EFFECTS OF LAND-USE CHANGE AND AEROSOL RADIATIVE PROPERTIES ON THE WEST AFRICAN CLIMATE SYSTEM

BY

AWOLEYE PEACE OLUBUKUNMI

B.Tech (Meteorology), M.Tech (Meteorology and Climate Science)

MET/09/7287

A Thesis of the Doctoral Research Programme of the West Africa Climate Systems, under the West Africa Science Service Centre on Climate Change and Adapted Land Use, in the Department of Meteorology and Climate Science submitted to the School of Postgraduate Studies in partial fulfilment of the requirements for the award of the degree of Doctor of Philosophy in Meteorology and Climate Science of the Federal University of Technology, Akure, Nigeria.

MAY, 2023

DECLARATION

I hereby declare that this thesis was written by me and is a correct record of my own research work. It has not been presented in any previous application for any degree of this or any University. All citations and sources of information are clearly acknowledged by means of references.

Candidate's Name: Awoleye, Peace Olubukunmi

Signature: Date

CERTIFICATION

We certify that this Dissertation entitled "Effects of Land Use Change and Aerosol Radiative Properties on the West African Climate System" is the outcome of the research carried out by John Stone under the WASCAL DRP-WACS in the Department of Meteorology and Climate Science of the Federal University of Technology, Akure.

Prof. K. O. Ogunjobi ……..

(Major Surpervisor) Signature
Date
Department of Meteorology and Climate Science,
Federal University of Technology,
Akure, Nigeria.

Prof. I. A. Balogun ……..

(Co-Surpervisor) Signature
Date
Department of Meteorology and Climate Science,
Federal University of Technology,
Akure, Nigeria.

Prof. Zachariah Debo Adeyewa ……..

(Director) Signature
Date
Doctoral Research Program – West African Climate Systems
West African Science Service Center on Climate Change and
Adapted Land Use (DRP-WACS, WASCAL),
Federal University of Technology,
Akure, Nigeria.

ABSTRACT

West Africa due to its climatological and geographical conditions is an essential domain for the characterization of atmospheric radiative forcing across the globe. This study investigated the interaction between aerosols and solar radiation over West African climatic zones (Sahara, Sahel, Savannah, and the coast of Guinea) between December 2005 and February 2006. The study further analyzed the dynamics of various aerosol sources and types and their contribution to the observed forcing effect in the climatic zones. The study identifies the distinguishing characteristics of the aerosol radiative properties, a greater amount of radiation is absorbed at the top of the atmosphere, and the radiative properties vary with changing aerosol concentration and distribution in the atmosphere. Additionally, an increase in anthropogenic aerosols leads to an increase in SSA. The study included the regional climate model RegCM 4.7.1 to conduct a sensitivity study, identifying the optimal cumulus convective precipitation scheme, planetary boundary layer (PBL), and land-surface scheme. The resulting simulation demonstrated a strong correlation with observed precipitation patterns and well-simulated temperatures. This study also aimed to explore how radiative mechanisms linked to seasonal dynamics in natural vegetation and abrupt land cover changes caused by human activities can influence the West African climate. In taller vegetation, such as forests and savannas, albedo increased during the growing period, leading to a decline in net shortwave radiation, while in shorter vegetation, such as grasslands and shrublands, albedo decreased, resulting in an increase in net shortwave radiation. However, the cooling and warming impacts of albedo during the growing period in taller and shorter vegetation, respectively, were significantly outweighed by ET cooling, which had a greater impact on LST seasonality in West Africa. Land cover changes caused an average increase in albedo, with the highest surge observed in the dry period. The albedo changes resulting from all land cover changes combined generated a regional instantaneous shortwave surface radiative forcing of -0.03W/m^2. Despite this small regional forcing, the study showed

that land cover changes from forest to cropland and savanna to grassland conversions had a more significant contribution to LST cooling than other changes in class. However, these conversion classes displayed the largest observed LST warming of up to 1.2°K and 0.4°K, respectively.

DEDICATION

This thesis is dedicated to Almighty God for His grace in completing this dissertation.

ACKNOWLEDGEMENTS

Firstly, I would like to express my sincere appreciation to God for His grace and guidance throughout my Ph.D. program. Without His divine intervention, I would not have successfully completed this journey. Furthermore, I am grateful to the Federal Ministry of Education and Research (BMBF), Germany for sponsoring the WASCAL program at the Federal University of Technology, Akure (FUTA DRP-WACS). This opportunity has enabled me to gain valuable knowledge and skills that have been instrumental to my academic and professional development.

I am also indebted to my supervisor, Prof. K. O. Ogunjobi, for his unwavering support, patience, and understanding throughout the research process. His guidance and mentorship were invaluable, and I am grateful for his contributions to my academic success.

Additionally, I would like to extend my appreciation to the entire staff of the FUTA DRP-WACS Centre, including the Centre Director, Prof. Z. D. Adeyewa; Deputy Director, Prof. I. A. Balogun; Scientific Coordinator, Prof. A. Oluleye; Head of Department, Dr. A. Akinbobola; and all the staff of the Meteorology and Climate Science Department for their assistance, commitment, and the knowledge imparted on me. Their collective efforts contributed significantly to the realization of my dream of acquiring a Ph.D. degree.

I am also thankful to my German host, Prof. M. Wendisch, for his constant support and advice. I appreciate him, the staff and management for being a great host during my research at the Leipzig Institute of Meteorology, Faculty of Physics and Earth Sciences, Uni-Leipzig.

I would also like to acknowledge the unwavering support of my brother, Dr. Stephen Ogungbenro, and the moral encouragement of Dr. A. Akinsanola and Dr. T. Morakinyo, which were instrumental in keeping me focused throughout the program.

Lastly, I express my profound gratitude to my selfless parents, Mr. and Mrs. Awoleye, my siblings, and my indefatigable partner, Adesua, for their emotional and physical support

throughout my program. Their encouragement and unwavering support kept me motivated, and I could not have accomplished this feat without them.

TABLE OF CONTENTS

LIST OF FIGURES

LIST OF TABLES

CHAPTER ONE

1.0 INTRODUCTION

1.1 Background to the Study

Aerosols influence climate directly by the scattering and absorption of solar radiation through their role as cloud condensation nuclei (Ogunjobi et al., 2004; Levy et al., 2013a), and its role on changing climate has been under scrutiny during the past decades (Ogunjobi et al., 2003; Kinne et al., 2013). Scattering (sulphate) and absorbing (black carbon) particles cool the Earth's surface; however, their radiative effects in the atmosphere vary with altitude (Kinne, 2019; Bellouin et al., 2020). For scattering particles, the top of the atmosphere forcing is almost the same as the surface forcing, while for absorbing aerosol species, the surface forcing is about 2–3 times larger than the top of the atmosphere forcing, which gives rise to a large atmospheric warming (Bozzo et al., 2020b). The greenhouse gases are longer lived and globally well mixed and their radiative effects are homogeneous and are of warming throughout the atmosphere starting from the surface. In contrast, aerosols reside in the atmosphere for about a week, exhibit regional signatures and can either warm or cool the atmosphere. Although aerosols are abundant near source regions, they impact the global climate as aerosols and their radiative influence can be transported to other regions due to atmospheric circulation. On temporal scales, the forcing due to aerosols is greatest during daytime and in summer (Li et al., 2016). In contrast, the greenhouse gas forcing acts over the full diurnal and seasonal cycles. Thus, aerosols perturb the earth–atmosphere radiation budget differently from greenhouse gases.

Vegetation impacts climate through its influence on water, energy, and gas exchange between the land surface and atmosphere (Bonan, 2008; Davin and de Noblet-Ducoudre, 2010). The degree to which vegetation impacts climate depends on the type of vegetation and season, and it is affected by land cover changes caused by human perturbations. Hence, improving our

understanding of the role of vegetation dynamics in ecosystem processes is crucial for delineating effective mitigation strategies against climate change.

The magnitude of the direct forcing of aerosols at a particular time and location depends on the amount of radiation scattered back to space, which itself depends on the size and optical properties of the particles, their abundance and the solar zenith angle. Indirect effects arise as a result of an increase in aerosol concentrations from anthropogenic sources. This leads to an increase in cloud condensation nuclei concentrations, which, in turn, develop into clouds with larger concentrations of droplets with smaller radii, and consequently to higher cloud albedo.

Atmospheric aerosols exert a cooling effect on the Earth's climate through direct and indirect effects which partially offset the warming caused due to greenhouse gases. The sources of aerosols can be natural (dust, sea salt, biogenic and volcanic) and anthropogenic (combustion of fossil fuel from urban/industrial processes and biomass burning). Dust, sea salt and sulphate produced over the ocean surfaces dominate the natural global aerosol abundance; however, a fraction of the dust in the atmosphere could be due to anthropogenic activities (Lu et al., 2010; Ginoux et al., 2012; Despres et al., 2012). Similarly, smoke from natural burning such as forest fires is treated as a natural component of biomass burning, while the burning of fuel wood or dung cake and crop waste burning are anthropogenic processes. Atmospheric aerosols modify the earth–atmosphere radiation budget by scattering and absorbing the incoming solar radiation (direct effect), and the processes of formation of clouds and precipitation (indirect effect). The direct and indirect aerosol radiative effects remain a significant uncertainty in climate studies (Solomon et al., 2007).

Aerosol observations are essential for understanding the Earth’s radiation budget and the complexities of climate change. Satellite-based remote sensing plays a vital role in gaining a good knowledge and understanding of global aerosol variations and interaction with the Earth’s climate [Kaufman et al., 2002]. Aerosol transport occurs in spectacular storm-like event, when

clouds of the desert aerosol particles take the shape of giant plumes that span the over large regions west of Africa and extend more than one thousand kilometres from the source. Deserts are the main sources of aerosol injected daily into the atmosphere, with mineral dust comprising more than 35% of the emitted primary aerosol mass (Remy et al., 2019). Half of this amount is attributed to the Saharan desert and influences the aerosol loading of Africa, the Atlantic Ocean, South America, the East coast of USA, and Europe. Atmospheric aerosols during the harmattan dust spell from the Sahara Desert is composed of minute particles borne by the north-east trade winds. Dusts are transported from these regions over land and sea to regions in Europe, the Middle East and across the Atlantic to as far away as Mexico City reducing visibility, relative humidity, solar radiation reaching the surface and temperature. Many factors have been attributed to the raising of dust in the source region. The primary factor is attributed to the behaviour of the sub-tropical anticyclone over the desert region.

Ground- based instruments measure local observations while the air borne sensors have the ability to monitor aerosols on a global scale. Satellite-based remote sensing plays a vital role in gaining good knowledge and understanding of global aerosol variations and their interaction within the earth's climate (Kaufman et al., 2002). Satellite data have long been employed for aerosol studies however with some major challenges in almost every step of the retrieval process, such as, sensor calibration, cloud screening, corrections for surface reflectivity and variability of aerosol properties; size distribution, refractive index (Bennonua et al., 2011; Middleton, 2017).

Aerosol optical depth is the single most comprehensive variable to remotely assess the aerosol burden in the atmosphere from ground-based instruments. This variable is used in local investigations to characterize aerosols, assess atmospheric pollution and make atmospheric corrections to satellite remotely sensed data. It is for these reasons, that a record of aerosol optical depth spanning most of the 20th century has been measured from sun photometers. The

vast majority are site specific, short term investigations with little relevance for seasonal, annual or long-term trend analysis, however a few multi-year spatial studies have contributed to the knowledge and experience.

1.2 Aerosols and Climate Change

The Earth's climate varies on numerous timescales that range from very long geological timescales and glacial–interglacial timescales typically of the last million years, to shorter timescales caused by external factors, such as volcanism, or the internal variability of the system. The latter includes a number of quasi-periodic oscillations involving the cryosphere, the ocean, and the atmosphere and their interactions. Human activity has modified profoundly the chemical composition of the atmosphere, well beyond variations observed over the last thousands of years or those encountered during the succession of glacial and interglacial conditions of the last million years. The rate of anthropogenic changes is also very large in comparison to past changes. Among greenhouse gases of anthropogenic origin, one can mention carbon dioxide, methane, and nitrous oxide that are responsible for an additional greenhouse effect. Observations show a warming of the planet since preindustrial times that has amplified and accelerated since the 1950s. The observed warming cannot be explained by natural factors (changes in the sun, volcanism, and natural variability) alone but requires anthropogenic factors including an enhanced greenhouse effect. This is how the Intergovernmental Panel on Climate Change (IPCC) has reached the conclusion that the observed climate change of the past century is extremely likely due in part to anthropogenic factors (Bindoff et al., 2013; Weinzierl et al., 2017; Ohneiser et al., 2020). Atmospheric aerosols form an integral part of the climate system and interact with the atmosphere, the cryosphere, the biosphere, and the ocean. Aerosols interact strongly with the water cycle and a number of biogeochemical cycles. Greenhouse gases are indeed not the only anthropogenic driver of climate change. It is now widely understood that anthropogenic aerosols have masked

a fraction of the warming effect expected from the increase in greenhouse gases, since the beginning of preindustrial times.

Vegetation impacts climate through its influence on water, energy, and gas exchange between the land surface and atmosphere (Bonan, 2008; Davin and de Noblet-Ducoudre, 2010). The degree to which vegetation impacts climate depends on the type of vegetation and season, and it is affected by land cover changes caused by human perturbations. Hence, improving our understanding of the role of vegetation dynamics in ecosystem processes is crucial for delineating effective mitigation strategies against climate change.

1.3 Sources of Aerosols and Aerosol Precursors

1.3.1 Marine Aerosols

The wind friction at the ocean surface ejects fine particles of salty marine water into the atmosphere. A fraction of the water evaporates, so that the concentration of salt in the particle increases. This gives rise to sea salt particles that are more or less hydrated according to the ambient humidity. Although these particles are often called sea salt aerosols, this is yet another misuse of language because these particles may also contain biological material and other impurities. It is therefore more appropriate to refer to them as sea spray aerosols. Sea spray aerosols cover sizes that range from typically 100 nanometres (nm) to several tens of micrometres (μm). The largest particles fall back fairly quickly to the ocean surface and are therefore of lesser climatic importance.

1.3.2 Desert Dust

The wind friction on continental surfaces can detach soil particles and suspend them in the atmosphere. This is particularly the case in desert, arid, and semiarid regions where the wind is not slowed down by the vegetation that is either completely absent or fairly sparse. The raising of soil particles to the atmosphere also requires a reduced soil humidity so that cohesive forces between soil particles are also reduced. As for sea spray aerosols, desert dust particles

span sizes that range from typically 100 nm to tens of μm. Larger particles can also be lifted but they fall down quickly. Desert dust aerosols are also called mineral dust or mineral aerosols. The raising of desert dust depends very much on environmental and meteorological conditions. They are sporadic in nature.

1.3.3 Volcanic Aerosols

Volcanoes can emit fragments of pulverized rocks and minerals, usually called volcanic ash, during explosive eruptions. These particles have sizes typically ranging from a micrometre to millimetres. Volcanic ash can be transported over distances of a few hundreds to a few thousand kilometres but being micronic particles they tend to fall down rapidly. Hence their climate effect is limited. Volcanoes also emit sulphur-rich gases (in the form of Sulphur dioxide, SO_2, and hydrogen sulphide, H_2S) that get oxidized in the atmosphere to form submicronic sulphate aerosols. If these Sulphur-containing gases are emitted in the troposphere, the residence time of the subsequent aerosols will be short, a few weeks at most. However, if the eruption is powerful enough to inject the Sulphur gases in the stratosphere, then the volcanic aerosols have a much longer residence time, of the order of a few months to more than a year, depending on the region and altitude of injection.

1.3.4 Biogenic Aerosols

The terrestrial biosphere is a source of primary biogenic aerosol particles. They comprise plant and insect debris, pollen (a fine powder produced by seed plants that contains the male gametes that serve for reproduction), spores (a reproduction cell or organ from many plants and fungi), bacteria and viruses. Once airborne, these particles can be transported by the wind on varying distances depending on their size. Debris are usually larger than 100 μm, pollen, spores and large bacteria are generally in the range of 1–100 μm, while small bacteria and viruses are generally smaller than 1 μm. Seawater also can contain biological material, some of which is transferred to sea spray aerosols during the emission process. This primary organic matter is

found preferentially in particles smaller than 200 nm in diameter (Leck and Bigg 2008) and its amount has been found to depend on the biological activity in ocean waters (Facchini et al., 2008). Terrestrial and marine ecosystems are also an important source of aerosol precursors. Some species of phytoplankton produce dimethyl sulphide (DMS), a gaseous compound that is oxidized in the atmosphere to form Sulphur-containing aerosols. Plants and algae emit volatile organic compounds (VOCs) that are oxidized in the atmosphere and condense and contribute organic material to the atmospheric aerosol. These aerosols are referred to as secondary biogenic aerosols. Their sizes are typically of the order of a few tenths of a micrometre.

1.3.5 Aerosols from Fossil Fuel Combustion

The combustion of coal and oil derivatives also produces black carbon and organic carbon, as well as sulphur dioxide that converts into sulphate aerosols. These are essentially submicronic particles, which are also a source of air pollution in developing and industrialized countries. Air pollution due to particles and gas-phase pollutants, such as ozone and nitrogen oxides, is responsible for a wide range of adverse health and environmental effects. Effects on human health include increased respiratory and cardio-vascular diseases and associated mortality. Aerosols and acidic deposition are responsible for damages on historical buildings.

1.3.6 Biomass Burning Aerosols

In biology, biomass refers to material produced by living organisms, but adjusting the definition here to mean all biological (organic) material that comes from the living world and can potentially burn (i.e. vegetation, dead wood, animal dung, peat) while excluding so-called fossil fuels (coal, gas, and oil) that are formed on geological timescales. The burning of biomass generates primary aerosols that stem from the incomplete combustion of the organic matter. Biomass burning aerosols include organic carbon, that is associated with hydrogen and oxygen atoms, and black carbon, where the carbon content is very high. These aerosols are generally

submicronic and are clearly visible in smoke plumes. The sources of biomass burning aerosols are both natural and anthropogenic. The combustion of biomass also emits gaseous compounds, such as volatile organic compounds and Sulphur dioxide, which are aerosol precursors.

1.4 Climate Effects of Aerosols

The role aerosols play in influencing climate in a number of ways as they scatter and absorb solar radiation. Backscattering of solar radiation towards space results in a reduction of incoming solar radiation at the Earth's surface, a loss of energy and a cooling of the climate system. Absorption of solar radiation is accompanied by a heating within the aerosol layer, but also by a reduction of incoming solar radiation at the Earth's surface. Such effects occur preferentially, but not uniquely, in clear sky conditions. The absorption of solar radiation by aerosols modifies the vertical temperature profile. This impacts the relative humidity, atmospheric stability, and therefore cloud formation. This effect has traditionally been called the aerosol semi-direct effect, but it can also be seen as a rapid adjustment of the atmospheric state that follows aerosol–radiation interactions.

Aerosols serve as cloud condensation nuclei in liquid water clouds, thus exerting a partial control of cloud microphysical and optical properties. An increase in the concentration of aerosols leads to an increase in the concentration of cloud condensation nuclei, and generally to an increase in the concentration of cloud droplets. For a fixed cloud liquid water content, this is accompanied by a reduction in the cloud droplet size and an increase in the cloud reflectivity. Altogether this leads to less solar energy absorbed and a cooling of the climate system. This effect has been traditionally called the aerosol first indirect effect, these processes have traditionally been called the aerosol direct effect. The modification of cloud microphysical properties is expected to have an impact on cloud evolution, in particular in terms of the ability of clouds to generate droplets that are large enough to initiate precipitation. This effect is traditionally called the aerosol second indirect effect.

Aerosol impacts the properties of mixed-phased and ice clouds, in particular through their role as ice nuclei. This has been referred to in the past as yet another indirect effect of aerosols, or a glaciation effect. It is also part of aerosol–cloud interactions. Absorbing aerosols may deposit onto snow and ice surfaces, thus making these surfaces less reflective (i.e. more absorbing). This contributes to warm the surface and thus the climate system. This effect is known as the aerosol on snow effect but can be categorized as part of aerosol–radiation interactions. Aerosols also interact with vegetation through changes in incoming solar radiation, fraction of diffuse radiation and as a source of nutrients. These are other contributions to aerosol–surface interactions.

1.5 Statement of the Research Problem

Land-use change has a significant impact on aerosol compositions. Emissions from biomass burning, desertification, deforestation and agricultural practices play a major role in modifying atmospheric aerosol compositions and radiative properties. Aerosols from urban and industrial air pollution play major roles in the climate system. Changes in land-use, such as bare surfaces, are major prerequisite for raising of dust particles in which wind friction can detach soil particles and suspend them in the atmosphere or transport them. Surface wind speed, soil humidity, and vegetation cover are three important factors that govern desert dust emissions. Vegetation contributes to the emissions from biomass burning and vegetation fires. These factors vary over multiple timescales because of the changes in land use which makes attributing recent variations in aerosol radiative properties to land-use change difficult and in choosing a reference period.

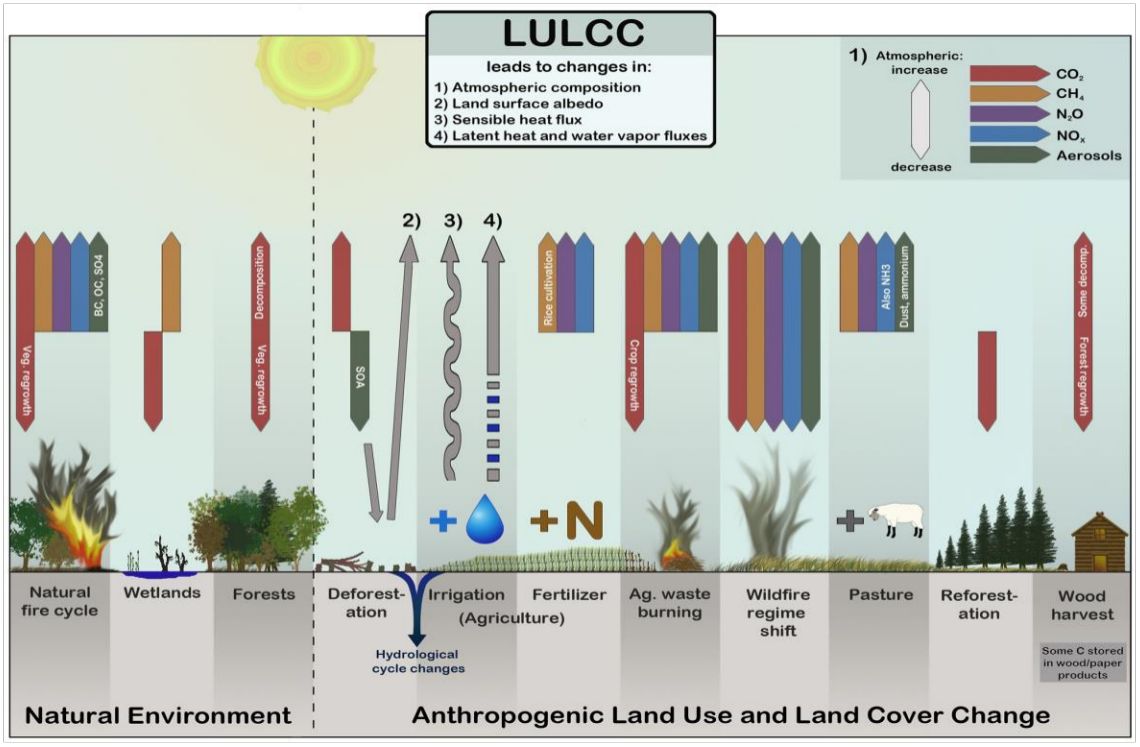

Figure 1.1: A schematic illustration of the climate impacts of land use and land cover change (Ward et al., 2014)

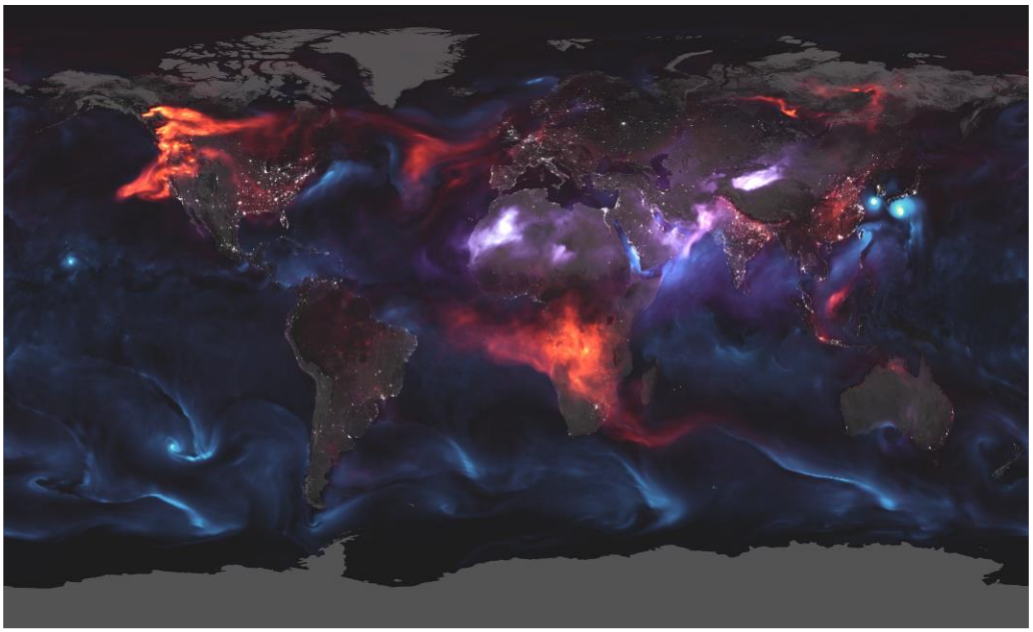

Figure 1.2: Visualization of the aerosol output from NASA model Goddard Earth Observing System Forward Processing on 2018-08-23 (Dunbar, 2018). Sea salt aerosol is shown in blue, black carbon in red and mineral dust in purple.

Aerosol particles absorb and scatter radiation, which leads to a radiative forcing due to aerosol–radiation interactions. They influence cloud micro-structure and precipitation processes, which in turn affect the radiative properties of clouds, atmospheric circulation and thermodynamics, as well as radiative budgets. Furthermore, aerosols affect clouds by heating atmospheric layers when they absorb a considerable amount of the solar radiation. Cloud condensation nuclei (CCN) are the subset of aerosol particles which are able to form cloud droplets, and has implications at various scales. In terms of radiative forcing, aerosol radiative properties which includes light scattering, light absorption, light extinction, single scattering albedo, angstrom exponent and radiative forcing efficiency, are the least understood influence on climate change. At the regional scale, such as West Africa, land-use can be a major driver in the radiative properties of aerosols that can alter radiation and dynamic processes. Reducing the large uncertainty in land-use effects is a major challenge in increasing confidence in global and regional climate change projections.

Man is altering the aerosol environment through land cover change, combustion of fossil fuels and the introduction of particulate and gas species to the atmosphere. Each perturbation has some impact on the aerosol-radiation interaction. How much aerosol man is contributing to the atmosphere is not known. Even more fundamental, we do not know the current total aerosol loading; thus, we have no definitive measure of change for future assessment (Andrea, 1996). Regardless of current conditions, the extent of aerosol-radiation interaction on a global scale is the subject of extensive aerosol radiative forcing modelling. Investigations have been initiated by concerns ranging from radiative forcing by aerosols, long term impacts on climate and public health, aesthetic and ecological impacts, as well as the future of sea level habitations and political entities. The resources put into these studies have been local and contributed to an enormous, yet mostly uncoordinated radiative forcing sub-regional assessment.

West Africa currently suffers from inadequate characterization of atmospheric aerosols due to its pressure on land resources which is expected to increase as global population continues to climb and the world becomes more affluent, resulting in a far reaching consequences on its inability to quantify precisely the climatic impacts of the radiative forcing inhibited by aerosol. Changing climate may exert additional pressures on natural lands as present-day productive regions may shift due to intense anthropogenic activities, and the recent rise in demand for biofuels increases competition with well vegetated land surfaces. Given these projected trends there is a need to understand the uncertainties revolving around the radiative forcing impacts of land use on the West African climate system.

1.6 Significance and Justification of Study

The study of the of radiative forcing due to aerosol and land-use changes are important for various application including, radiative forcing modeling, studies of aerosol interaction with radiation and clouds, and also in land-use changes.

Atmospheric aerosol concentrations and their radiative properties are also considered as one of the largest sources of uncertainty in current assessments and predictions of global climate change. Hence, it is significant to obtain such information via simulating forcing due to aerosol-radiation interaction using regional climate models. Therefore, for comprehensive understanding of the role of land-use changes and aerosol radiative properties and also its variation in a changing climate, their properties, spatial and temporal variations must be properly understood. This study investigates the effects of land-use and aerosol radiative properties on the West African climate system during the 2005-2006 (DJF) “dust episode”. These effects could have strong implications on convection, cloud development and the ratio of direct to diffuse radiation, which impacts carbon uptake and the photosynthetic rate of the forest. A good knowledge on the effects that land-use changes has on aerosol radiative properties is therefore key to attributing observed climate change to a forcing mechanism.

Therefore, it becomes crucial to examine the dynamics of aerosol radiative properties due to changes in land-use and the interactions with the West African climate system. This will help in making effective land-use policy scenarios for a changing climate. Attempts have been made to classify various aerosol episodes in West Africa in relation to their radiative properties because dust particles have been attributed to be the largest contributor to the radiative forcing over West Africa depth, this study further investigates other significant contributors to the changes in the abundance of these atmospheric constituents generating forcing onto the West African climate.

1.7 Aim and Objectives

This study aims at conducting a detailed study of the effects of changes in land-use and aerosol radiative properties on the West Africa climate during the December to February (2005-2006) dust episode.

The specific objectives of this study therefore are to;

i. determine the dynamics of aerosols radiative properties (size, volume, reflective and radiative properties) in the study area;
ii. evaluate model performance in simulating aerosol radiative properties over West Africa, and;
iii. evaluate the radiative forcing effect on climate due to changes in land-use.

The daily and spatial variations of aerosol radiative properties were discussed, with emphasis on the advection of dust, black carbon, organic carbon and sea-salt aerosols. Furthermore, various classes of land features were also examined to explain the land surface albedo and its role in the forcing experienced during the study period based on the land surface temperature.

CHAPTER TWO

2.0 LITERATURE REVIEW

The existing scientific literature extensively documents mineral dust aerosols (Akinyoola et al., 2019; Fawole et al., 2019; Frol'kis and Kokorin, 2019; Bellouin, 2020; Bockarie et al., 2020; Solmon et al., 2021) in the atmosphere and their impacts on aerosol radiation forcing (Saidou et al., 2020; Gryspeerdt et al., 2020; Liu et al., 2021; Fung et al., 2022).

2.1 Aerosol-Radiation Interactions

A fundamental measure of the strength of the direct interaction of aerosol with radiation in the atmosphere is the Radiative Effect from aerosol–radiation interactions (REari) (Boucher et al., 2014). It is computed as the difference of the net irradiance with aerosol particles and in hypothetical pristine conditions. While some climatological studies only consider the effect at the top of the atmosphere, many others are also focused on the radiative effect of the total atmosphere or surface to investigate the resulting heating or cooling by aerosol. The best estimate of the change in global mean effect caused by anthropogenic aerosol particles is called the aerosol radiative forcing. The Intergovernmental Panel on Climate Change (IPCC) report from the year 2014 constrains the effective aerosol forcing to values between −0.95 and $+0.05 Wm^{-2}$ (Myhre et al., 2014). This large confidence range is one of the major uncertainties for estimating the total radiative forcing of the climate system. The most recent IPCC report from the year 2021 further constrains the forcing to values between −0.6 and $0 Wm^{-2}$ (Forster et al., 2021), which is consistent with the comprehensive review study from Bellouin et al. (2020), where the effective aerosol radiative forcing is constraint to the range between −0.71 and $-0.14 Wm^{-2}$. For radiative effect, a distinction is made for short-wave (solar) and long-wave (terrestrial) radiation, with solar and terrestrial radiation being defined as the electromagnetic radiation received from the sun and emitted by the Earth, respectively.

The radiative effect of aerosols varies strongly depending on the aerosol type. For example, pure sulphates, nitrates and sea salt aerosol particles scatter almost all solar radiation they encounter, thus cooling the atmosphere (e.g., Bauer et al., 2007; Yue & Liao, 2012). Black carbon, on the other hand, has strongly absorbing properties and warms the atmosphere (e.g., Bond et al., 2013; Wang et al., 2016). Organic (brown) carbon is less absorbent than black carbon, causing that its radiative effect for the atmosphere therefore depends on the reflectivity of the surface in the region of interest (e.g., Myhre et al., 2013; Lin et al., 2014). The radiative effect of mineral dust, on the other hand, varies strongly depending on the composition of minerals that make up the dust grains, their anthropogenic or natural origin, and whether they are coated with, e.g., black or brown carbon (e.g., Ansmann et al., 2011; Miller et al., 2004b; Chaibou et al., 2020).

This study is focused on the clear sky short-wave radiative effect at the surface and clear sky long-wave radiative effect at the top of the atmosphere. Therefore, clouds are completely ignored and, for further simplification, aerosol particles from natural or anthropogenic sources are considered only in combination. At the surface, the aerosol radiative effect is relevant for our understanding of the climate system due to its influence on the surface energy budget, and thus its influence on latent and sensible heat fluxes (e.g., Chaibou et al., 2020). In addition, the effect of aerosol on the surface *solar* irradiance is of high interest for the renewable energy sector, e.g. the planning of photovoltaic power plants (e.g., Schroedter-Homscheidt et al., 2012). In addition, the radiative effect is studied exclusively with focus on the short-wave radiation, thus the effect of aerosol on terrestrial radiation is not considered.

Considerable effort has been spent over the last decades to quantify the radiative effect due to aerosol-radiation interaction. This radiative effect is studied at global (e.g., Yu et al., 2006; Bellouin et al., 2013; Kinne, 2019) and regional scales (e.g., Papadimas et al., 2012; Esteve et al., 2016; Bartok, 2016). For Europe, Nabat et al. (2014) quantified the radiative effect by

utilizing a coupled regional climate system model (CNRM-RCSM4). Bartok (2016) used the MAGIC radiation code with aerosol and water vapour climatology from Aerocom and ERA-INTERIM, respectively, for calculating the radiative effect. Esteve et al. (2016) utilized a different radiation scheme (ES96) along with aircraft measurements of aerosol optical properties during the EUCAARI-LONGREX campaign. These studies found annual mean values of radiative effect ranging from −7 to −15Wm^{-1}, with uncertainties of about 5Wm^{-2}. The discrepancies in the methods found in the literature are the result of different methods and models used, variations in the assumed aerosol types and optical properties, and the different remote sensing techniques used for the underlying databases.

As indicated in Figure 1.2, aerosol particles are not homogeneously distributed across the globe. Therefore, the corresponding radiative effect also shows strong regional dependencies. Despite significant progress in recent decades, estimating the direct climate impact of aerosol remains a challenge. Of the 25 climate models considered by the IPCC, only a few parametrize the direct impacts of aerosol types other than sulphates (Boucher et al., 2014). For progress in climatological modelling studies, remote sensing of aerosol optical properties from ground-based, airborne and satellite platforms is required. In particular, events with smaller spatial and temporal scales such as desert dust storms or forest fire plumes require detailed insight with remote sensing methods, as such events are challenging to represent realistically in models.

Apart from determining the optical properties of aerosol particles, the influence of aerosol on the radiation budget in the form of the radiative effect can directly be determined from the narrow- or broadband irradiance measured by ground-based sensors. Data of measured broadband irradiance and energy budget on Earth's surface is important for applications in, e.g., agriculture, astronomy, hydrology, climate change, and the renewable energy sector. Furthermore, these datasets offer the possibility to assess the radiative closure in combination with explicit or empirical radiative transfer modelling. The aim of a radiative closure study is

the comparison of simulated and measured radiation to evaluate the parametrization of coincident-state measurements such as aerosol optical and radiative properties (e.g., Michalsky et al., 2006; Sussmann et al., 2016). As with ground-based measurements of aerosol optical properties, measurements of broadband irradiance are organized in global networks.

Non-dust aerosols, such as black carbon and organic matter, are significant contributors to the radiative forcing of aerosols in West Africa and their impact is greatest in the Savanah and Guinea zones. Boiyo et al., 2019 explained that both dust and non-dust aerosols have a significant impact on the radiative forcing and that the magnitude of their effect depends on their size distribution and concentration. Black carbon can have a much stronger radiative effect than dust aerosols, particularly in areas with high levels of pollution.

Bond et al., (2013) focused on the role of black carbon in the climate system, including its radiative effects. The authors found that black carbon is a significant contributor to the radiative forcing of aerosols and that it can have a strong warming effect in regions near sources of emissions. They also emphasized the importance of quantifying the interaction of black carbon and other non-dust aerosols with solar radiation in order to improve our understanding of their radiative effects. The role of black carbon in the climate system, including its radiative forcing and effects on the atmosphere and surface temperature cannot be ignored. The authors found that black carbon is a significant contributor to global warming and that its radiative forcing is comparable to that of other greenhouse gases.

Radiative forcing of aerosols over West Africa, including both dust and non-dust particles, is significant and it can have a significant impact on the surface temperature and precipitation patterns (Quaas, J., et al. 2013). Prospero et al., 2002 showed that dust aerosols can have a significant impact on the radiative balance of the Earth, especially in regions downwind of desert sources, such as West Africa as it is of utmost importance to quantify the interaction of

dust and non-dust particles with solar radiation in order to improve our understanding of their radiative effects (Kaufman et al., 2002; Boucher et al., 2013; Gbobaniyi et al., 2013).

To obtain the radiative effect from irradiance observations with aerosol, the irradiance of the aerosol-free (pristine) atmosphere has to be simulated. The complexity of the methods for these simulations ranges from simplified semi physical models to explicit radiative transfer calculation. A large variety of CSM has been developed, ranging from simple to highly complex schemes developed for different applications (Sun et al., 2019). The accuracy of these models to simulate the clear sky irradiance at the surface is intensively evaluated in numerous studies, most recently and detailed by Sun et al. (2019). CSM are widely used to estimate the solar irradiance at the surface in cloud-free conditions. Applications range from the evaluation of power generation of photo-voltaic power plants (Bright et al., 2017) to the determination of the global radiation budget for regions where ground based observations are not available (Ruiz-Arias & Gueymard, 2018). These models can also be used for the quality control of observational data (e.g., Long & Ackerman, 2000; Ineichen, 2014; Reno & Hansen, 2016).

The characterization of aerosols in response to radiative forcing has been widely discussed by several authors. Due to the ability of aerosols to interfere with the earth's radiation balance at regional and global scales, atmospheric aerosols have recently gained significance in climate studies (Haywood and Boucher, 2000; Penner et al., 2004). Over West Africa, mineral dust is found to be the most dominant aerosol having a huge radiative forcing than other aerosol types such as black carbon, organic matter, and sea salt, amongst others. (Korgo, 2014; Eresanya et al., 2017). Emission and transportation of aerosols over West Africa concerning volume size distribution and concentration have been discussed. The behavioral pattern of aerosols during the wet and dry seasons over West Africa has been found to vary seasonally with high concentrations found during winter due to the transport from the Sahara (Kaufman et al., 2002; Andrae et al., 2005; Ming and Ramaswamy 2011; Titos et al., 2016). The cooling radiative

effect experienced during this season has been linked to the high deposition of absorbing aerosols in this region mobilized and transported from the Sahara (Ogunjobi and Awoleye, 2019). Aerosol characteristics with different species and emission in the West Africa region have been widely discussed. Specific inventories of different aerosols including carbonaceous aerosol from biomass burning and mineral dust (Marticorena et al. 2010) have been developed. Clouds play a key role in Earth's radiation budget, and aerosols serve as the seeds upon which cloud droplets form.

Anthropogenic activity has led to an increase in aerosol particle concentrations globally and an increase in those particles that act as cloud condensation nuclei (CCN) and ice nucleating particles (INP). The effect of an increase in aerosols on cloud optical properties, and associated radiative forcing, is the most uncertain component of historical radiative forcing of Earth's climate caused by aerosols. For instance, the global DRF due to anthropogenic aerosols is estimated as −0.5 (±0.4) Wm-2 (Forster et al., 2007). However, the top of the atmosphere (TOA) DRF of aerosols varies strongly both spatially and temporally. Indeed, unlike greenhouse gases, aerosols show a large variability in their spatial distribution due to shorter lifetime (Rosenfeld et al., 2008; Boucher et al., 2013). Their physical chemical optical properties also vary greatly depending on emissions sources and aging (i.e., physical and chemical changes via mixing and other processes) during transport. The magnitude, and even the sign, of the TOA DRF varies among different regions and is controlled by several factors including aerosol absorption capacity, surface reflectivity, and the reflectivity of the underlying cloud and/or aerosol layers (Russell et al., 2002; Haywood et al., 2003; Johnson et al., 2008b). Land-use changes could be a major factor in the behaviour. Dust and biomass aerosols are major aerosols influencing the West African climate system, and they can be either due to anthropogenic emissions or natural phenomenon. It is evident that biomass aerosols are majorly due to human activity in the burning of biomass in West Africa, while the raising of dust is

majorly natural due to high pressure to the north of the Bodélé intensifying the north-east trade winds, leading to an increased entrainment of dust in the Bodélé Depression (Wolfgang et al., 2007).

Due to the uncertainties revolving around the characteristics of aerosols present in the atmosphere leading to the cooling radiative forcing experienced during the winter season, it is therefore essential to understand the dynamics and the roles different aerosols play in interfering with the solar radiation assuming the atmosphere is free of clouds. Because dust, black carbon and organic matter aerosols can affect radiation balance both near the source and far downwind, especially in regions where the optical and chemical properties of the particles vary, determining the optical parameters requires careful consideration, especially since these are required inputs in climate prediction models. This study also focused on characterizing the radiative forcing induced by major dominant aerosols during the notable termed dust episode of the 2005-2006 dry season (December, January, and February) under a clear-sky idealized atmospheric condition over West Africa. General circulation models (GCMs) are unable to include the effects of regional features (Xue et al., 2010) due to their relatively coarse resolution. Regional climate models (RCMs) are relevant tools for this purpose since they allow for land surface heterogeneity and fine-scale forcing such as complex topography and vegetation variations (Paeth and Feichter 2006; Paeth and Hense, 2006).

2.2 Radiative Forcing of Land Use Change

The radiative forcing concept is a common currency that allows us to compare and contrast various perturbations to the climate system, such as changes in the emissions of CO 2, tropospheric aerosols, solar activity or land-use, amongst others (e.g. Sherwood et al. 2015). A radiative forcing arises in response to changes in land cover (e.g. forest to pasture and crops) predominantly because different surface types have different albedos. Forests are generally darker than grasses or croplands and so deforestation tends to increase the Earth's albedo and

reflect more solar radiation to space—a negative radiative forcing which causes cooling (e.g. Myhre et al. 2013). However the forcing from changes in land-use is further complicated by its impact on hydrology and non-radiative fluxes (Brovkin et al., 2006; Betts et al., 2007; Davin et al., 2007; Davin and deNoblet-Ducoudré 2010; deNoblet-Ducoudré et al., 2012) as well the coincidence of land-cover change and snow cover at higher latitudes (e.g Betts 2000; Pitman et al. 2011).Changes in land-use are also expected to have large bio-geochemical effects through altered CO2 emission and uptake(e.g. Betts 2000; Brovkin et al. 2013) due to uncertainties regarding the magnitude of the imposed land use perturbations (Schmidt et al., 2012), the resulting alterations in land surface properties, the interplay between radiative (related to albedo) and non-radiative processes (related to changes in evaporative fraction and roughness), and the influence of atmospheric feedbacks and non-local effects (Winckler et al., 2017, 2019).

More than half of the Earth's land surface has been affected by land use and land cover change activities over the last 300 years, largely from the expansion of agriculture (Hurtt et al., 2011), leading to numerous climate impacts (Foley et al., 2005). Conversion of land from natural vegetation to agriculture or pasturage releases carbon from vegetation and soils into the atmosphere (Houghton et al., 1983), often quickly through fires, which emit carbon dioxide (CO_2), methane (CH_4), ozone (O_3) producing compounds, and aerosols (Randerson et al., 2006). Deforested areas have a diminished capacity to act as a CO_2 sink as atmospheric CO_2 concentrations increase (Arora and Boer, 2010). Furthermore, agriculture and pasturage emits CH_4 and nitrous oxide (N_2O), accelerates soil carbon loss (Lal, 2004), and changes aerosol emissions (Foley et al., 2011). For instance, land management can enhance mineral dust aerosol emission by modifying surface sediments and soil moisture (Ginoux et al., 2012), but reduces fire aerosol emissions (Kloster et al., 2012) and emissions of low-volatility products of oxidized biogenic organic compounds that condense to form secondary organic aerosols (Heald et al.,

2008). Changes in the abundance of these atmospheric constituents generate forcing onto the climate system (Figure 1.1), quantified in this study as radiative forcing.

The global radiative forcing and associated climate response attributable to land use changes are often portrayed as a balance between cooling bio geophysical effects (changes in surface energy and water balance) and the warming biogeochemical effect of increases in atmospheric CO_2 (e.g., Claussen et al., 2001; Brovkin et al., 2004; Foley et al., 2005; Bala et al., 2007; Cherubini et al., 2012). Claussen et al. (2001) found that the cooling from bio geophysical effects of land cover change dominated over the warming from associated CO_2 emissions in high-latitude regions, where the land may be snow covered for part of the year, whereas tropical land use changes leads to a warming due to a weaker albedo forcing. This regional contrast in the dominant forcing from deforestation also applies to natural forest disturbances (O'Halloran et al., 2011). On a global scale, model estimates have shown both cancelling climate responses to historical land cover change bio geophysical effects and CO_2 emissions (Brovkin et al., 2004; Sitch et al., 2005) and a net warming (0.15^{o}c) from the same effects (Matthews et al., 2004).

Additional land use change forcing are often grouped together with fossil fuel burning and other activities for assessment of the total anthropogenic RF (e.g., Forster et al., 2007; Myhre et al., 2013). Nevertheless, there is some recognition of the importance of evaluating emissions of non-CO2 greenhouse gases attributable to land use separately from fossil fuel emissions for targeting emission reduction policies (Tubiello et al., 2013). Less attention is given to forcing from short-lived atmospheric species that are affected by land use changes. Foley et al. (2005) acknowledge that changes in the concentrations of short-lived species, aerosols and O_3, attributable to land use change are important for air quality assessment but do not estimate the impacts of these species on climate. Unger et al. (2010) partition sources of global, anthropogenic RF into economic sectors, including agriculture. They consider non-CO_2 greenhouse gas and aerosol forcing agents but only for present-day land use emissions and they

do not include land cover change. The full contribution of land use change to global and regional radiative forcing compared to the contribution from other anthropogenic activities remains unquantified.

Seasonal changes in vegetation structure (e.g., leaf area index (LAI) and canopy height) and physiology (e.g., photosynthesis and transpiration) affect the surface biophysical properties (albedo, canopy conductance, and surface roughness length), which directly impact the surface energy balance, net radiation partitioning Moore et al., 1996; Pielke et al., 2007; Richardson et al., 2013), and hence land surface temperature (LST) (Schwartz, 1992). Climate patterns, on the other hand, directly affect vegetation phenology and temporal patterns of ecosystem functioning. The interacting mechanisms and feedbacks of these processes across different ecoregions are not yet fully understood, particularly in remote regions, where observation data on key climate and biophysical variables are scarce. For instance, in the Horn of Africa, the dominating bimodal rainfall pattern, associated with the Intertropical Convergence Zone (ITCZ), often results in multiple vegetation growing periods (Nicholson, 2017). This pattern influences the role of vegetation phenology in regulating the radiation balance and LST through their effect on albedo seasonality.

Previous ground-based albedo measurements in grasslands (Song, 1999), bushlands (Allen et al., 1994), shrublands (Williamson et al., 2016), and forests (Hollinger et al., 2010; Moore et al., 1996) have shown that the albedo of a vegetated surface is strongly affected by phenology. Soil moisture content can also influence the observed seasonal variations in albedo over vegetated surfaces (Allen et al., 1994). Furthermore, other factors not related to the land surface, such as solar zenith angle (SZA) variations, have an impact on the seasonal course of albedo (Song, 1999). However, the extent to which such albedo dynamics affects seasonality of the radiation regime, and how it is partitioned to determine the residual energy available to warm the land surface need further investigation.

Land cover changes also affect the energy balance and LST through modification of surface biophysical properties, particularly albedo, surface roughness and evapotranspiration (ET) (Pielke Sr et al., 2007; Lee et al., 2011; Li et al., 2015; Alkama and Cescatti, 2016). Changes in the net radiation balance of the Earth due to anthropogenic perturbations (e.g., changes in land cover, aerosols, and greenhouse gas concentrations) or natural variability (e.g., solar irradiance and volcanic eruptions) are commonly known as radiative forcing (Myhre et al., 2013). When land cover changes result in the replacement of a darker surface in favour of a brighter one (e.g., in the case of tropical forests being replaced by brighter background soil during deforestation), albedo tends to increase, resulting in negative radiative forcing (Zhang et al., 2017; Ding et al., 2022). On the other hand, when the conversion happens from a brighter to darker surface (e.g., through afforestation), albedo decreases, resulting in positive radiative forcing.

Although the radiative impact of land cover changes at a global level is the least uncertain of all anthropogenic forcing, the best estimate of -0.2 ± 0.2 W m^{-2} for pre-industrial times has been produced by climate models (Myhre et al., 2013). Recent studies based on Moderate Resolution Imaging Spectroradiometer (MODIS) data, however, have given smaller estimates (-0.09 W m^{-2}) and it has been argued that the radiative impact could have been previously overestimated (Myhre et al., 2013). The wide range in global radiative forcing estimates arises from uncertainties in accurately measuring albedo and land cover changes. Although the impact of land cover change on air temperature and LST has been much studied at a global scale (refer to Perugini et al. (2017) for an extensive literature review), relatively few studies have examined the impacts of individual radiative (albedo) and non-radiative (surface roughness and evapotranspiration) processes using either modelling (Davin and de Noblet-Ducoudre, 2010) or observations (remote sensing and in situ) (Luyssaert et al., 2014; Lee et al., 2011; Bright et al., 2017; Peng et al., 2014). Davin and de NobletDucoudre (2010) have shown that surface

albedo change due to globalscale replacement of forest by grassland could cause −1.36 K cooling globally, whereas non-radiative process could cause warming of up to 0.24 K via ET and 0.29 K via surface roughness reductions. Hence, further studies at a global or regional level are still needed in the areas that have undergone significant land cover changes.

2.3 Gaps in Literature

It is unavoidable that there is a gap in knowledge between acquiring an understanding of atmospheric processes and incorporating them into climate models, and this is particularly evident in the case of aerosol processes. Important uncertainties in terms of land-use changes that alters the properties of atmospheric aerosols and their interactions with the West African climate system still remain uncertain, despite the better assessment of emissions, improvements in remote sensing satellite observations, dedicated field campaigns and aerosols surface networks which offer better constraints for numerical models. Unfortunately, there are still fundamental gaps in our knowledge on the dynamics of West African Aerosols and the interaction between its associated features such as cloud and radiation. This is partly due to the lack of appropriate observational datasets (Dubovic et al., 2000; Oluleye et al., 2012) and rare capability of climate models to incorporate other processes affecting the properties and dynamics of West African aerosols (Coakley et al., 1982). However, several studies have shown that climate models are useful tools to study and understand aerosols variability and its associated features but unable to resolve processes due to land-use changes in the dynamics of aerosol properties, most especially the radiative properties over West Africa.

CHAPTER THREE

3.0 METHODOLOGY

3.1 Description and local meteorology of the Study Area

West Africa's climate is controlled by the interaction of two air masses; the maritime tropical air mass coming from the Atlantic Ocean and the continental tropical air mass originating from the Sahara Desert, the influence which varies throughout the year with the north-south movement of the Intertropical Discontinuity (ITD). Hot, dry continental air masses originating from the high-pressure system above the Sahara Desert give rise to dusty harmattan winds over most of West Africa from November to February. In summer, moist equatorial air masses originating over the Atlantic Ocean bring annual monsoon rains (Nicholson, 2013).

As a result of these interacting air masses, West Africa's precipitation regime is characterized by latitudinal belts of decreasing rainfall and wet season length. At the Gulf of Guinea, precipitation is abundant year-round without a marked dry season. At higher latitudes, precipitation decreases and is limited to a wet season of decreasing duration. This latitudinal pattern is somewhat modified by altitude, with higher mountain elevations, e.g. the Guinean Highlands and the Jos Plateau in central Nigeria, receiving more precipitation than lowlands of the same latitude. Along the south–north gradient of decreasing rainfall, Abidjan, Côte d'Ivoire (5° north latitude) records a mean annual rainfall of 1,600 mm; Ouagadougou, Burkina Faso (12° northern latitude) 700 mm within a 5-month rainy season; and Agadez, Niger (18° northern latitude) 165 mm annually in a short 2.5-month rainy season. Temperatures in the lowlands of West Africa are high throughout the year, with annual means usually above 18°C. In the Sahel, maximum temperatures can reach above 40°C. (eros.usgs.gov).

Figure 3.1: Study area showing the four major climatic zones according to USGS, 2017

3.2 Data and Model Description

Land-use and aerosol data sources includes derivation of MODIS land-use and aerosol data, MISR aerosol product data and ground-based AERONET observations for model performance evaluation in simulating aerosol properties and land-use changes over West Africa. Reanalysis climate data which will be used is the National Center for Environmental Prediction/Department of Energy (NCEP/DOE) Atmospheric Model Intercomparison Project (AMIP)-II reanalysis, hereafter referred to as NCEP-2 (Kanamitsu et al. 2002), for the period 2001–2006. Note that the observation minus reality (OMR) method proposed by Kalnay and Cai (2003) is based on the assumption that surface observations are not being used in the reanalysis; therefore, not all reanalysis datasets are suitable for this method. NCEP-2 is designed to improve the NCEP/NCAR reanalysis, which is used in Kalnay and Cai (2003), by fixing the errors and by updating the parameterizations of the physical processes. NCEP-2 is believed to more accurately characterize soil moisture, clouds, and near-surface temperature over land (Kanamitsu et al. 2002) than NCEP/NCAR reanalysis, and has been used to estimate the urbanization effect in South China (Zhou et al. 2004). Data to be used from NCEP-2 include the monthly Tmax and Tmin at 2 m, monthly downward solar radiation flux at the surface (hereafter referred to as downward SSR), monthly precipitation and monthly total cloud cover at entire atmosphere considered as a single layer. They are all Gaussian grids with 192 × 94 grid points.

3.2.1 Model Description and Configuration

The fourth generation of the Abdus Salam International Centre for Theoretical Physics (ICTP) regional climate model (RegCM4) (Giorgi et al., 2012) has been used in this study. The RegCM's dynamical core is based on the hydrostatic version of the mesoscale model MM5 of National Center for Atmospheric Research (NCAR) and Pennsylvania State University (Grell et al. 1994). Radiative transfer in RegCM is based on the parameterization of NCAR's

community climate model CCM3 (Kiehl et al. 1996). RegCM consists of the biosphere–atmosphere transfer scheme (BATS; Dickinson et al. 1993) with supplementary amendments to take account sub grid variability of topography and land cover using mosaic-type approach (Giorgi et al., 2003) and community land model (CLM) (Steiner et al., 2009) as land surface packages. This study CLM version 4.5 (Oleson et al., 2013) as land-surface scheme (LSS) and both the available PBL schemes of Holtslag et al. (1990) and that of the University of Washington (UW) (Grenier and Bretherton 2001; Bretherton et al. 2004; O'Brien et al. 2012) for the sensitivity analysis. RegCM 4.4 includes several options for cumulus convection: Grell (1993), the Massachusetts Institute of Technology (MIT) scheme (Emanuel 1991; Emanuel and Rothman 1999), Tiedtke scheme (Tiedtke 1989), Kain and Fritsch scheme (Kain and Fritsch 1993) and there is also possibility of using different convective schemes over ocean and continent in the same simulation which is referred to as "mixed convection". The convection is triggered for Grell scheme when the lifted air parcel attains moist convection. The current study follows Fritsch-Chappell (FC) closure (Fritsch and Chappell 1980) for the Grell scheme where available buoyant energy is released within a specified period. In the Emanuel scheme where the mixing in clouds is highly inhomogeneous and episodic, convection triggers when the level of neutral buoyancy is higher than cloud-based level. Air lifts between these two levels and a fraction of the condensed moisture forms precipitation. Whereas the rest forms cloud that mix with the environment, of which the mixing entrainment and detrainment rate are proportional to vertical gradients of buoyancy in clouds. Tiedtke convective scheme is a mass flux convection scheme in which the closure assumptions for shallow convection are maintained by the supply of moisture from surface evaporation. Whereas, penetrative and mid-level convection is determined by large-scale moist convergence. Kain and Fritsch scheme is a revised version of Fritsch-Chappell scheme (Fritsch and Chappell 1980) with modifications in detrainment effect and cloud model. The main

components of Kain and Fritsch are a trigger function, moist convective updraft, moist convective downdraft, compensating circulation and a closure assumption. Convection triggers when Lifting Condensation Level (LCL) temperature of the ascending parcel exceeds the environmental LCL temperature.

The closure assumption of Kain and Frisch scheme is the same as that of Fritsch-Chappell scheme (1980): to reduce convective available potential energy (CAPE) over a specific timescale. For obtaining the best parameterization schemes: cumulus convective precipitation, PBL and land surface, we have conducted 5 sensitivity simulations as explained in Table 3.1. Five sensitivity simulations (TDK, GR, EM, KU, and K-F) were conducted with all the five available cumulus convective precipitation schemes using UW PBL scheme and coupling RegCM with CLM4.5 to test for the best convective scheme in simulating the aerosol radiative effects. PBL scheme Holstag sensitivity under CLM4.5 is investigated using Tiedtke cumulus convective precipitation scheme. Three observational datasets are used to evaluate the model precipitation and temperature: the, Tropical Rainfall Measuring Mission (TRMM; Huffman et al. 2007), National Center for Environmental Prediction/Department of Energy (NCEP/DOE; Kanamitsu et al. 2002) and Copernicus Atmosphere Monitoring Service (CAMS; Granier et al., 2011; Inness et al., 2019).

As mentioned previously, the aim on this study is to investigate how and to what extent land-use changes and varying aerosol loadings and their interactions have been affecting climate of West Africa. For the purpose of the study, the model simulates radiative properties of aerosols from November 2005 to April 2006 (plus 1 month spin-up period) which covered the transition in aerosol mixture between “dust + carbonaceous” aerosols and “pure dust” aerosols cases. This particular period was chosen because of the data available from the African Monsoon Multidisciplinary analysis, Special Observing Period - Dust and Biomass Burning Experiment

(AMMA SOP-DABEX) campaign (Haywood et al., 2008) that help to constrain and evaluate the aerosol parameterization in RegCM4, especially concerning black carbon particle

Table 3.1: Different RegCM4.7.1 model sensitivity simulation description.

Simulation	Convective Scheme	Land Surface Model	Boundary Layer Scheme	Significance
EM	Emanuel 1991	CLM4.5	UW-PBL	Climate evolution using Emanuel precipitation scheme
GR	Grell	CLM4.5	UW-PBL	Climate evolution using Grell precipitation scheme
B-M	Betts – Miller 1986	DOES NOT WORK!		
K-F	Kain and Fritsch 1990, 2004	CLM4.5	UW-PBL	Climate evolution using Kain and Fritsch precipitation scheme
KU	Kuo	CLM4.5	UW-PBL	
MM5	MM5 Shallow Cumulus	DOES NOT WORK!		No precipitation but only mixing
TDK	Tiedtke 1996	CLM4.5	UW-PBL	Climate evolution using Tiedtke precipitation scheme

Table 3.2: Comparison of BATS and CLM4.5 land-surface schemes configuration in RegCM4 Model.

Parameters	BATS	CLM4.5
Land use Parameters	20(GLCC)	5 land units, 17 vegetation types
Soil texture	FAO soil world map	IGP soil dataset
Soil freezing	Yes	Super cooled soil water model
Number of soil layers	3	10
Surface datasets	Leaf area index	MODIS products
Number of snow layers	1	5
Soil temperature calculation	Force-restore method	Head diffusion equation

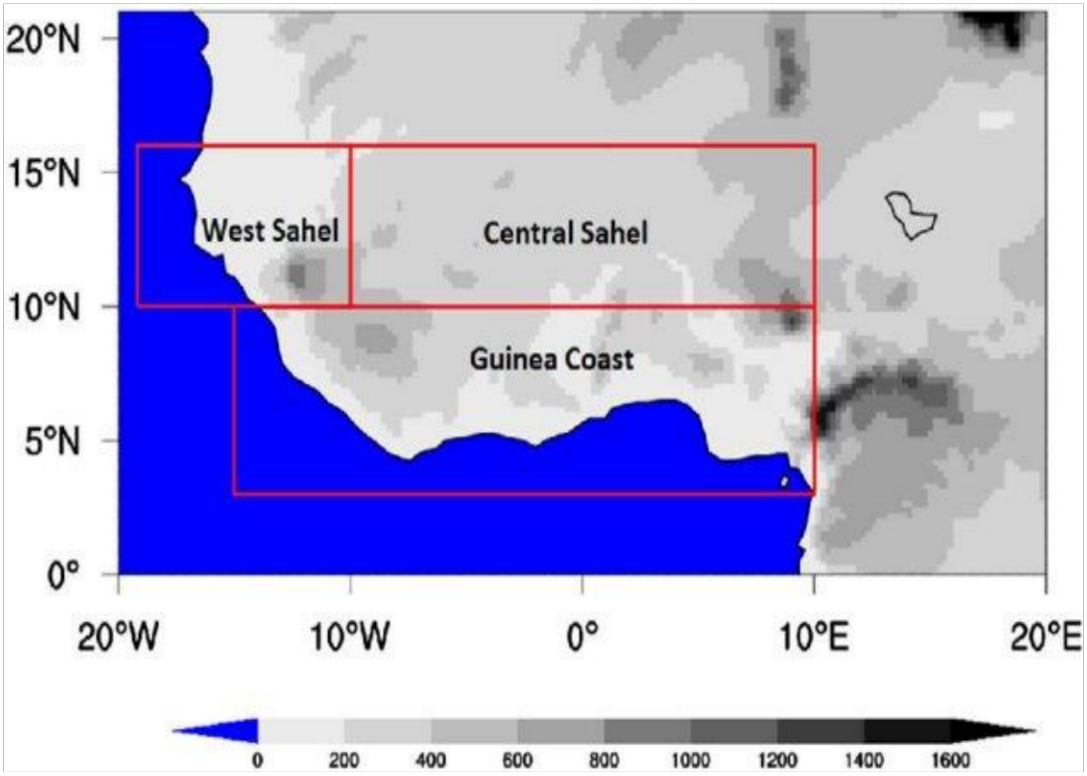

Figure 3.2: Topography (m) of simulation domain, with the entire West African domain.

The model ran over the West African region, on 23 hydrostatic sigma levels in the vertical, and at 45 km horizontal resolution. The simulation domain in this study spanned from longitude 20W to 20E and latitude 05S to 21N. The horizontal grid resolution is 25 × 25 km about 0.23˚ × 0.23˚ (Figure 3.2). We have 174 grid points (lon.) and 114 (lat.) and the vertical grids are composed of 18 sigma (σ) levels stretching from near the surface to the model top (10 hPa). The simulations are initialized and forced every six hours, by the ERA-Interim reanalysis with a grid spacing of 1.5˚ × 1.5. Sea-air temperatures (SSTs) were acquired from NOAA optimal interpolation weekly SST data resolution. In order to maintain the model computational stability, an integration time step of 60 seconds was used. Each simulation (CLM) starts from 01 September 2001 to 31 November 2006. The results from the first 03 months were discarded as the model spin up.

RegCM4 predecessor (CCM2) accounted for the effects of H_2O, O_3, O_2, and CO_2. The CCM3 is structured in the same way that it includes new features such as the effect of additional greenhouse gases (NO2, CH4, and CFCs), atmospheric aerosols, and cloud ice. The solar radiation scheme of the RegCM4 employs the delta-Eddington approximation for radiative flux calculations, and the wavelength spectrum is divided into 18 discrete intervals from 0.2 to 4.5 μm (Kiehl et al., 1996). Seven of these span the ultraviolet (0.2 to 0.35 μm), one covers the visible (0.35 to 0.7 μm) while the remaining bands cover the infrared or special absorption windows. The radiative transfer calculations were fully coupled with an aerosol scheme [Solmon et al., 2007] to perform the simulation, including aerosol radiative effects in order to study the feedbacks on atmospheric dynamics.

3.2.2 Radiative Transfer Model

The Copernicus Atmosphere Monitoring Service (CAMS) makes available a worldwide reanalysis dataset of atmospheric composition that includes aerosol properties. This dataset focuses on the composition of the atmosphere (Inness et al., 2019). This dataset allows for

explicit radiative transfer modelling as a result of the comprehensive coverage both spatially and temporally, as well as the availability of all variables that are required. The optical properties of the aerosol are profoundly affected by the aerosol mixture, which is reflected in the underlying aerosol model of the CAMS RA as a collection of seven distinct aerosol types. In comparison to free-running models, the radiative forcing estimations provided by this reanalysis, which integrates atmospheric composition variables derived from satellite, are more accurate. The improvements are directly derived from the observational limitations placed on reactive gas columns, aerosol optical depths, and vertical profiles in the case of ozone. In addition, data integration imposes limits on emissions of gaseous and biomass-burning aerosols, which leads to improvements in the simulation of atmospheric concentrations that are indirect in nature (Agusti et al., 2016, Inness et al., 2019). As a result, the process that produces radiative forcing places the utmost importance on variables that have been enhanced by the integration of data. However, it is not possible to rely solely on integrated variables because other aspects of the model affect radiative forcing either directly or indirectly. This means that it is not possible to rely solely on assimilated variables. Aside from that, auxiliary datasets provide information on characteristics like aerosol size distributions that are necessary for the radiative forcing calculation but aren't simulated by the global reanalysis.

Aerosol direct forcing can be estimated only from observations, and these estimates have been done, although it has been done mostly via a radiation model. For example, the SBDART is a radiative model developed by the atmospheric science community that has been widely used for radiative transfer calculations over various environments by a number of authors such as Srivastava et al. (2013), Kang et al. (2016), Yu et al. (2016), Patel et al. (2017), and Vachaspati et al. (2018). Input variables such as AOD (aerosol optical depth, SSA (single scattering albedo), AE (angstrom exponent) and ASY (asymmetry factor are employed in all radiation models used to estimate aerosol direct forcing. The radiative transfer equations are numerically

modified and integrated with this module using the Discrete Ordinate Radiative Transfer (DISORT) model, which was developed for a vertically inhomogeneous, non-isothermal, plane-parallel atmosphere. Aerosol direct radiative effects have been estimated using the input variables obtained from Copernicus ECMWF CAMS Reanalysis datasets. The net radiation is computed by;

$$\Delta f = f_{\downarrow} - f_{\uparrow} \tag{3.1}$$

where net radiation upward fluxes $f_{\uparrow}$ and downward fluxes $f_{\downarrow}$. The forcing at the TOA can be computed from the difference between the TOA and the surface net radiation. If the result is positive, it indicates atmospheric heating and atmospheric cooling when it's negative (Boiyo et al., 2019; Witthuhn et al., 2021).

$$\Delta f_{toa} = \left(f^{a}{}_{toa\downarrow} - f^{a}{}_{toa\uparrow}\right) - \left(f^{o}{}_{toa\downarrow} - f^{0}{}_{toa\uparrow}\right) \tag{3.2}$$

$$\Delta f_{sfc} = \left(f^{a}{}_{sfc\downarrow} - f^{a}{}_{sfc\uparrow}\right) - \left(f^{o}{}_{sfc\downarrow} - f^{0}{}_{sfc\uparrow}\right) \tag{3.3}$$

where the ↑ calculates the upward fluxes and ↓ calculates the downward fluxes under a generally clear sky condition. Ricchiazzi et al., 2008, reported additional information about the model, its components, and sensitivity.

3.2.3 Land-Use Changes Model Description

The Community Land Model is the land model for the Community Earth System Model (CESM). It examines the physical, chemical, and biological processes by which terrestrial ecosystems affect and are affected by climate across a variety of spatial and temporal scales. The central theme is that terrestrial ecosystems, through their cycling of energy, water, chemical elements, and trace gases, are important determinants of climate. The Model components consist of: bio geophysics, hydrologic cycle, biogeochemistry and dynamic vegetation. For this research, the land surface will be represented by 4 primary sub-grid land cover types (bare-surface, water body, urban, vegetated) in each grid cell (Lawrence et al., 2012). The vegetated portion of a grid cell will further be divided into patches of plant

functional types, each with its own leaf and stem area index and canopy height. Simulations for RegCM4 will be conducted with CLM4.5 at 2^{o} resolution, and include an interactive Carbon and Nitrogen cycle (CN) and an interactive crop model (CROP). A transient land cover and land use change, including wood harvest, capability was introduced to enable the evaluation of the impact of historic and future land use change (Heald et al. 2008).

3.2.4 Remote Sensing Data

Five distinct land cover classification schemes that were obtained using a supervised decision-tree classification algorithm are included in the MODIS Terra and Aqua Combined Land Cover product. The primary land cover scheme identifies 17 IGBP classes, comprising 11 classes of natural vegetation, 3 classes of human-altered vegetation, and 3 classes of non-vegetated land. The seasonal cycles are marked by layers in the Land Cover Dynamics product that detail the timing of vegetation development, maturity, and senescence. The product can capture two growth cycles if necessary by providing estimates of vegetation phenology twice a year from the two 12-month focal periods, July-June and January-December (Friedl et al., 2010). This takes into account hemisphere differences in the growing seasons. MODIS Land Cover Type product was created annually since 2001. Five land cover schemes, created by several research groups, are available for each year. The USGS provides data in standard MODIS grid tiles at a resolution of 500m. These tiles are 10 degrees by 10 degrees at the equator and cover an area of about 1200 by 1200 km using the sinusoidal projection.

The MODIS Terra and Aqua Combined Land Cover product includes a total of five different land cover classification schemes. These land cover classification schemes were generated through the use of a supervised classification algorithm. The major land cover scheme identifies a total of 17 IGBP classifications, 11 of which are classified as natural vegetation, 3 of which are classified as human-altered vegetation, and 3 of which are classified as non-vegetated land. In the land cover dynamics product, the seasonal cycles are denoted by layers

that provide specific information regarding the times of vegetation development, maturity, and senescence. Estimates of the phenology of the vegetation are provided twice a year by the product, based on the two 12-month focal periods of July–June and January–December by allowing the product to capture two growth cycles (Friedl et al., 2010). This takes into account the different planting seasons in hemisphere differences. Since 2001, a new iteration of the MODIS Land Cover Type product has been consistently developed each year. Every year, five different land cover patterns were developed by a number of different research teams. At a resolution of 500 meters, the United States Geological Survey (USGS) supplies data in the form of standard MODIS grid tiles. Using the sinusoidal projection, these tiles cover an area of approximately 1,200 by 1,200 kilometres and have a latitude and longitude of 10 by 10 degrees, respectively, at the equator.

A large variety of remotely sensed environmental data, including albedo, leaf area index (LAI), LST, emissivity, air temperature, ET, land cover, and surface incoming shortwave radiation (SIS). All the data covered the period between 2001 and 2006. For consistent spatial analysis, all products were compared at 1 km spatial resolution. The products with 500m resolution (LAI and land cover) were aggregated to 1 km to match the resolution of the other products. In aggregating land cover data, the dominant land cover type was assigned for each pixel (i.e., at least three out of the four 500mpixels should belong to the same class, otherwise were removed from the analysis). Air temperature and SIS data were resampled to 1 km resolution using bilinear interpolation. A summary of the data used in this study is presented in Table 1.

Shortwave broadband black sky albedo (SBSA) (0.3-5.0μm) at local solar noon was obtained from the MODIS collection 6 MCD43B3 product, at 1 km spatial resolution (NASA LP DAAC, 2016b). I chose black-sky albedo for this study since it represents albedo at local noon and is consistent in time with empirical model used in this study (e.g. Eq. (3.7)). Furthermore, black-sky, white-sky, and blue-sky albedo are so strongly correlated in the region that the

selection of albedo type does not affect the results (Li et al., 2015). LAI was obtained from the MODIS MCD15A2H product at 500m resolution, prepared from atmospherically corrected surface reflectance (MOD09) and the revised multiyear land cover product (MCD12Q1) (Myneni et al., 2015). I used the quality flags provided with the product to select only the best quality retrievals based on the main radiative transfer method without saturation (Yang et al., 2006).

The product used for LST was the MOD11A2, which provides 8-day average radiometric temperature for clear-sky conditions at 1 km resolution (Wan et al., 2015). To ensure the use of only high-quality and cloud-free pixels, we used quality assessment flags to filter valid LST pixels using quality control flag bits with a value of zero. Previous studies indicate that this product has an accuracy better than 1^{o}K over vegetation, soil, and lakes (Wan et al., 2015). Estimates of ET were obtained from the MOD16A2 gap-filled product at 1 km resolution (Running et al., 2017). This product is based on the Penman-Monteith equation, daily meteorological data (air temperature, surface downward solar radiation, vapour pressure deficit, wind speed, and relative humidity), and MODIS 8-day albedo, LAI, and land cover data. It has a mean absolute error of around 0.3 mm/day when compared with eddy flux towers (Running et al., 2017). Land cover was mapped using the collection 051MCD12Q1 product at 500m resolution (NASA LP DAAC, 2016a). The product has an overall accuracy of around 75% (Friedl et al., 2010). I used the International Geosphere-Biosphere Programme (IGBP) type 1 classification schemes in the study.

To identify land cover changes, stable land cover maps representing initial and final conditions were prepared using the MODIS 2001-2006 product. Only pixels in which land cover was stable for at least three years were used, while pixels below this threshold were removed. To know the impact of land cover changes on albedo, I compared the average albedo of the first and year, for each land cover change pixel, respectively. Then, the impact of shortwave albedo

change on the surface radiation was estimated from instantaneous shortwave surface radiative forcing (ISRF) using Eq. (3.4):

$$ISRF = -SW_{in} \times (\alpha_f - \alpha_i) \quad (3.4)$$

where SW_{in} is incoming shortwave radiation, and α_i and α_f are albedo before and after the change, respectively. The regional instantaneous shortwave surface radiative forcing (RISRF) was estimated from the individual land cover change contributions using Eq. (3.5) (Bright, 2015; Jin & Roy, 2005):

$$RISRF = \sum_{I=1}^{7} \left(ISRF_i \times \frac{A_i}{A_t} \right) \quad (3.5)$$

where $ISRF_i$ is the instantaneous shortwave surface radiative forcing for land cover change i; *Ai* is the land surface area covered by land cover change i; *At* is the total land surface area of the study region ~5,112,903 km^2; i (land cover change codes) =1-7: grassland to shrubland=1; shrubland to grassland=2; savanna to mixed=3; grassland to savanna=4; savanna to cropland=5; savanna to grassland= 6; forest to cropland=7.

For estimating the contribution of radiative mechanisms to LST shift due to albedo changes associated with land cover change, we used an analytical expression based on the energy balance approach initially proposed by Lee et al. (2011):

$$\Delta T_s = \frac{\Delta_0 \times \Delta S}{(1+f)} + \frac{(-\lambda_0) \times R_n \times \Delta f}{(1+f)^2} \quad (3.6)$$

where ΔT_s is the calculated surface temperature change; ΔS is the net shortwave radiation change; f is the monthly mean energy redistribution factor; Δf is the change in energy redistribution due to land cover change; R_n is the monthly mean net radiation; λ_0 is the 2001-2006 monthly mean temperature sensitivity from the longwave radiation feedback (K $(W/m^2)^{-1}$).

The first term on the right-hand side of Eq. (3.6) represents the temperature change due to the radiative mechanism and the second term shows the remaining impact from the non-radiative mechanisms (evapotranspiration and surface roughness). The λ_0 was computed using Eq. (3.7).

$$\lambda_0 = \frac{1}{4 \times e_s \times \sigma \times T_s^3} \quad (3.7)$$

e_s and T_s are 2001-2006 monthly mean surface emissivity and surface temperature (K), respectively; σ is the Stefan-Boltzmann constant (W/m^2 K^{-4}).

The energy redistribution factor (f) was estimated using Eq. (3.8) (Lee et al., 2011) from surface and air temperature, net radiation, and ground heat flux (G):

$$f = \frac{\lambda_0}{T_s - T_a}(R_n^* - G) - 1 \quad (3.8)$$

where $R_n^* \approx R_n$ is the apparent net radiation. G was estimated by multiplying the ratio of G and net radiation (R_n) by Rn. The G/R_n ratio was estimated using an empirical equation by Bastiaanssen (2000), which represents values near local noon:

$$\frac{G}{R_n} = (T_s - 273.15)(0.0038 + 0.0074 \times \alpha)(1 - 0.98 \times NDVI^4 \quad (3.9)$$

The SBSA (α) used in this equation represents albedo at local noon and thus is consistent in time with the model. NDVI is the normalized difference vegetation index, which was calculated using surface reflectance imagery obtained from the MODIS albedo model parameter product (MCD43B1), using the following formula: NDVI = (NIR-R) / (NIR+R), where NIR is the near infrared reflectance and R is the red reflectance. All surface reflectance values were corrected for the sun-sensor geometry (by fixing the view angle at the nadir and the sun angle at 45°) to avoid non-vegetation signals from bidirectional reflectance distribution function (BRDF) effects. Rn was estimated using Eq. (10) (Cleugh et al., 2007):

$$R_n = SW_{in}(1 - \alpha) + \sigma \times (e_a - e_s) \times T_\alpha^4 \quad (3.10)$$

$$e_a = 1 - 0.261 \times exp(-7.77 \times 10^{-4} \times T_a^2) \quad (3.11)$$

where e_a is air emissivity; T_a is air temperature. In estimating net radiation, we estimated surface emissivity (e_s) from averages of MODIS band 29 (8.40-8.70μm, in the broadband region), 31 (10.78-11.28μm), and 32 (11.70-12.27μm), instead of the average of the emissivities in bands 31 and 32, as doing so could overestimate emissivities in arid and semi-arid regions (Wan et al., 2002). We used the MOD11B3 product, which contains monthly emissivity in band 29 at 6 km resolution, and resampled it to 1 km resolution to match resolutions of bands 31 and 32.

CHAPTER FOUR

4.0 RESULTS AND DISCUSSION

4.1 Quantification of Aerosol Radiative Properties

The single scattering albedo, asymmetry factor, angstrom exponent and aerosol optical depth are the critical parameters crucial in the estimation of aerosol radiative forcing as shown in Figures 4.1, 4.2 and 4.3. Significant variation in the daily average of the aerosol optical depth during DJF in 2005-2006 can also lead to large variations in the asymmetry factor and single scattering albedo. The SSA and AF were at their lowest in the early days of February due to the high concentration of absorbing dust aerosols and large AOD values. The AOD of each aerosol layer (dust and biomass burning aerosol) had a strong influence on the radiative budget, according to sensitivity analyses (Raut and Chazette, 2008, Granier et al., 2011). Minimum SSA and AF were also observed in January when non-dust particles were observed over West Africa. Accordingly, Raut and Chazette, 2008 reported that the biomass-burning layer's single-scattering albedo values can range from 0.78 to 0.82 while the dust plume's values can also range from 0.9 to 0.92, likewise, asymmetry parameters in mineral dust layers can be from 0.73 to 0.75 and in biomass-burning layers from 0.71 to 0.73.

Single scattering albedo is a very crucial aerosol radiative property as the forcing at the top of the atmosphere basically depends on the single scattering albedo. The reduction in SSA leads to positive forcing at the top of the atmosphere (Malavelle et al., 2011), but as the single scattering albedo increases, the forcing turns negative. Surface net radiation becomes lower with lower single scattering albedo. In order words, the forcing at the surface increases as the single scattering albedo increases. Sulfate, nitrate, and sea salt are known to have SSA values that are near 1.0. The brown carbon component of OM, which was formerly considered to be completely scattering (Stier et al., 2007; Arola et al., 2010), is now commonly acknowledged to include a large absorption component.

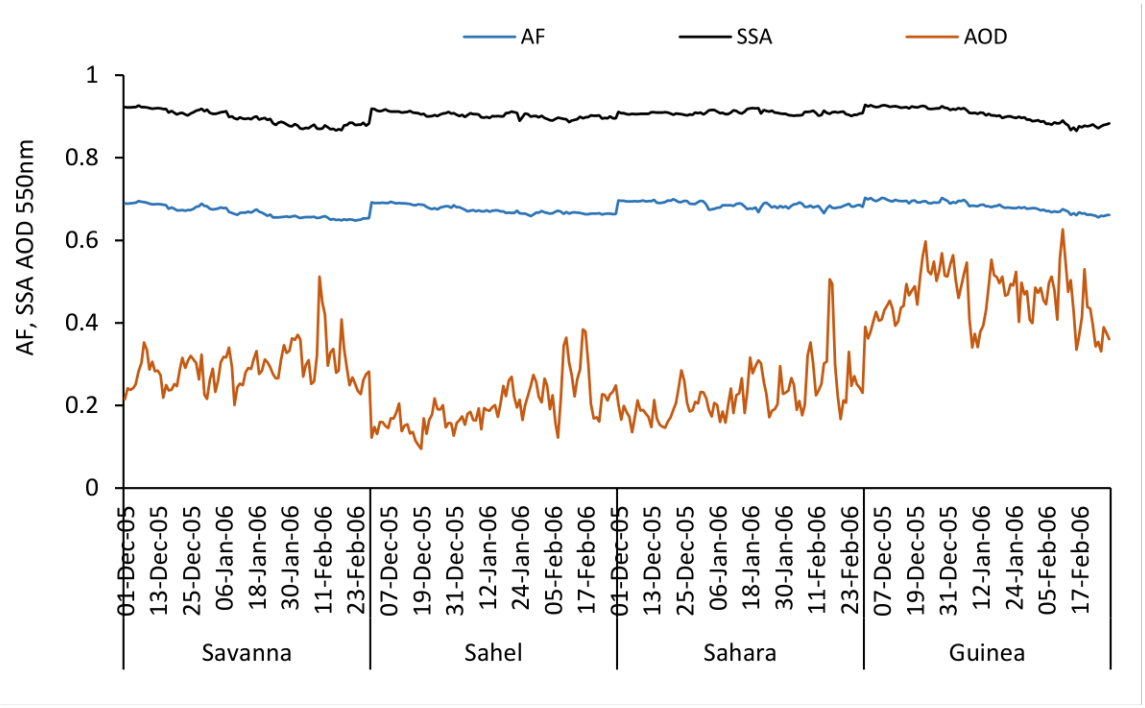

Figure 4.1: Time series of daily average asymmetry factor, single scattering albedo, and aerosol optical depth, all at 500nm (DJF, 2005-2006) over West Africa.

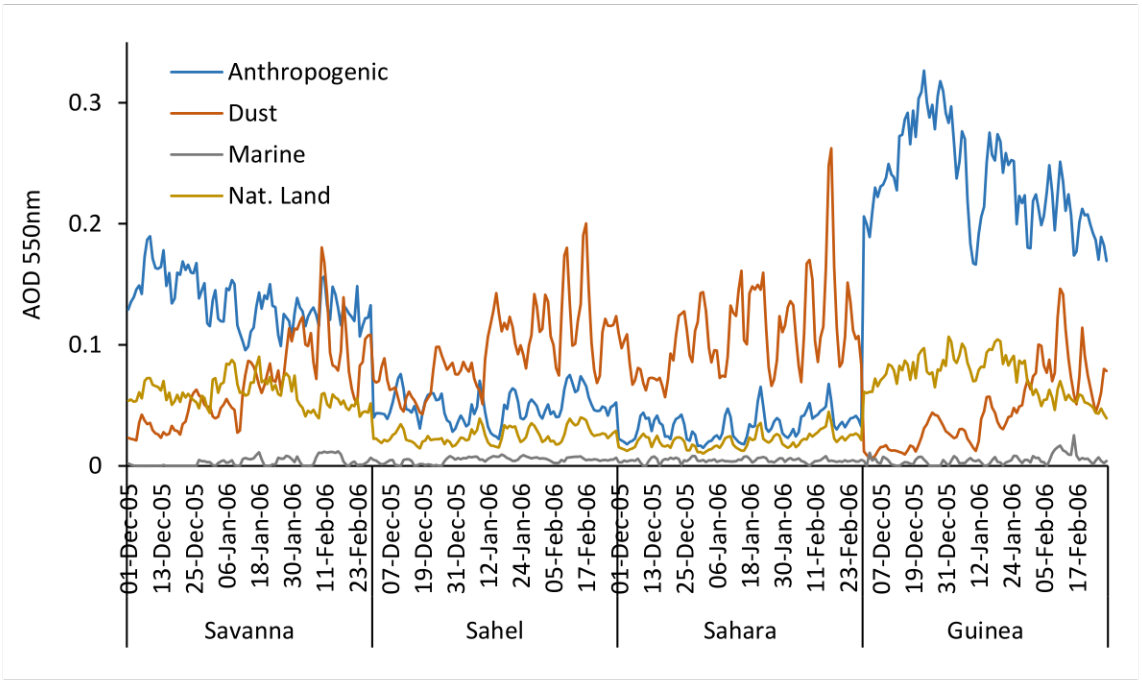

Figure 4.2: Time series of daily average anthropogenic, dust, sea-salt, and marine aerosols optical depth, at 500nm (DJF, 2005-2006) over West Africa

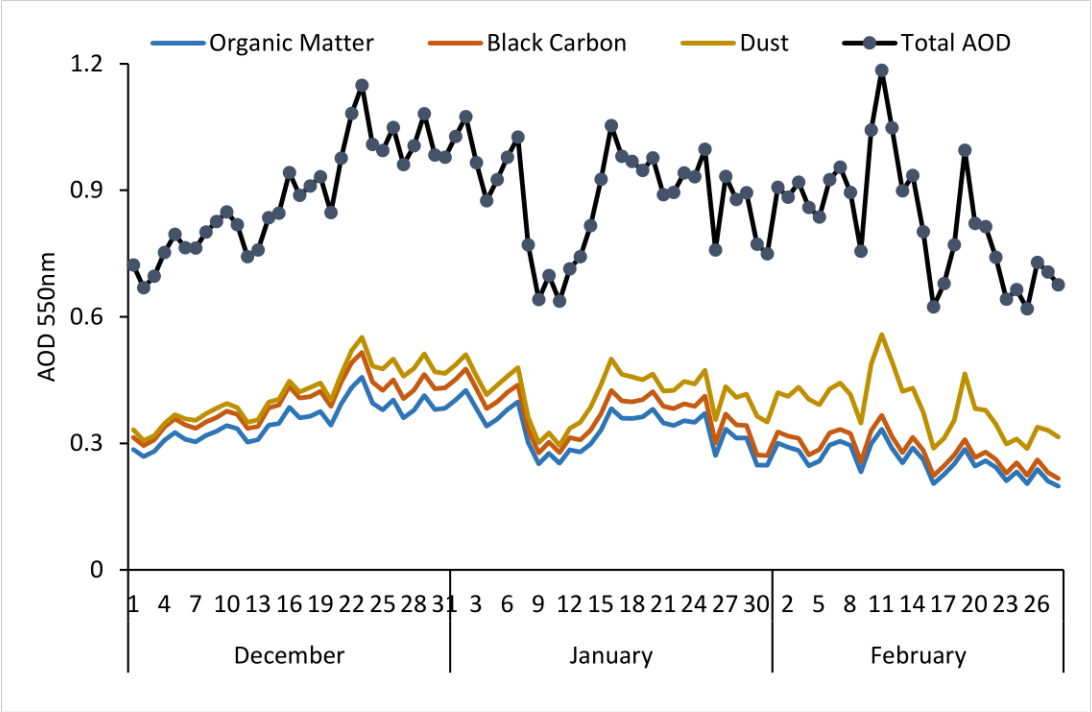

Figure 4.3: Daily variation of different types of aerosols optical depth in the Guinean climatic Zone

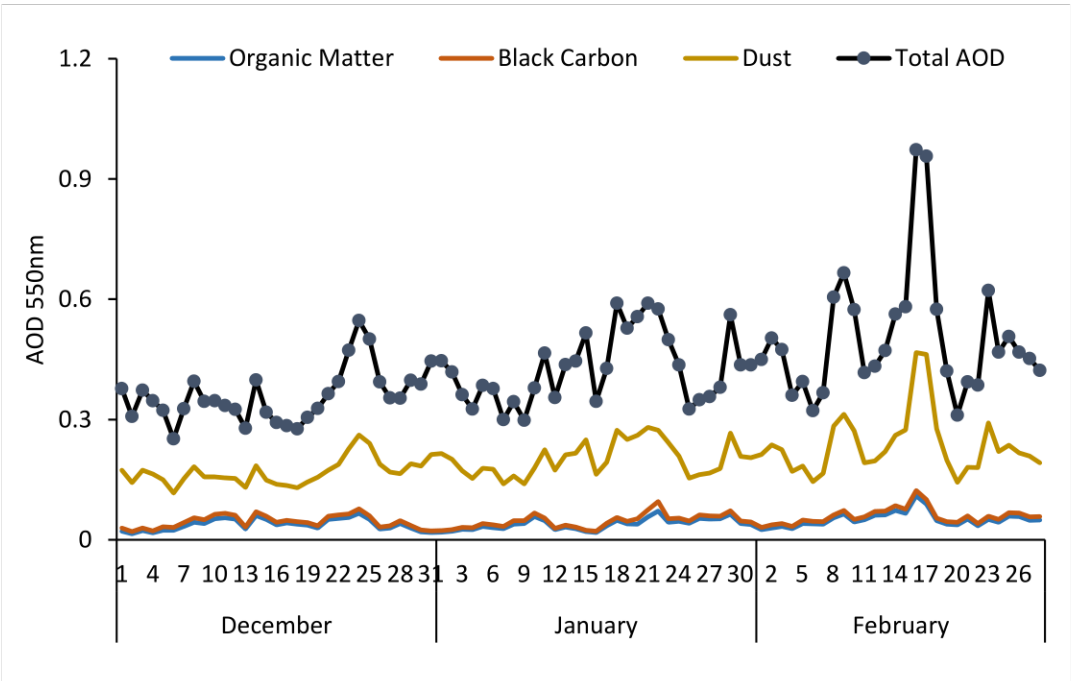

Figure 4.4: Daily variation of different types of aerosols optical depth in the Saharan climatic Zone

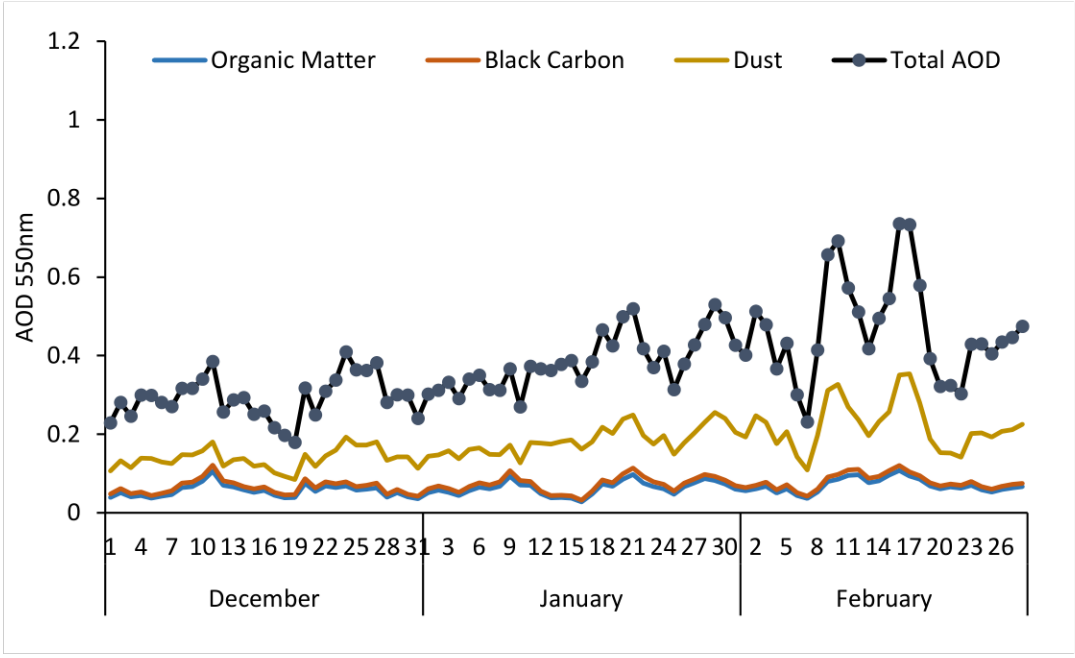

Figure 4.5: Daily variation of different types of aerosols optical depth in the Sahelian climatic Zone

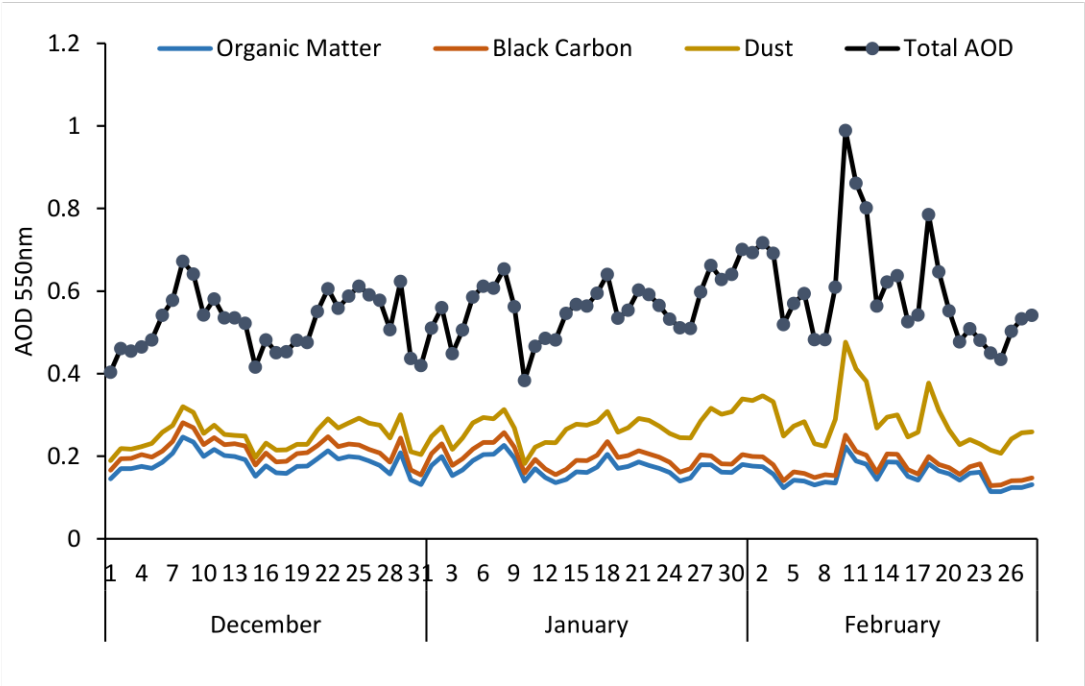

Figure 4.6: Daily variation of different types of aerosols optical depth in the Savanah climatic Zone

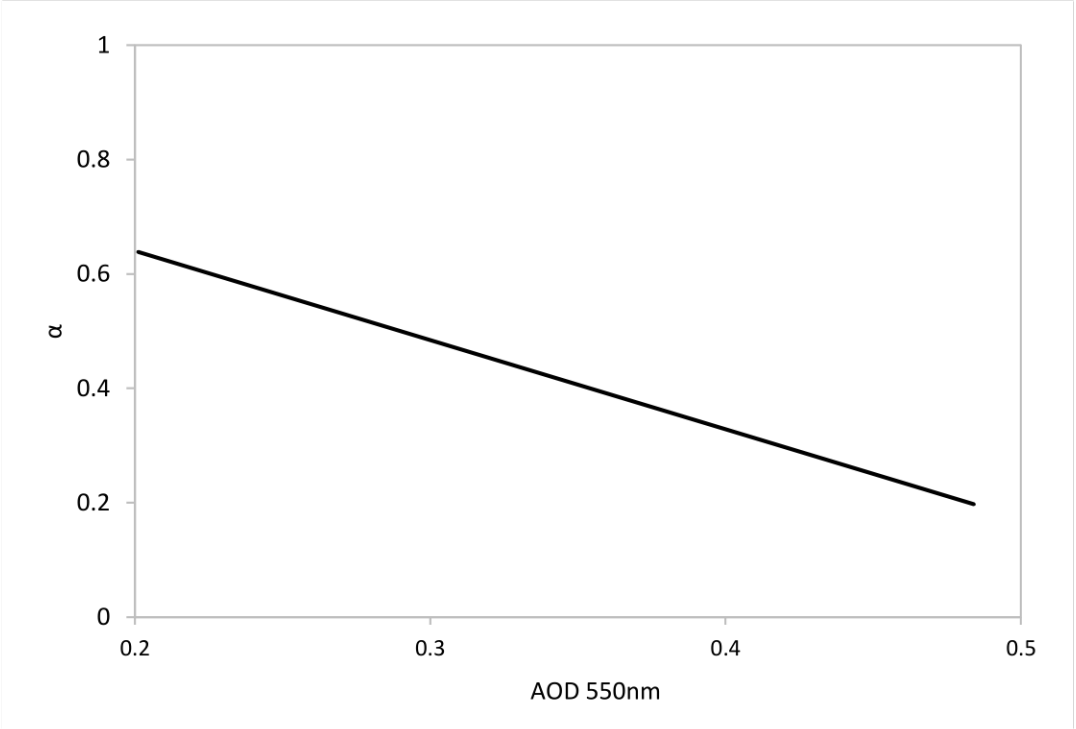

Figure 4.7: Scatter plot between daily average angstrom exponent α (340-870nm) and AOD (550nm)

The presence of these absorbing aerosols leads to the surface becoming cooler. Strongly absorbing aerosols have a warming effect only at the top of the atmosphere.

It can be observed that asymmetry doesn't effectively change the aerosol absorption in the atmosphere. Change in asymmetry does not change atmospheric aerosol absorption. Thus, no significant change in the forcing at the surface. The impact of the asymmetry factor on aerosol forcing at the top of the atmosphere is more than the impact it has on aerosol absorption within the atmosphere and at the surface. The intensification in the asymmetry factor leads to an increase in the aerosol forcing at the top of the atmosphere due to the ability of aerosols with a large asymmetry factor to scatter less radiation back to space. ASY is 0 when the forward scattering equals the backward scattering. As forward scattering surpasses backward scattering, ASY increases. The ASY is higher for larger particles. Monthly-mean aerosol ASY in the atmosphere have been to range from 0.6 to 0.82 (Holben et al., 2001).

It can be observed in Figure 4.7 that dust particles contributed substantially to the high radiative forcing observed in the early days of February 2006. This result correlates with the dust episode observation made during the AMMA-SOP campaign over West Africa in DJF, 2005-2006. During this period, the solar radiation was not able to penetrate the aerosol-loaded atmosphere, which means that the surface has little energy to reflect back to space as this increases the surface albedo.

Absorbing aerosols such as dust, black carbon, organic matter and sea salt, dominate the atmosphere of West Africa. These aerosols are intensified during the winter period leading to an increase in the aerosol optical depth and atmospheric absorption. Atmospheric absorption increases with increasing aerosol optical depth, while the positive aerosol forcing at the top of the atmosphere increases with a negatively increased surface net radiation. An increase in the aerosol optical depth warms the top of the atmosphere because the dominating aerosols are good absorbers of the heat from the sun and prevent the heat from escaping to the surface,

hence the cooling effect at the surface. AOD should double when aerosol mass quantity is doubled. However, unlike AOD, the aerosol mass amount does not immediately correlate with aerosol forcing. Furthermore, AOD, not aerosol mass quantity, can be inferred from satellite measurements. AOD is the most important factor in the interaction between aerosols and climate because of these combined factors (Eddy, 2012). This denotes that with increased optical depth, the radiation absorbed within the atmosphere likewise increases leading to a shrink in the radiation reaching the surface. This creates a cooling radiative effect at the surface experienced during this period irrespective of the surface albedo. (Eddy, 2012).

The atmospheric absorption dependent on the angstrom exponent shows a different pattern from the AOD (Figure 4.7). Lower angstrom exponent is a signal that aerosol extinction is more wavelength independent for larger particles. A decrease in the angstrom exponent shows a consistent increase in atmospheric absorption. This implies that more radiation is absorbed and the forcing at the top of the atmosphere declines with increased angstrom exponent of aerosols. Because low-level clouds effectively reflect solar radiation, the absorption of aerosols above low-level clouds is greater (Podgorny and Ramanathan, 2001). Surface net radiation also intensifies as the angstrom exponent becomes larger. Reduction in total aerosol extinction of solar radiation is associated with an increase in the angstrom exponent. A low angstrom value can be associated with a dominance of larger size aerosol particles and a high angstrom value can signify the domination of smaller size aerosol particles. Thus, less aerosol forcing can be linked to a large angstrom exponent.

The effect of anthropogenic and dust sources of aerosols over the West Africa domain cannot be overemphasized (Figure 4.8). There still exist a lot of uncertainties in the estimation of these sources of aerosols with their corresponding radiative effects globally, most especially over West Africa. The estimated surface and TOA shortwave radiative forcing are found to be negative in the pre-monsoon season (Patel et al., 2017).

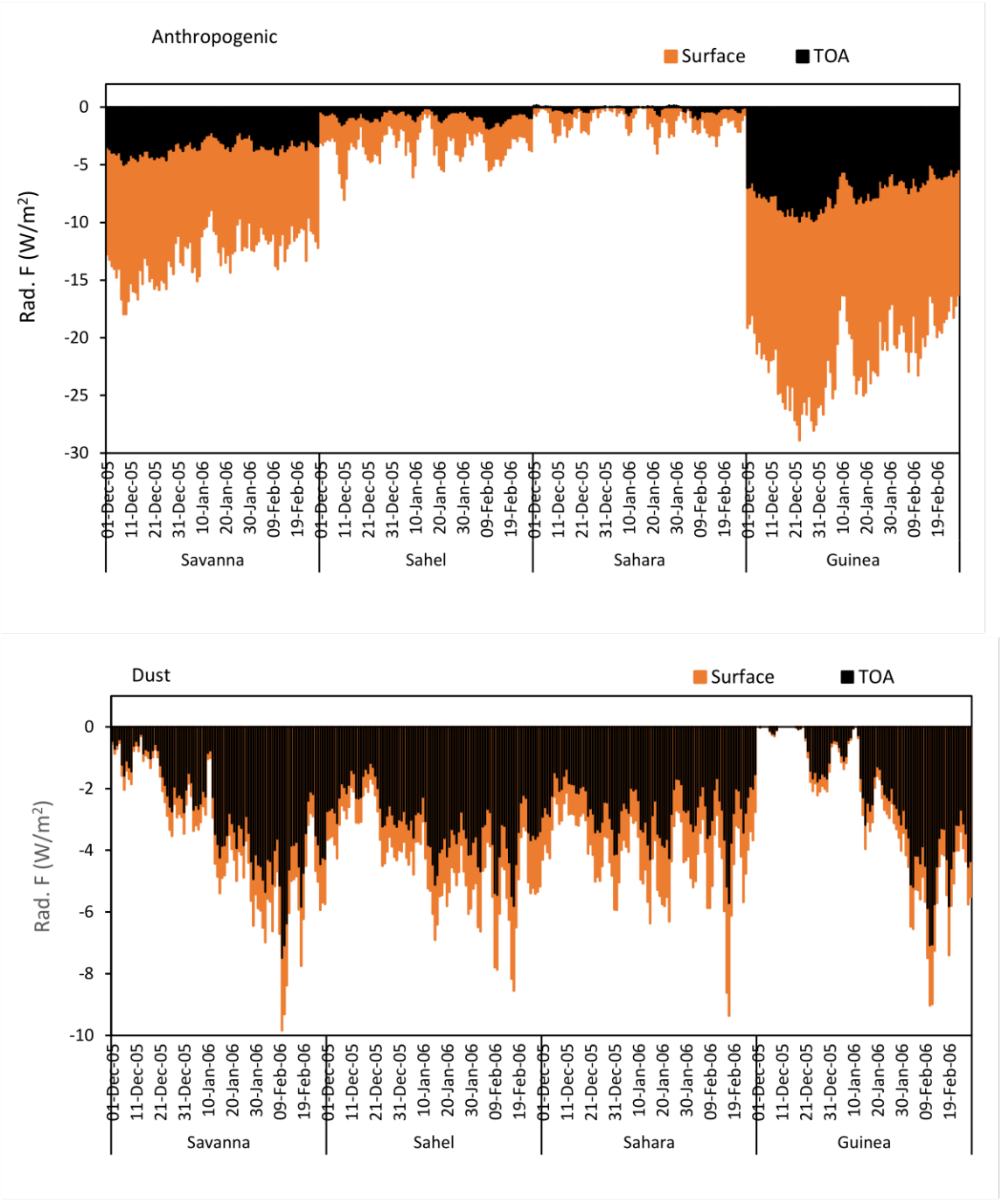

Figure 4.8: Daily average of Anthropogenic and Dust Aerosols Direct Effect (Clear Sky) at the Surface and Top of the Atmosphere.

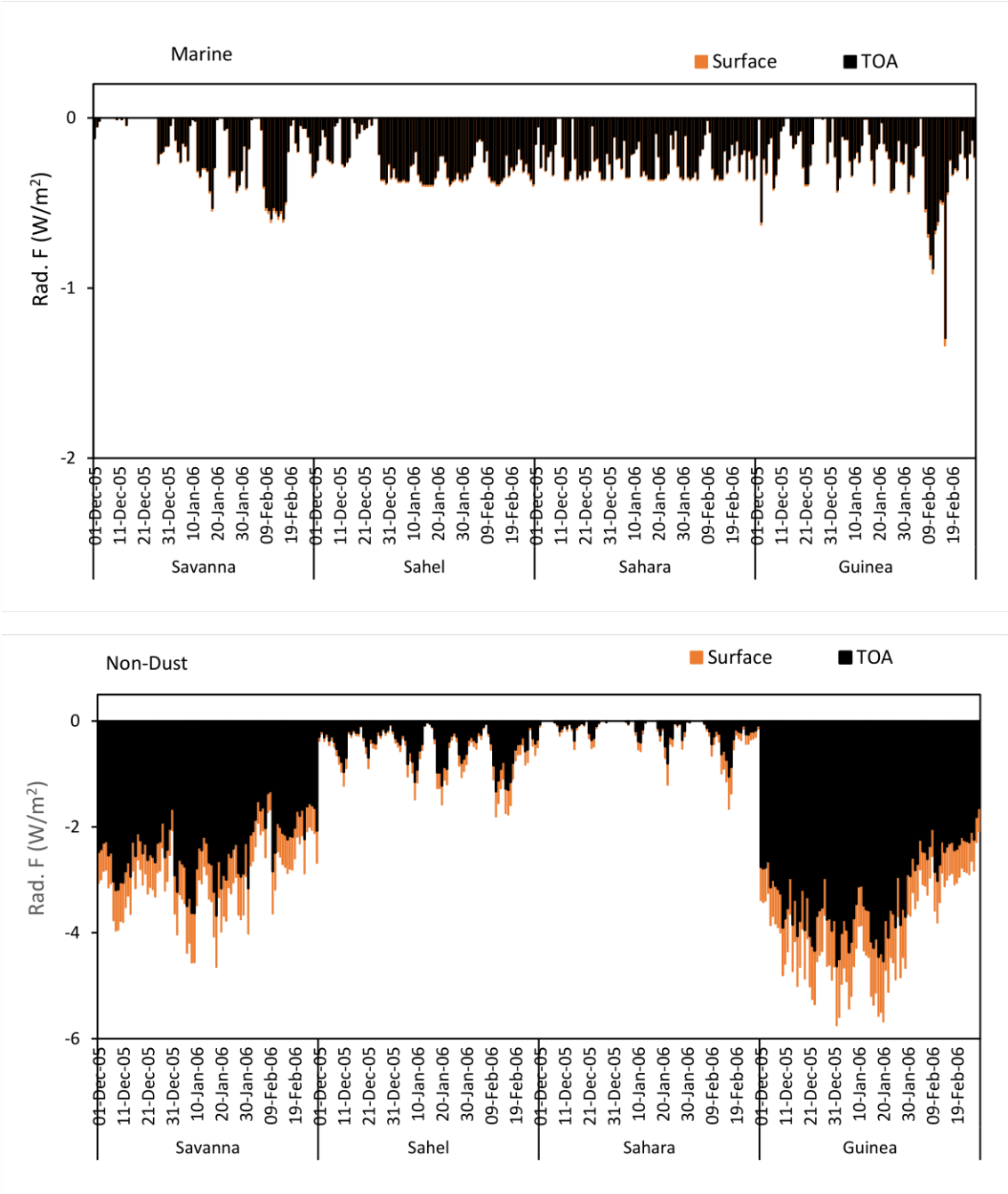

Figure 4.9: Daily average of Marine Aerosol and Non-Dust Direct Effect (Clear Sky) at the Surface and Top of the Atmosphere

Figure 4.8 shows the anthropogenic and dust aerosol radiative effect under clear sky conditions from December 2005 – February 2006 over different climatic zones in West Africa. Anthropogenic activities contribute to the low cooling effect observed in the Sahel and Sahara climatic zones while a higher cooling effect can be noted in the Savanah and Guinea zones. These findings show that maximum surface forcing occurs does not occur near aerosol emission sources. The prevailing north-easterly wind circulation transports aerosol particles, raising aerosol concentrations and AOD in neighbouring regions. This allows for the observed higher surface forcing. It can also be observed over West Africa that the radiative forcing at the top of the atmosphere is generally warmer compared to the surface. These can be connected to the strong presence of absorbing anthropogenic aerosols. Anthropogenic activities occurring in the Savanah and the Guinea zones lead to an increase in the cooling effect at the surface. Similar patterns can be noted in the forcing at the surface and the top of the atmosphere during this study period.

Direct radiative effect due to dust can be observed to be high over West Africa. The effect spreads across the four climatic zones which indicates the strong dominance of dust aerosols during the study period. Several works of literature have affirmed the role dust aerosol plays over West Africa in altering the radiative effect both at the surface and at the top of the atmosphere. These results corroborate with Liao and Seinfeld, 1998 who demonstrated that for pure dust, the TOA net forcing was more sensitive to variations in dust than surface cooling. It is noted in Figure 4.4 that the direct radiative effect of dust aerosol is exerted in all four climatic zones. The radiative forcing at the surface is weaker when there is an increased down-welling diffuse flux. The study period (December to January) is a period where dust prevails over other forms of aerosol in West Africa. There exists notable dust in the early days of February. This result is in line with the dust event captured by the AMMA-SOP campaign in 2006 (Raut and Chazette, 2008), where it was observed that the aerosol optical depth exponentially increased

due to this dust episode leading to a cooling radiative effect across the climatic zones. The deep occurrence observed in the Savanah and Guinea zones is associated with the prevailing dry and warm north-westerly winds propagation deepens southward, depositing dust along its routes of advection. It can also be attributed to the southward displacement of the Inter-tropical discontinuity (ITD).

Figure 4.9 shows the direct radiative effect of marine and non-dust aerosols under clear sky conditions over West Africa. Higher radiative is observed over the Guinea coast in the early days of February, most especially at the surface. This can be attributed to the more concentration of marine types of aerosols emitted from the ocean. The proximity of the Guinea coast to the ocean is another factor that enhances the mass concentration of sea-salt aerosols over the region with the addition of anthropogenic activities such as oil drilling occurring in the region. This anthropogenic activity can be considered to complement the already present sea-salt aerosols in the region, thereby increasing the cooling effect observed in the region. The Savannah region also demonstrates a similar pattern but with low radiative forcing when compared to the Guinea coast which can be attributed to the little amount of sea salt transported off the Guinea coast in the zone. Low radiative forcing was observed over the Sahel and Sahara as this implies that the marine type of aerosol (sea salt) does not have a significant radiative effect over these regions. Before sea salt is transported from the Guinea coast to the Sahel and Sahara, other dominant aerosols such as dust would have already gained momentum in altering the radiative transfer and imbalance over the region, hence, making sea salt so insignificantly effective. During the mobilization and transportation of dust particles over polluted areas, non-dust particles such as black carbon sulphate and organic matter, are often attached to dust. This effect can be observed in Figure 4.9 were a notable radiative effect of non-dust particles occurred in the Sahel and Sahara climatic zones. Non-dust aerosols likewise play a significant role in the alternation of solar radiation both at the top of the atmosphere and the surface. This

forcing effect can be significantly noticed in the Guinea coast region where notable emission of black carbon and organic matter is being emitted. The fraction of non-dust aerosols make up a significant percentage of the aerosol mixture in the summer, while they make up a lesser percentage of the aerosol mixture during winter (DJF). Due to the increased absorption, this would cause all through the year, these non-dust aerosols thereby created a significant cooling radiative forcing mechanism experienced in this region throughout the four climatic seasons (DJF, MAM, JJA, and SON). The same can be observed in the Sahara, which can be attributed to the major emission of black carbon in this region.

Figure 4.10 shows the daily radiative forcing of aerosols. This shows the slow transportation of the non-dust aerosols to the Guinea coast during the season. The same can be observed over the Savanah zone, even though non-dust particles contributed more to the cooling forcing observed at the TOA during this period. Both natural and human-induced bush fires sweep through the Savanah areas, burning up to 80% of the areas each year contributing to the anthropogenic induced radiative forcing observed in Figure 4.7. However, it is noted over the Sahel and Sahara region that dust is the major influence of the radiative cooling effect occurrence, while sea-salt can be insignificantly ignored. The high forcing observed at the surface (Figure 4.11), can be attributed to the role these aerosols play at the top of the atmosphere by causing the delay and reduction in the solar radiation reaching the surface, thereby creating a form of cooling effect at the surface (Haywood and Boucher, 2000).

Higher albedo also contributes to higher aerosol forcing at TOA by reducing aerosol scattering back to space (Figure 4.12). Deserts, ice, and snow all have high surface absorption. When the vegetated surface is covered with dew crystals, the surface albedo is enhanced causing a cooling effect. The observation that the radiative effect is greater at the surface than at the top of the atmosphere suggests that land-use plays a crucial role in the overall balance of the forcing.

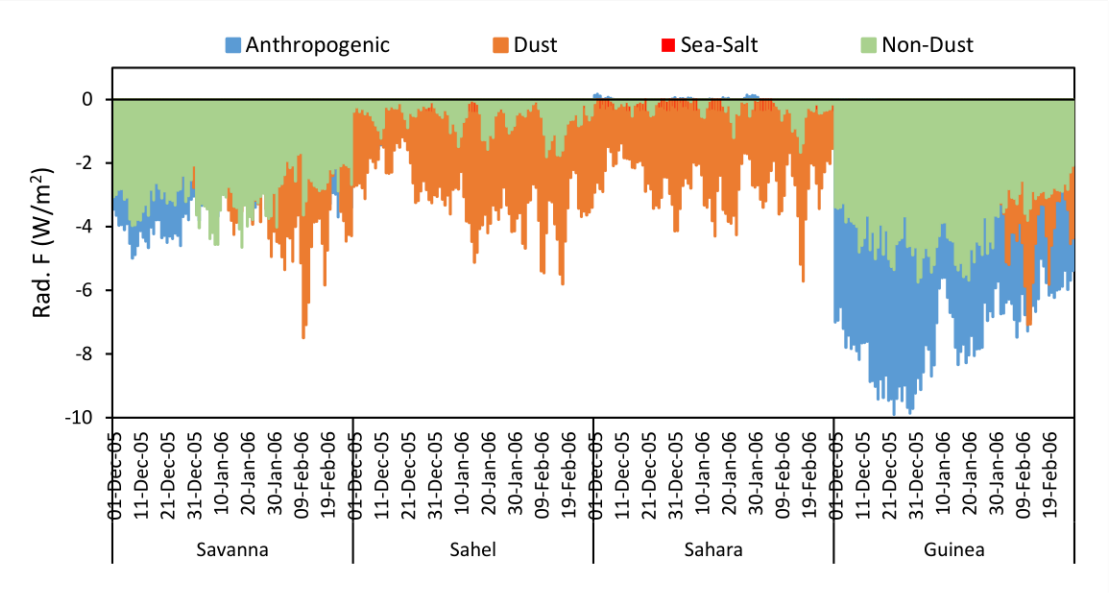

Figure 4.10: Daily average of Aerosols Direct Radiative Effect (Clear Sky) at the Top of the Atmosphere in DJF (2005-2006).

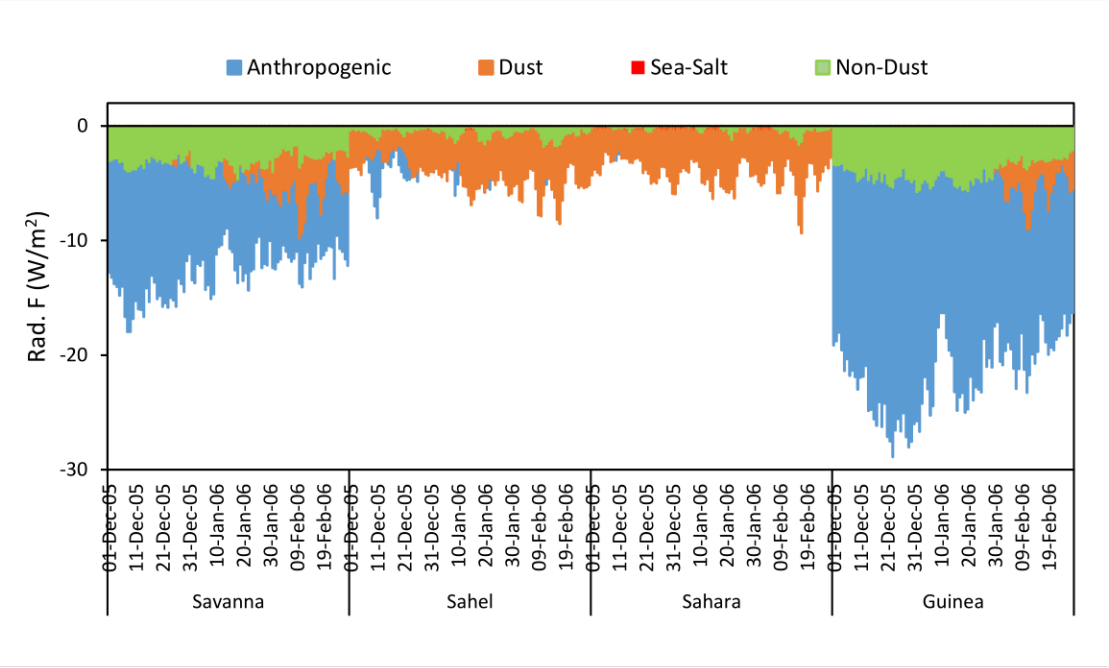

Figure 4.11: Daily average of Aerosols Direct Radiative Effect (Clear Sky) at the Surface in DJF (2005-2006).

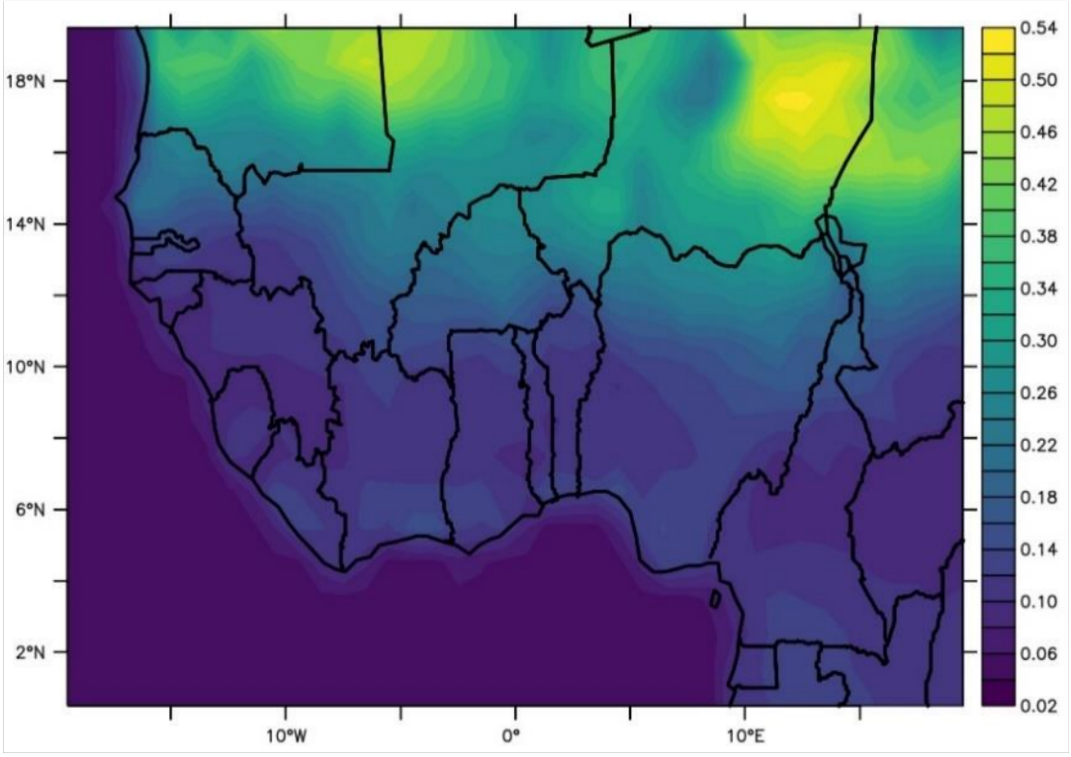

Figure 4.12: Daily average of the surface albedo over West Africa in DJF, 2005-2006.

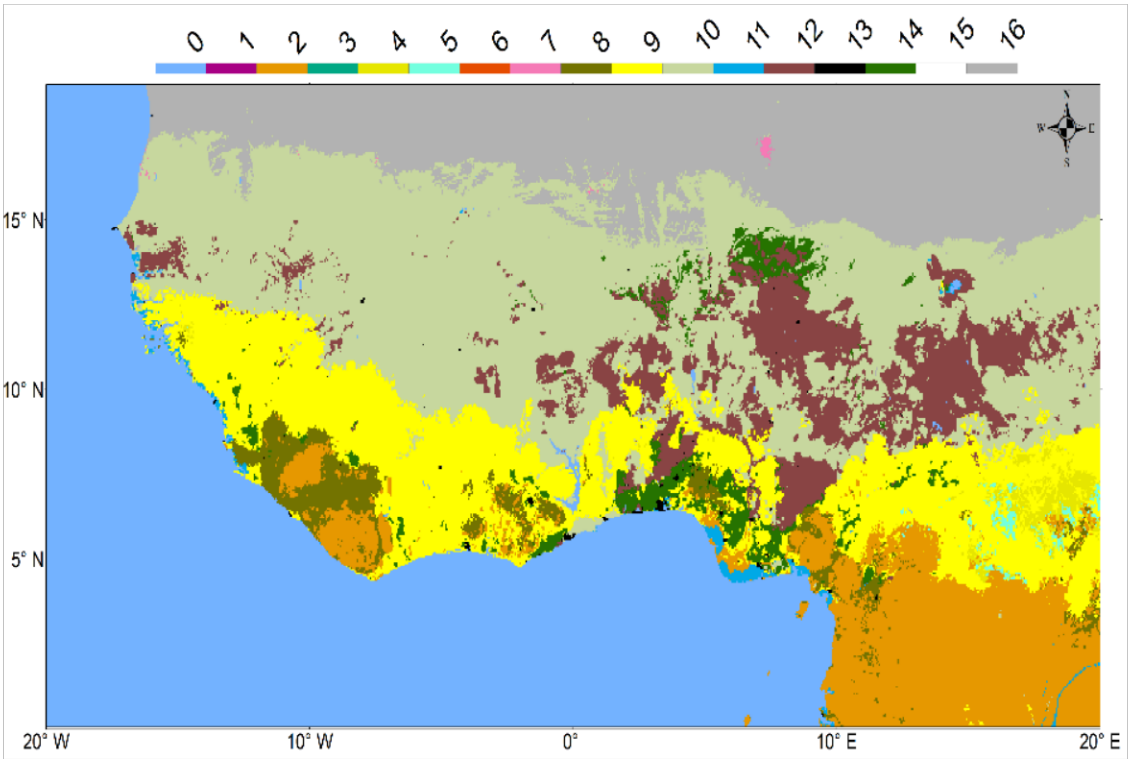

Figure 4.13: Land cover classification over West Africa in 2006 retrieved from MODIS.

Classifications: (0) Water bodies; (1) Evergreen Needle leaf Forests; (2) Evergreen Broadleaf Forests; (3) Deciduous Needle leaf Forests; (4) Deciduous Broadleaf Forests; (5) Mixed Forests; (6) Closed Shrub lands; (7) Open Shrub lands; (8) Woody Savannahs; (9) Savannahs; (10) Grasslands; (11) Wetlands; (12) Croplands; (13) Urban and Built; (14) Natural Vegetation; (15) Snow and Ice; (16) Barren Lands.

Considering the land-cover dynamics at the surface over these climatic zones, it can be easily concluded in Figure 4.13 that vegetated areas are larger in Guinea and the Savanah than in the Sahel and Sahara climatic zones of West Africa. The desertification of the Sahel and Sahara climatic zones cannot be ignored in the vegetation structure, thereby diminishing the surface albedo in these regions because there exist both direct and indirect correlations between albedo, direct solar radiation and the concentration of aerosols in the atmosphere. The surface is crucial when it comes to absorbing aerosols (i.e., aerosols with low SSA). Increased aerosol absorption and, consequently, aerosol forcing at the TOA as well as in the atmosphere are caused by higher albedo (more surface reflection). Because absorbing aerosols also absorb reflected upward solar energy, having a higher albedo improves aerosol absorption.

The average aerosol concentration in Figure 4.14 shows a large prevalence of small and medium dust particles in the Sahara and Sahel climatic zones with relatively low prevalence in the Guinea climatic zone. Large dust particles are observed to be prevalent in the Sahara region emanating from the Bodele depression in Chad, which has been described as the world's largest dust source. Small and medium dust particles are reportedly easily mobilized and transported by the wind at 12-14 m/s due to the low weight they possess when compared to larger dust particles (Legrand et at., 2001; Seinfeld et al., 2004, Ogunjobi and Awoleye, 2019). It can also be observed that black carbon and organic matter are deeply concentrated in the Guinea region. Apart from the Guinea coast being another major source of black carbon and organic matter, the prevailing north-easterly wind is also a major factor contributing to the observed BC and OM aerosol concentration in the region.

Largely over the Atlantic Ocean is the principal concentration of sea-salt aerosols, showing the small and the medium concentrates are more domineering than the large sea-salt aerosol. Aerosols' radiative effect depends on their size and chemical structure in addition to other factors such as the concentration. (Figure 4.15).

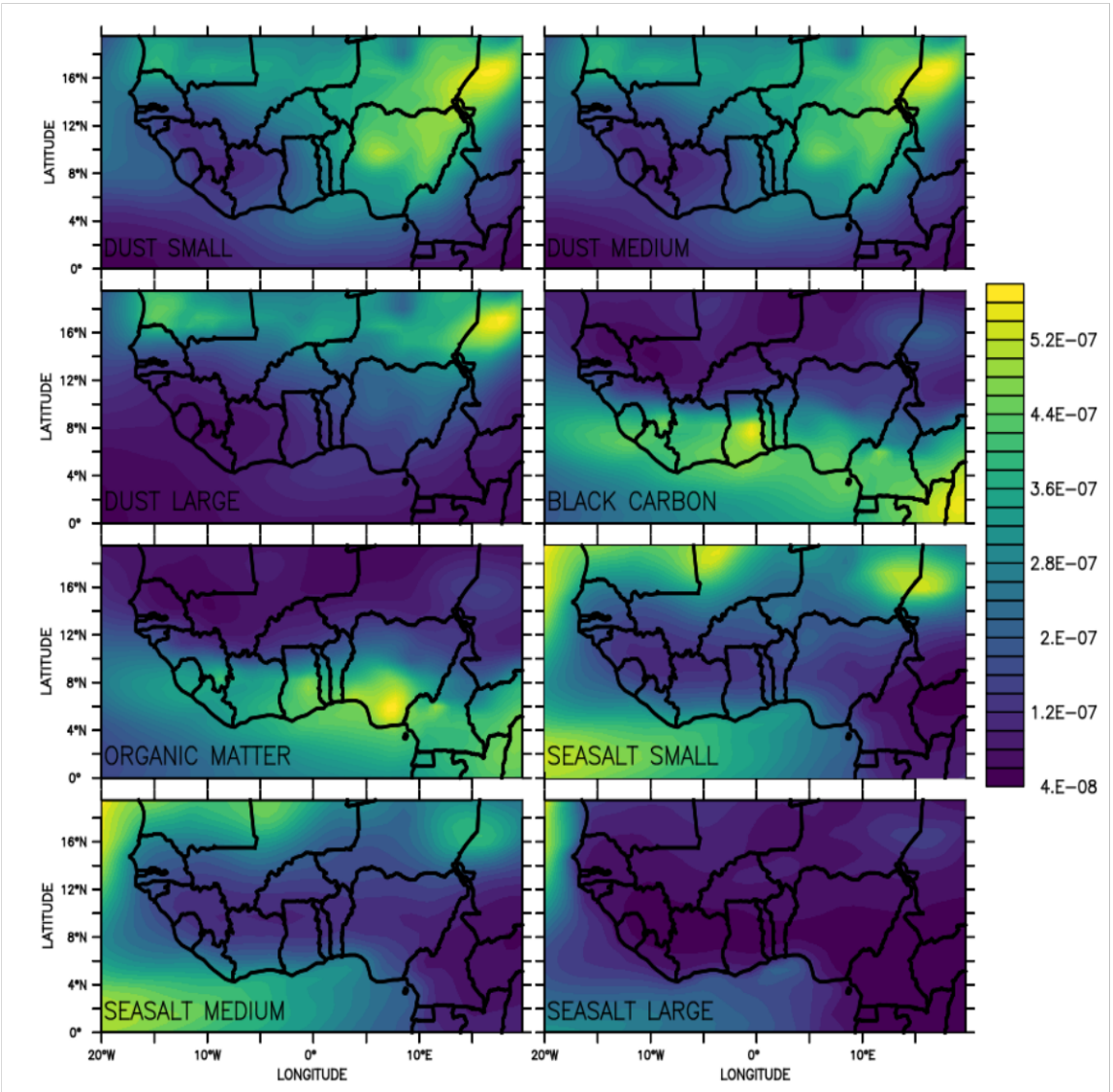

Figure 4.14: Daily average of Aerosol mass concentration (kg m^{-2}) over West Africa (DJF, 2005-2006).

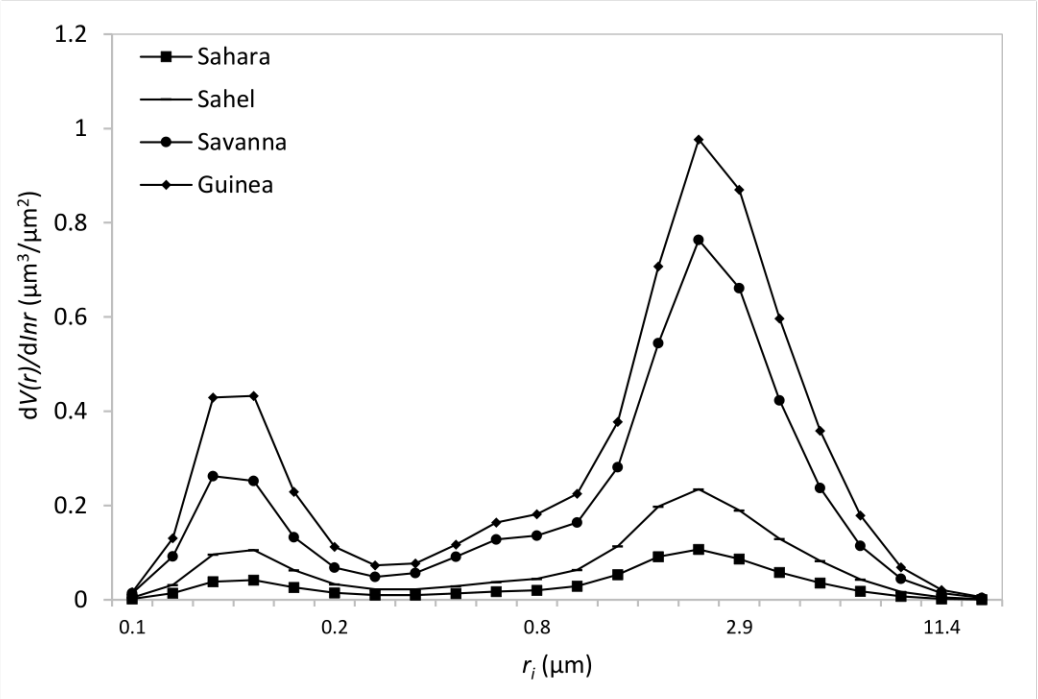

Figure 4.15: Derived volume size distribution of aerosols on an average daily basis from (DJF, 2005-2006) over West Africa.

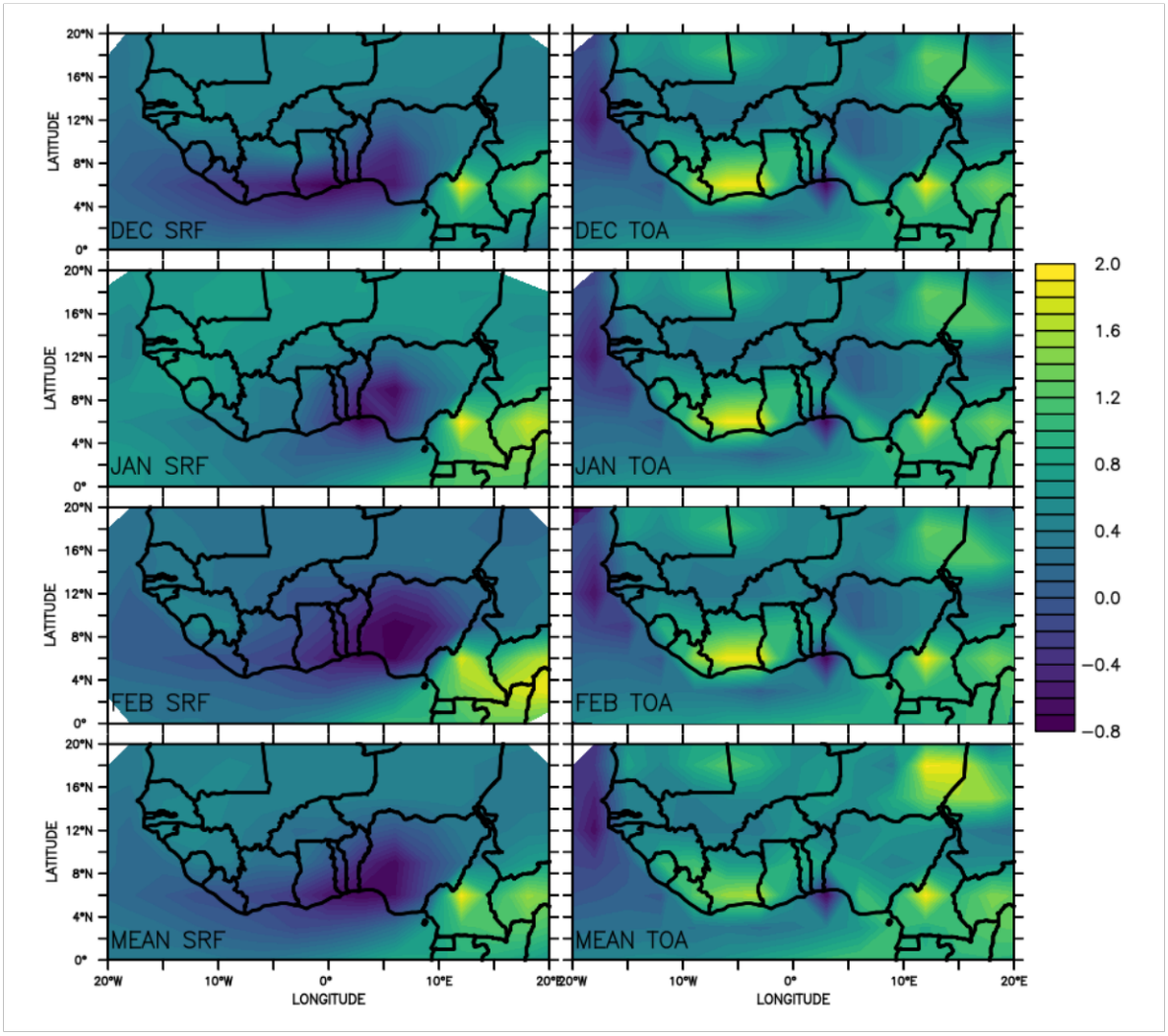

Figure 4.16: Daily average radiative forcing under all-sky condition at the surface and the atmosphere.

Desert dust is typically larger and has a more absorbing capacity at different wavelengths. Due to some greenhouse gases trapping the emitted solar energy, the top of the atmosphere becomes more heated (Lubin et al., 2002). The figure shows the daily average volume size distribution for December, January and February 2005-2006. Coarse mode particles have a substantial impact and could significantly influence the general characteristics of aerosols. It can be observed that the aerosol distribution follows a bimodal pattern with fine-mode aerosols around 0.1-0.2μm and coarse-mode aerosols around 2-4μm. Boiyo et al., 2019 reported a strong contribution of coarse mode aerosols to the total volume concentration which influenced the behaviour of aerosols.

Aerosols made up of black carbon and organic matter are predominately composed of fine-mode particles, whereas dust and sea salt aerosols are composed primarily of coarse-mode particles. (Boiyo et al., 2019). In contrast, the four climatic zones have more volume sizes of coarse-mode particles. Guinea and Savana climatic zones are observed to have a greater volume of fine particle fraction than the Sahel and Sahara region during the study period. A larger quantity of anthropogenic and non-dust aerosols, apart from the predominant dust aerosol in this region, could cause and boost the radiative forcing of aerosols, which is sensitive to the amount of precipitation along the Guinean coast and reduction in the Sahara region (Akinyoola et al., 2019). Daily averaged values of volume concentration, volume radius and the lognormal for both fine and coarse mode particles are given in Table 4.1. Coarse particle radius is higher with a value of 0.5 in the Sahara and 0.4 in the Sahel zone, describing the higher volume concentration observed of dust in the Sahara as it reduces southward to the Guinea coast.

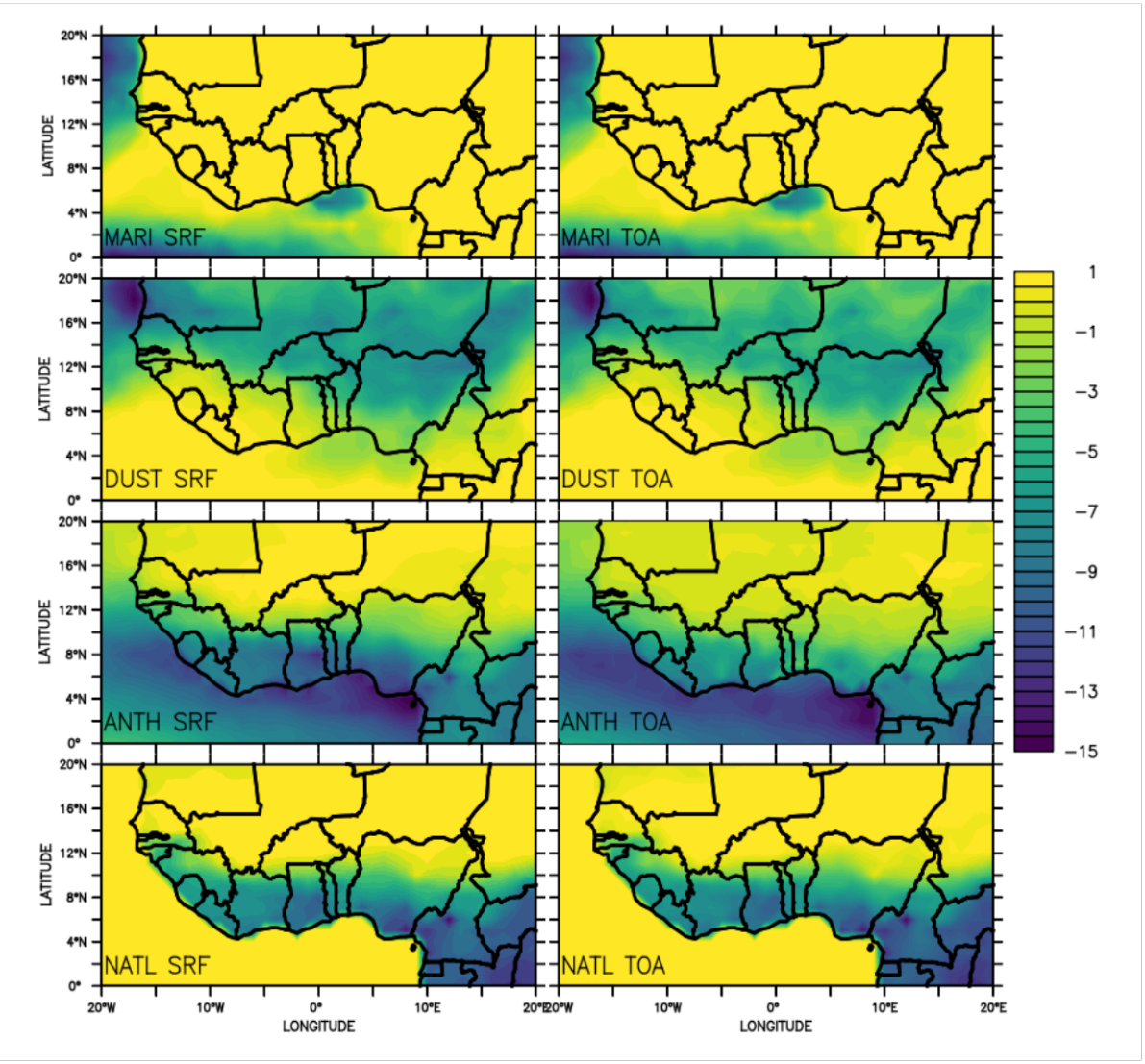

Figure 4.17: Daily aerosol radiative forcing (W/m^2) effect average in December 2005.

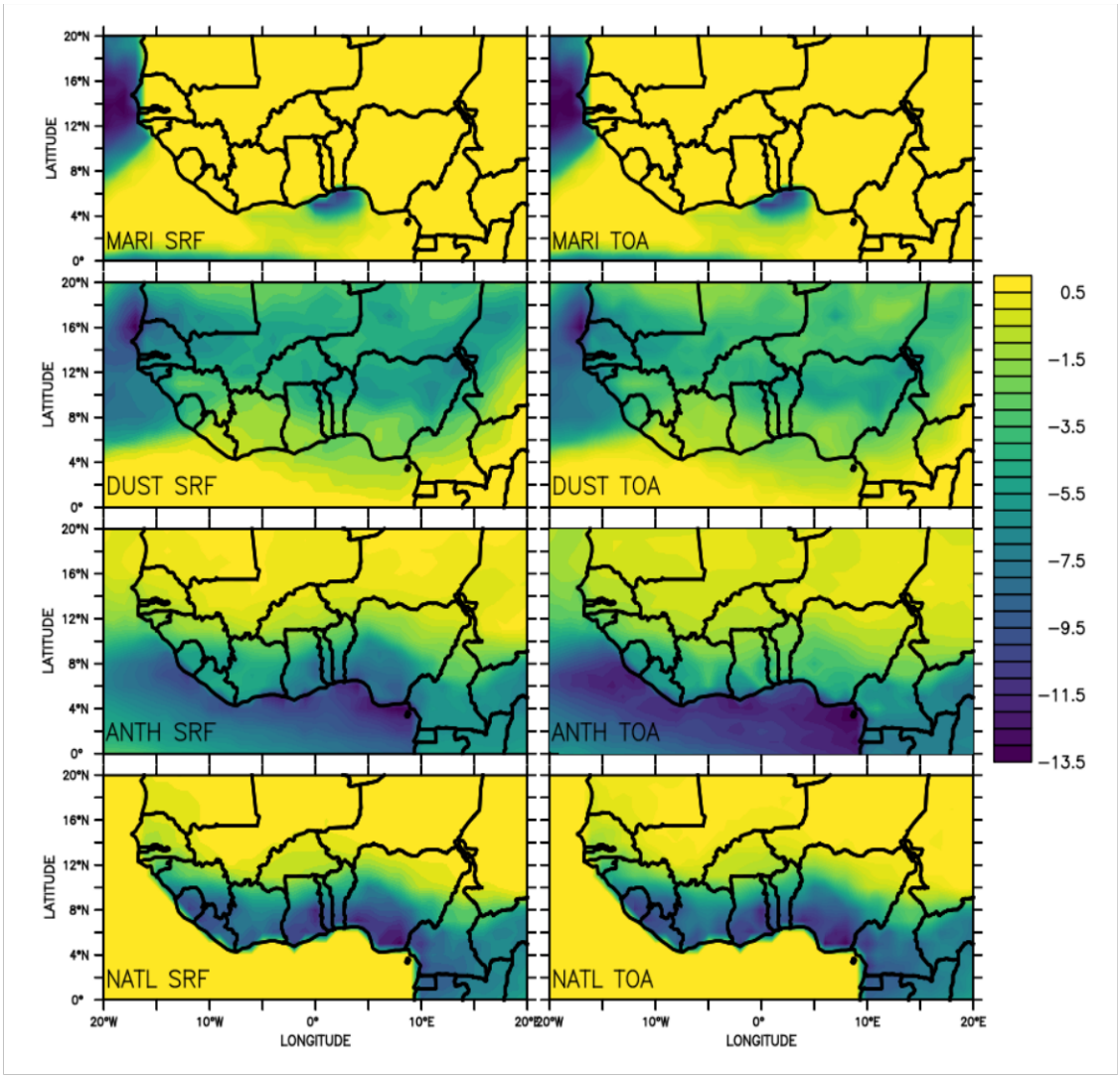

Figure 4.18: Daily aerosol radiative forcing (W/m^2) effect average in January 2006

Fine mode radius is more prominent in the Guinea and Savana region with a total volume concentration noticed in the Savana at 0.8 due to the excess mixture of both anthropogenic and dust aerosols. The impact of dust aerosol radiation can be altered in a variety of ways by adding black carbon and other aerosols to the dust particles (Chandra et al., 2004).

4.2 Obtaining the Best Parameterization Scheme for Chemistry Simulations

4.2.1 Model Precipitation, Circulation Climatology and Validation

Precipitation is one of the most studied climate variables to evaluate model performance. The spatial distribution of RegCM simulated precipitation for five experiments for the four seasons during 2002–2006 is presented in Figure 4.20 along with the TRMM precipitation combined with NCEP wind speed and direction. The results show that the RegCM is able to reproduce the seasonal circulation pattern over West Africa including the evolution of monsoonal pattern. Due to the intense surface heating and hence decrease in the atmospheric pressure of the landmass, a southern dominant moist wind originating from the Atlantic ocean moves from equator to the northern region during JJA. During the SON-DJF seasons, the West African subcontinent receives a “dry-season” precipitation. Scarce precipitation during DJF as observed from TRMM is also captured by the RegCM simulations for the five experiments. A precipitation band with ~ 6 - 8 mm/day over the ocean region near to the tip of coastal regions during DJF and MAM is well generated in most of the experiments. K-F experiment generates a wet bias over Sahara during MAM. The West African maximum precipitation is obtained during the monsoon season. A strong precipitation band ~ 7–8 mm/day is generally observed near the Sahelian and Guinea Coast region. EM and GR experiments fail to capture the low precipitation experienced over the Savanah region during DJF. EM noticeably generates a high precipitation over the deep coast of Guinea region during that period (DJF).

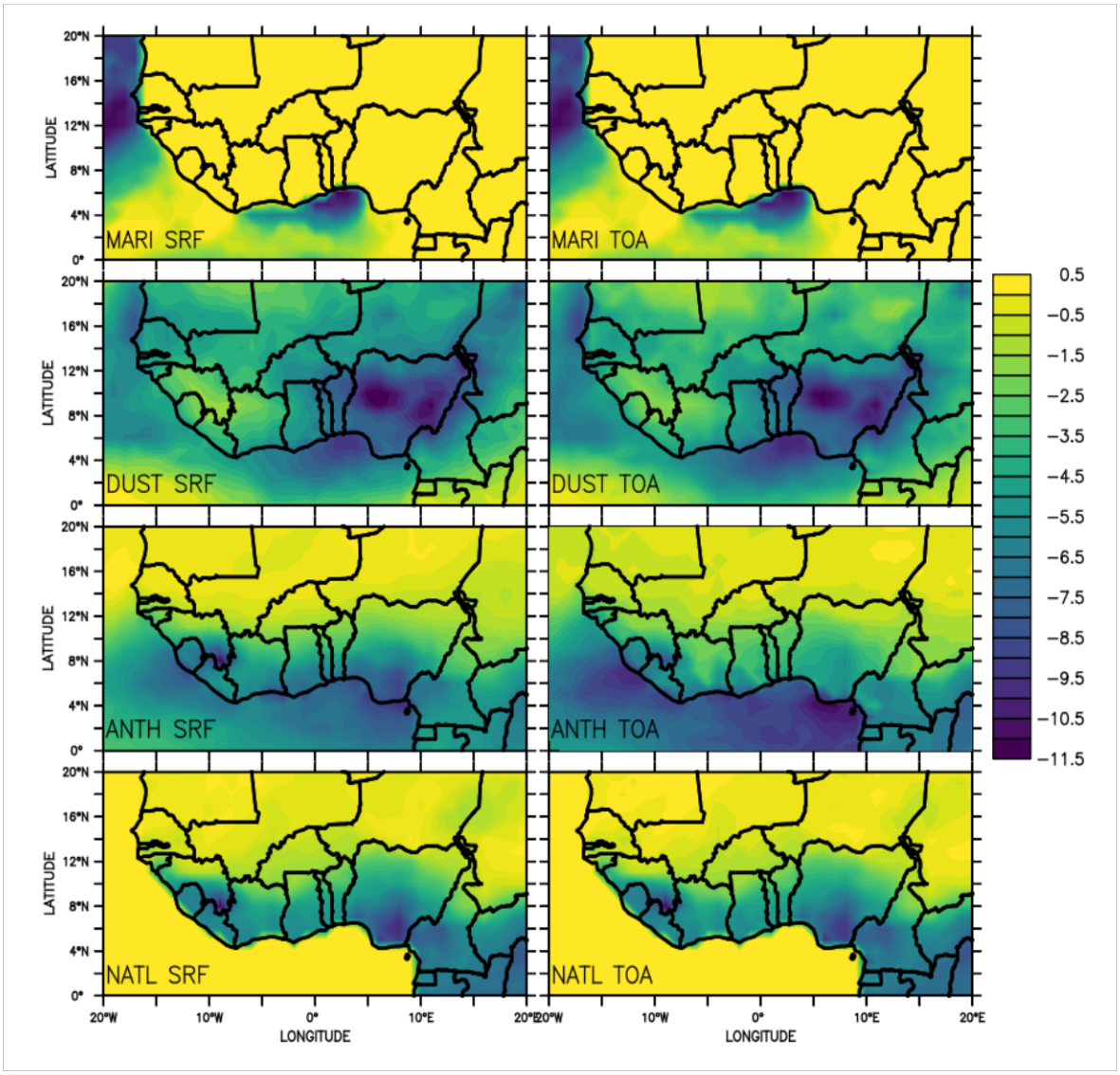

Figure 4.19: Daily aerosol radiative forcing (W/m^2) effect average in February 2006

Table 4.1: Daily Average Values of Volume Size Distribution Parameters over Climatic Zones from December to February (2005-2006) over West Africa

	$VolC_t$	VMR_t	Std_t	$VolC_f$	VMR_f	Std_f	$VolC_c$	VMR_c	Std_c
Guinea	0.493	0.333	0.949	1.504	0.160	0.117	0.126	0.322	0.333
Savanah	0.806	0.461	1.229	1.315	0.158	0.115	0.129	0.411	0.648
Sahel	0.236	0.477	1.154	1.312	0.063	0.124	0.135	0.494	0.174
Sahara	0.190	0.445	1.139	1.311	0.045	0.119	0.140	0.508	0.144

$VolC_t$: Volume Concentration of Total Aerosols

VMR_t: Volume Median Radius of Total Aerosols

Std_t: The lognormal size distribution's standard deviation of Total Aerosols

$VolC_f$: Volume Concentration of Fine-mode Aerosols

VMR_f: Volume Median Radius of Fine-mode Aerosols

Std_f: Standard Deviation of the lognormal size distribution of Fine-mode Aerosols

$VolC_c$: Volume Concentration of Coarse-mode Aerosols

VMR_c: Volume Median Radius of Coarse-mode Aerosols

Std_c: The lognormal size distribution's standard deviation of Coarse-mode Aerosols

The model precipitation bias with TRMM dataset is presented in Figure 4.21. During DJF EM, GR, K-F and KU experiments show minimal bias with the TRMM pattern over the Saharan desert. During MAM, the rainfall pattern of the Guinea and Savana simulated by GR and K-F experiments goes well with the TRMM pattern while EM, KU and TDK create a dry bias. EM, GR, KU and TDK different from K-F create a wet bias over the Sahara in JJA. K-F, EM, TDK, and GR create a wet bias over the Guinea while KU creates a dry bias. KU and TDK experiments simulate a wet bias over the Sahel and the Sahara region, whereas GR, KF and EM inhibit this. TDK generates a marginal dry bias over the Atlantic Ocean. During monsoon (Figure 4.22), when dominant rainfall occurs throughout the northern part of West Africa, cumulus convective schemes behave in dissimilar ways over the northern region. All the convective schemes other than the KU overestimate precipitation over northern region while other experiments create a dry bias. All the experiments create a dry bias over the study domain, comparatively, KF and TDKM simulate well in SON. In SON, KU experiments creates an intense dry bias that covers almost the entire region. Over Sahel, Savana regions, all experiments unanimously show a dry bias. Noticeably all the schemes except TDK generate a dry bias over the Sahel and Savana region in DJF. An underestimated peak monsoon precipitation during the mature phase in West Africa has also been reported (Kone et al., 2018; Ogunjobi and Awoleye, 2019 and Kouassi et al., 2022). During post-monsoon season, TDK generated rainfall go well with the observations throughout the study area with only a minimal bias. EM produces a drier climatology during the SON all over the Atlantic. K-F and TDK behavior is noble other than a bias over the Atlantic. EM and GR, even though well behave with observations, has a dry bias over the Savana and Guinea. The performances of different schemes are further discussed based on Taylor's diagram.

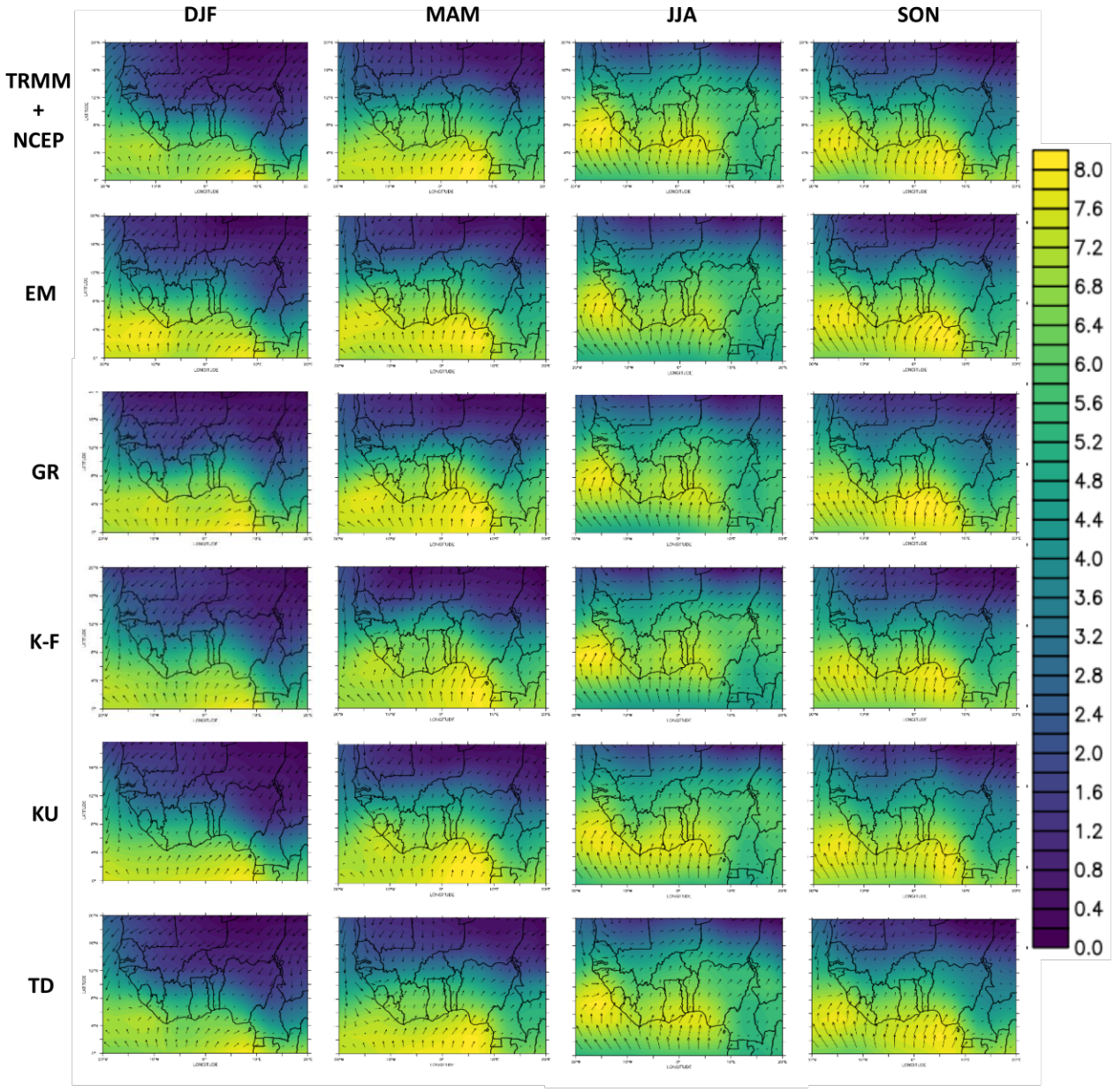

Figure 4.20: RegCM simulated and observed (TRMM with NCEP winds) seasonal average precipitation (mm/day) and wind (m/s) for different cumulus convective precipitation schemes – Emanuel (EM), Grell (GR), Kain-Fritsch (K-F), Kuo (KU), and Tiedtke (TDK).

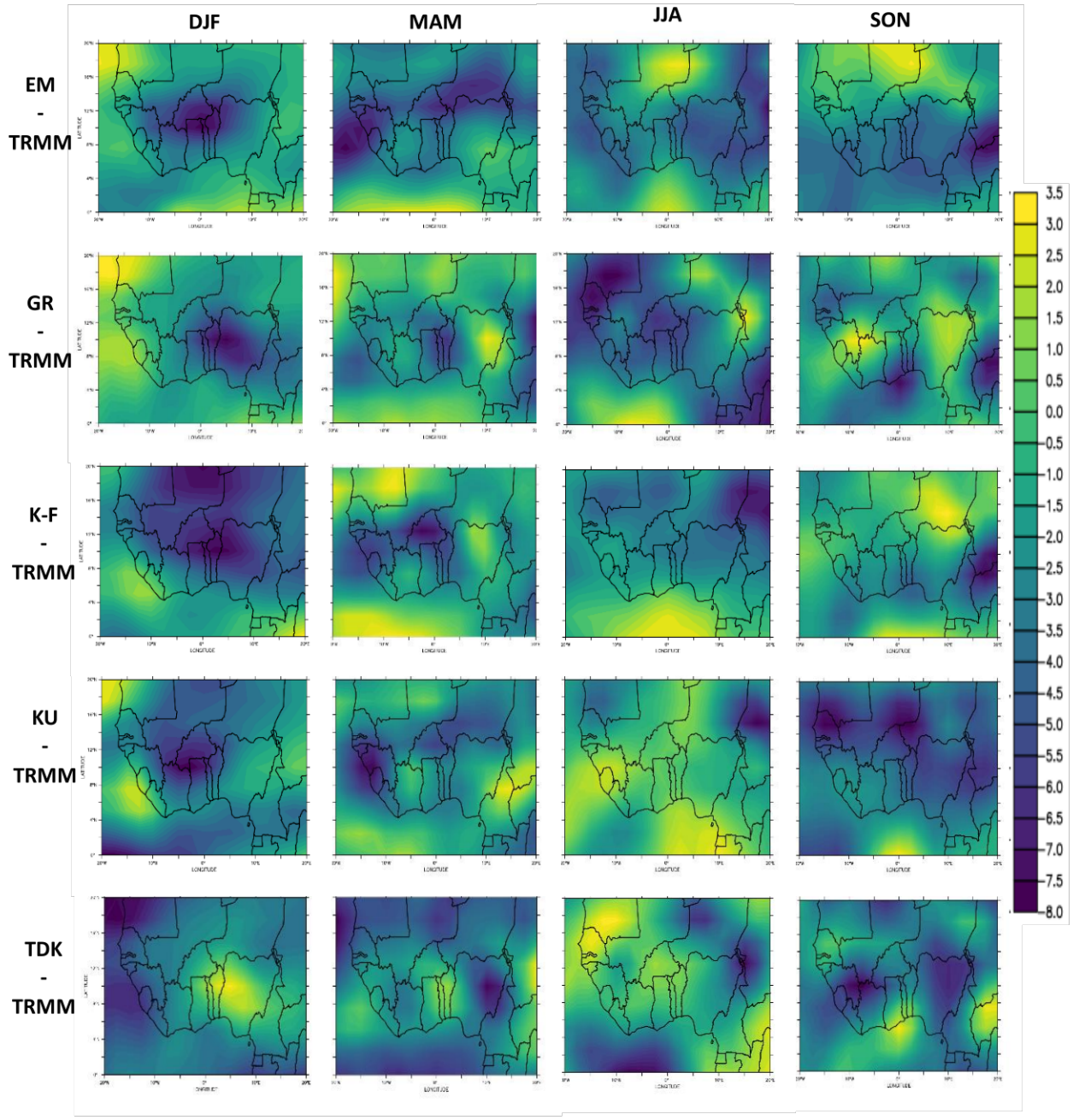

Figure 4.21: RegCM simulated precipitation bias with TRMM observation for different cumulus convective precipitation schemes.

4.2.2 Temperature Climatology and Validation

Simulated seasonal air temperatures were validated against Copernicus Atmosphere Monitoring Service (CAMS) dataset with 0.5° × 0.5° resolution (Granier et al., 2019; Inness et al., 2019). During DJF (Figures 4.23), the observed maximum is higher over the equator (> 40°C), reduces gradually moving northwards and the Sahara experience lowest maximum temperature (< 20°C) while the minimum temperature also observed over the southern region above 23°C decreases northward to values below 12°C. During December even though underestimation of temperature over the Sahara and Sahel exist, the model experiments comparatively perform well over other regions. There is a warm bias of ~ 3–4°C over the northern region and a cold bias over the southern region for all schemes (Figure. 4.21). KU experiment underestimates the temperature all over the West Africa subcontinent during SON, whereas all other experiments exhibit a warm bias and. TDK exhibits higher spatial warm bias over the Savana and Guinea coast than the rest while other schemes exhibit cold biases. A cold systematic bias of a few degrees has been reported over the Guinea and Savana by Kone et al., (2019).

With the Taylor diagram shown in Figure 4.27, the impact of cumulus convective schemes on precipitation and the modulations brought by changes in convective parameters over West Africa areas can be examined and the better performing convective scheme over different can be found out. This analysis makes an implication that all of the precipitation schemes is finest over the domain. TDK simulation, even though shows a good correlation with observation, it overestimates for the precipitation and underestimates for temperature. GR, EM and KU show better results comparatively. The Bodele depression in Chad is a hotspot and a major source region for aerosols over West Africa, as the pollution rate is extremely high in that region (Ogunjobi et al., 2004; Akinyoola et al., 2019).

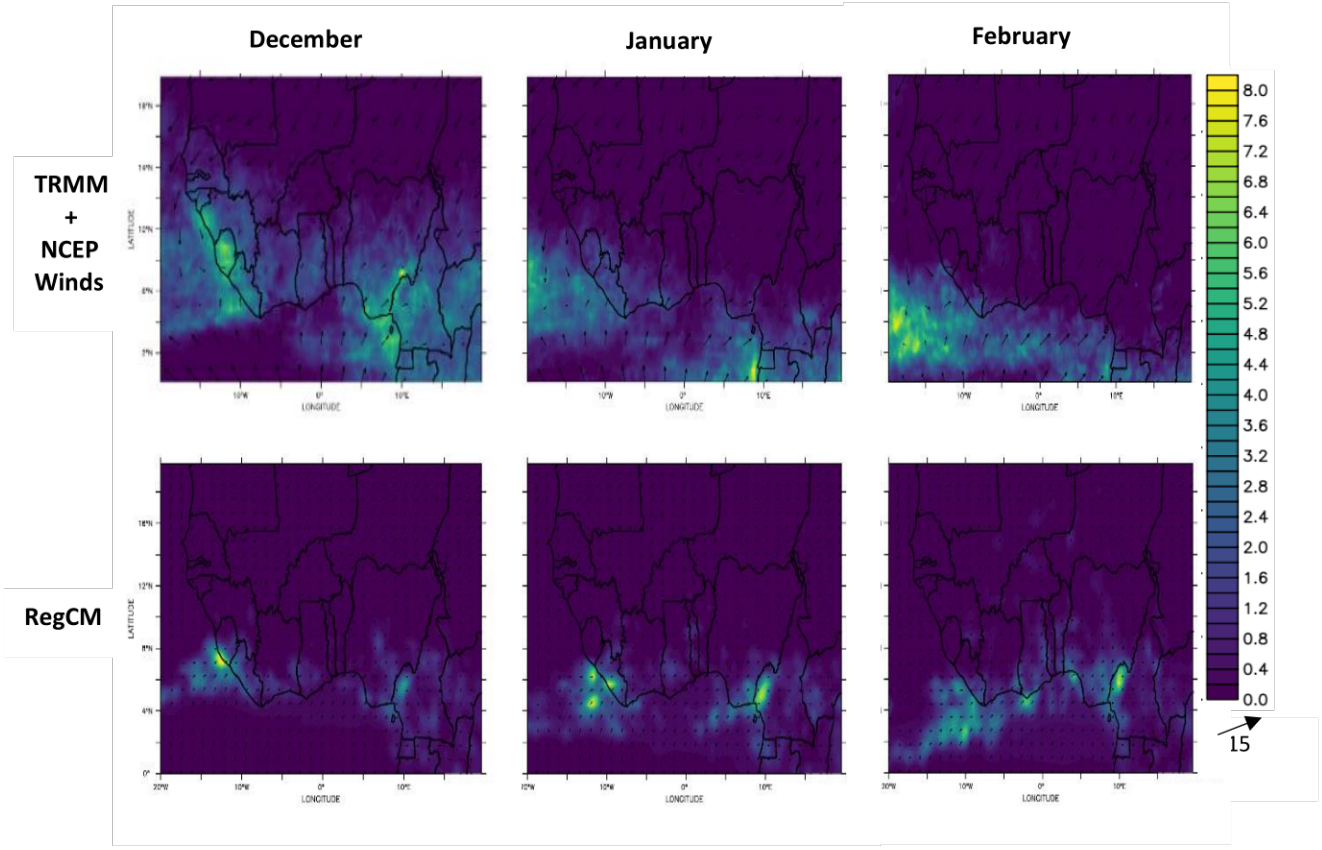

Figure 4.22: RegCM simulated and observed (TRMM with NCEP winds) seasonal precipitation (mm/day) and wind (m/s) using Kain-Fritsch (K-F) cumulus convective precipitation scheme.

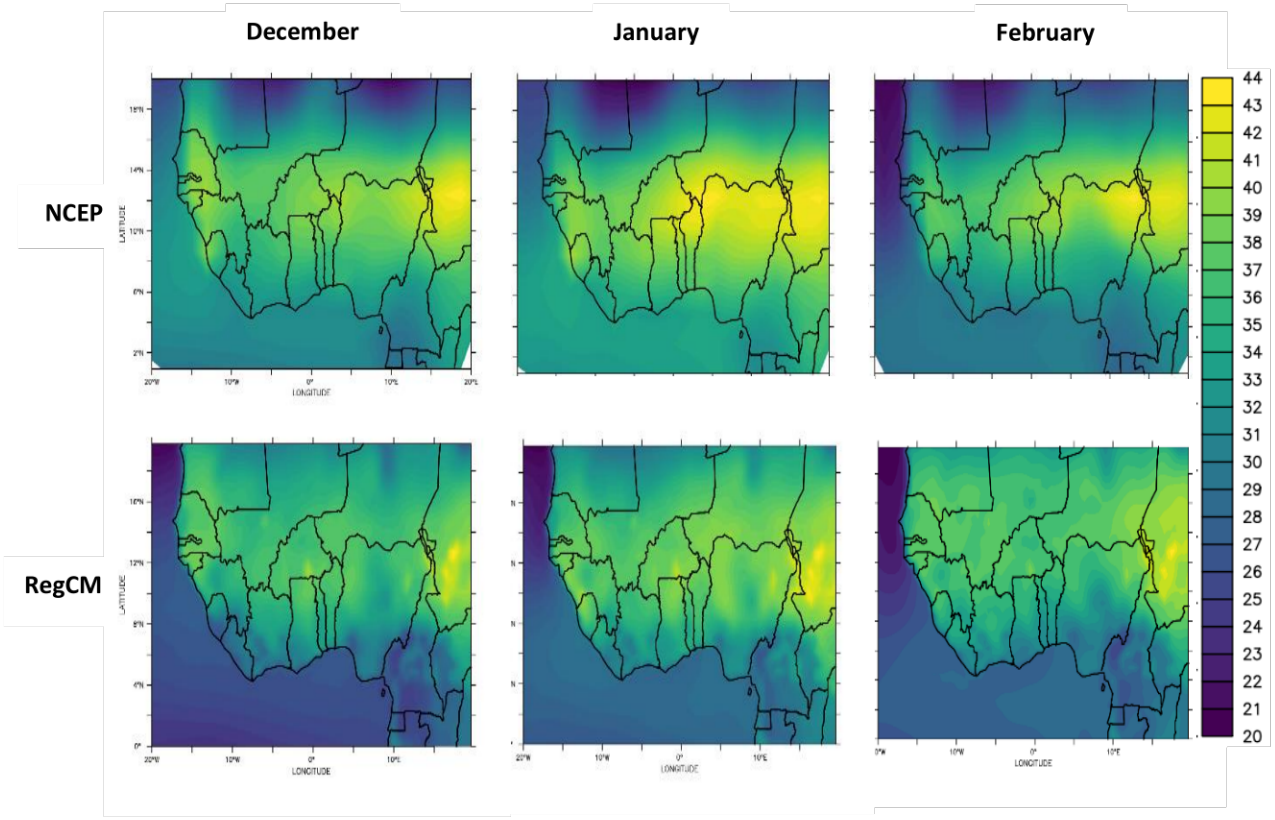

Figure 4.23: RegCM simulated and observed (NCEP) 2m near-surface maximum temperature (°c) using Kain-Fritsch cumulus convective precipitation schemes.

Hence, precipitation simulation over this region has to be considered important as it plays a major role in the aerosol removal from the atmosphere which explains the significant correlation the experiments showed. TDK simulation shows a very good correlation also with less deviation from observation and also has a perfect annual cycle (Gautam et al. 2009, 2010). The results in Figure 4.28 show that the model simulations of rainfall have good agreement with observations, except for a slight overestimation in the Guinea region. The Guinea region is a rainfall hotspot region of the study domain and is unique with its topography, which may have contributed to the overestimation in the RegCM simulation. In contrast, the rainfall simulations over the Sahel and Sahara regions show good agreements with the TRMM observations. This suggests that the model can capture the precipitation climatology and desertification experienced in those areas. Results also showed that the highest precipitation values occurred in December 2005 over Guinea, at above 50mm/day. In contrast, the lowest precipitation values were recorded in February 2006, with some days having no rainfall. The low precipitation values observed in early December 2005, with values below 25mm/day, indicate strong and deep aerosol concentration inhibiting the formation of deep convections. The model simulations show a small discrepancy with observations, with correlations above 95%. In simulating regional temperature. The results in Figures 4.27 and 4.28n further show that the model simulations exhibit less disagreement with observations, with GR showing less standard deviation from observations. However, the simulations of regional temperature and precipitation vary depending on the chosen cumulus convective parameterization schemes. The K-F scheme shows intense low-level westerlies during monsoon in good agreement with observed patterns as already shown in Figure 4.22. This highlights the importance of choosing appropriate cumulus convective parameterization schemes for accurate simulations. The high precision in simulating southwest monsoon precipitation entering the subcontinent through South India and the Southern Atlantic is the main reason for the good agreement. However, all

the experiments underestimate precipitation over the northern region, while those over the southern region perform well.

The K-F scheme exhibits a realistic precipitation and temperature over a large part of the domain and is in good agreement with observations over the sub-regions. The observed phase of annual precipitation cycle is well simulated by K-F scheme over the Sahel, Sahara and Savanah. Extensive sensitivity study of RegCM to cumulus convective precipitation schemes with reference to precipitation and temperature reveals that seasonal and monthly mean spatial distribution, as well as magnitude, are better simulated by K-F experiment (Sylla et al., 2013; Ajay et al., 2018; Wang et al., 2015) compared to the other experiment. In TDK scheme the shallow, midlevel and deep convection are represented by several cloud types and downdrafts. Performance of TDK scheme is better due to its different closure assumptions for shallow and deep, mid-level convection (Bhatla et al. 2016). Even though there is a difference in spatial distribution between observations across the other sub regions, the TDK scheme does well capture the seasonality. It is worthwhile to mention that other schemes are also performing well spatially in all the regions. Although RegCM4-CLM4.5 shows some weaknesses, such as a dry bias over most of the central Sahel and Guinea coast region, its performance in replicating the spatial distribution of rainfall appears in line with that documented in previous studies using the previous version RegCM3 (Sylla et al., 2009; Abiodun et al., 2012). However, as West Africa is the focused region for the aerosol simulation, this study is not considering TDK as the best parameterization scheme. Instead, K-F which is performing much better over the Sahara, Sahel, Savanah and Guinea and is considered further for the aerosol radiative effect simulations. It is worthwhile to mention that the Guinea is also affected by pollutants including sea-salt aerosols transported from the ocean compared to rest of the climatic regions considered in this study. Thus the K-F experiment with UW scheme is considered as the best combination for RegCM 4.7.1 coupled with CLM4.5.

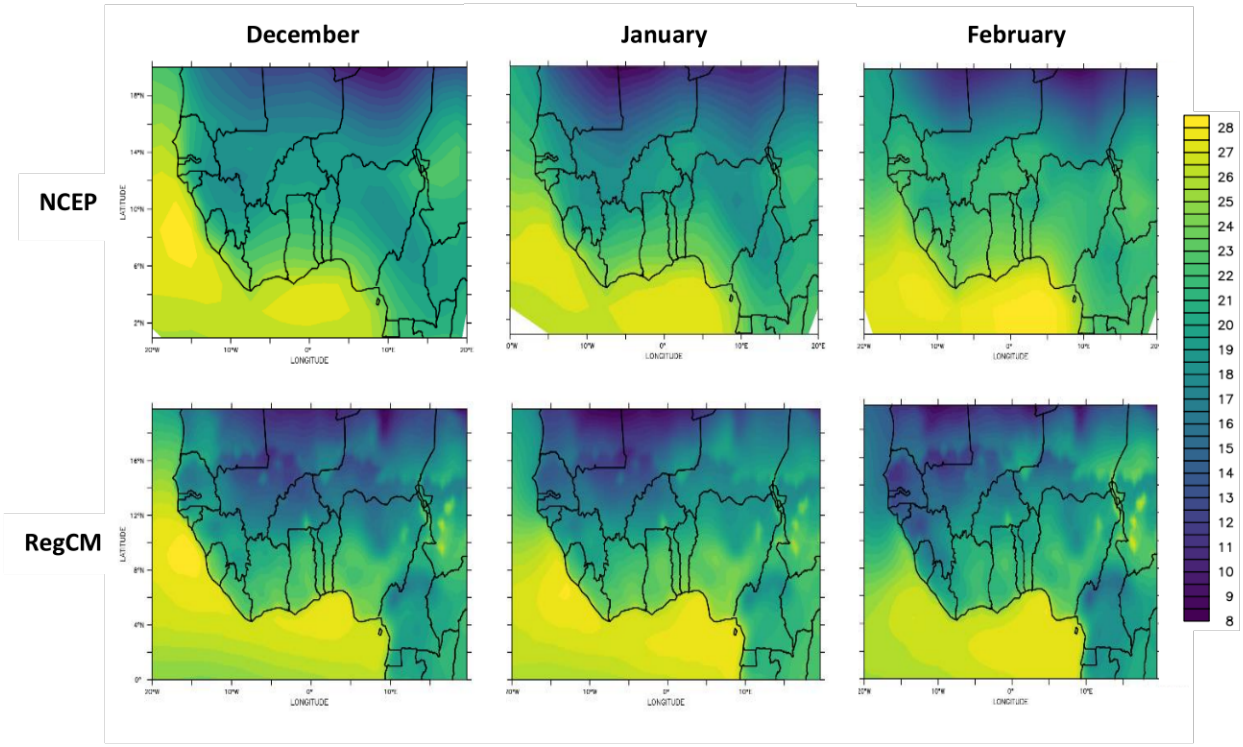

Figure 4.24: RegCM simulated and observed (NCEP) 2m near-surface minimum temperature (°C) using Kain-Fritsch cumulus convective precipitation schemes.

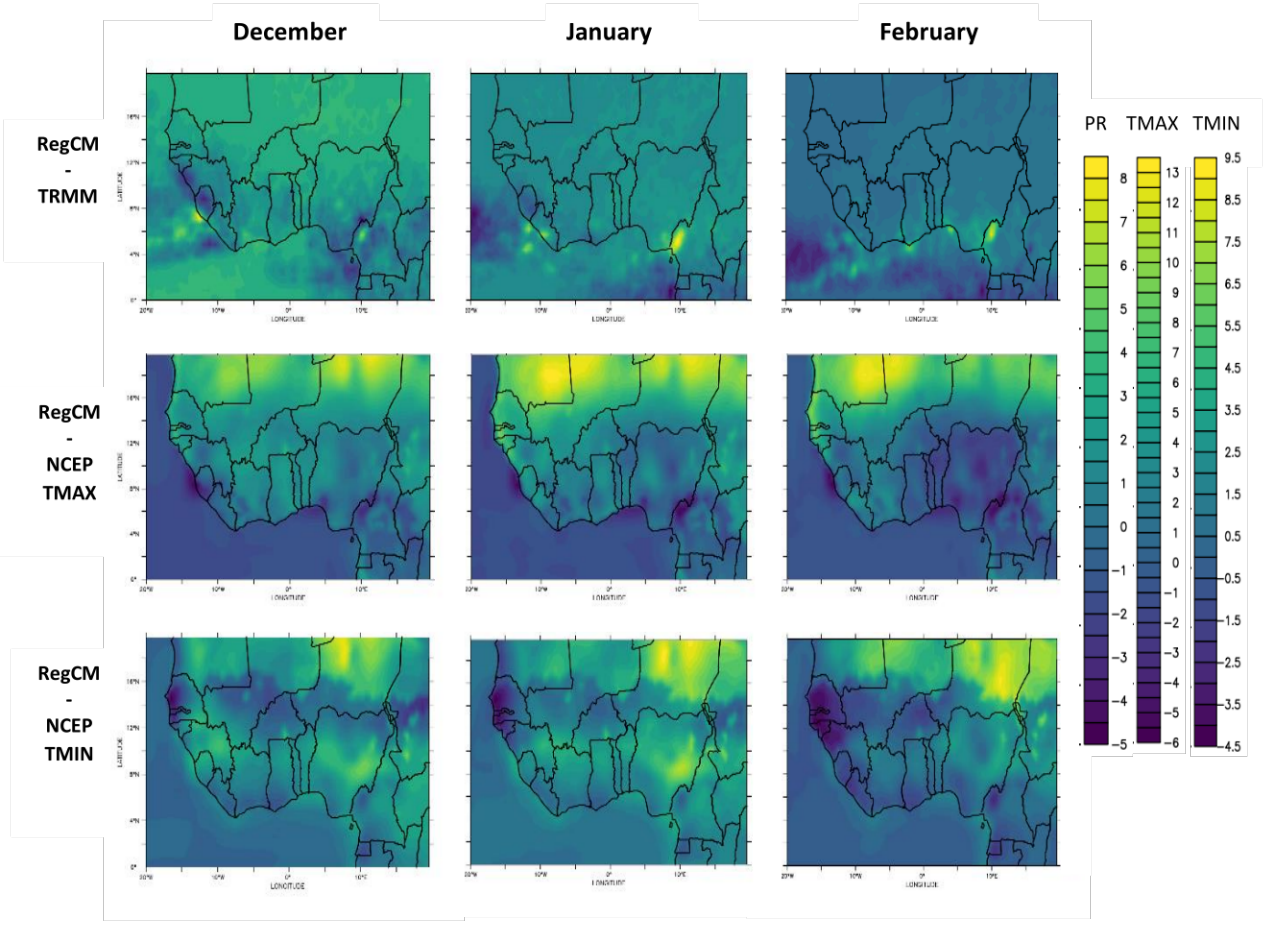

Figure 4.25: RegCM simulated precipitation bias using the Kain-Fritsch cumulus convective precipitation scheme with observed TRMM (precipitation) and NCEP 2m near-surface (maximum and minimum) temperature observation.

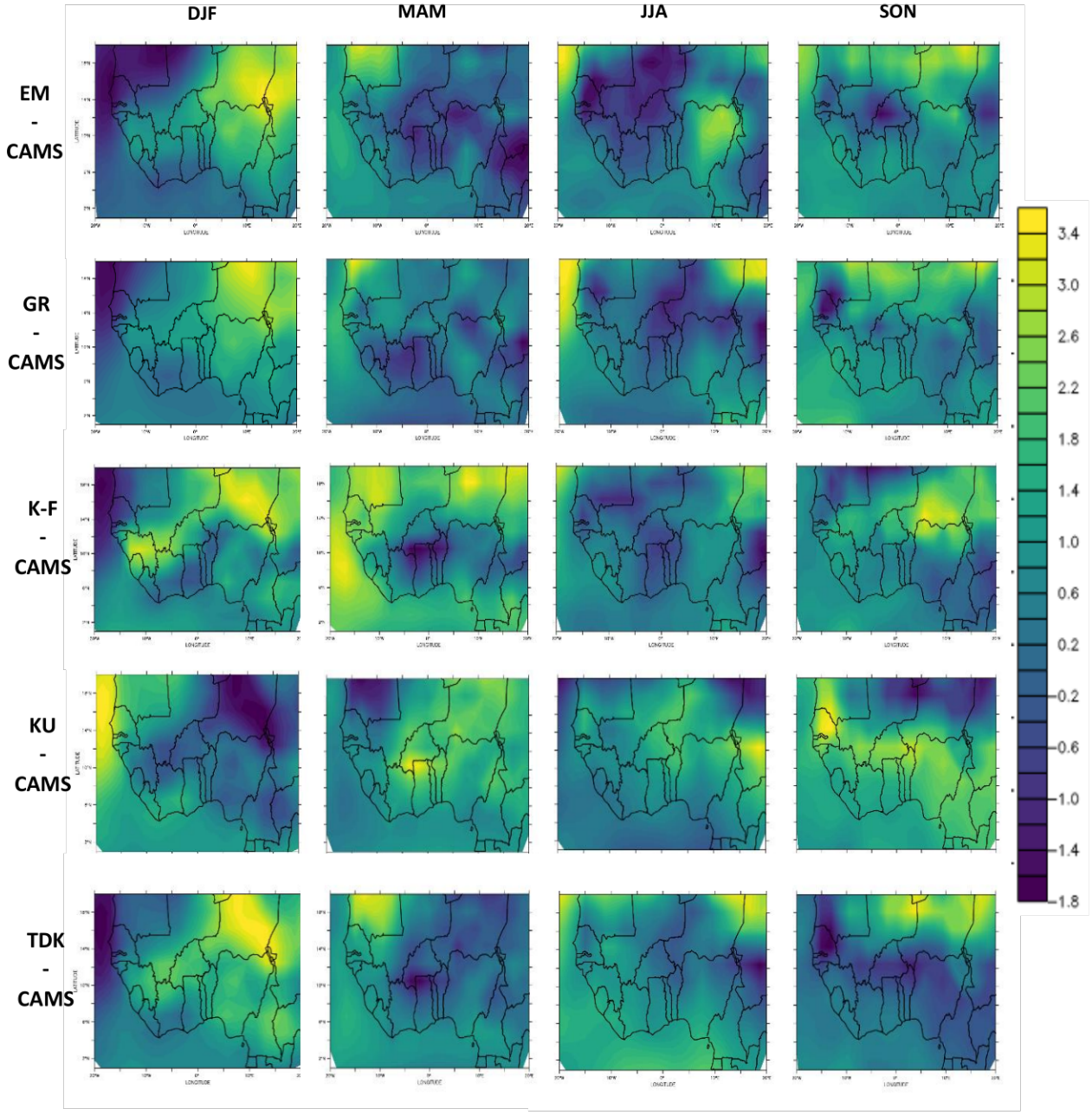

Figure 4.26: RegCM simulated and observed (CAMS) bias seasonal temperature (°C) for different cumulus convective precipitation schemes.

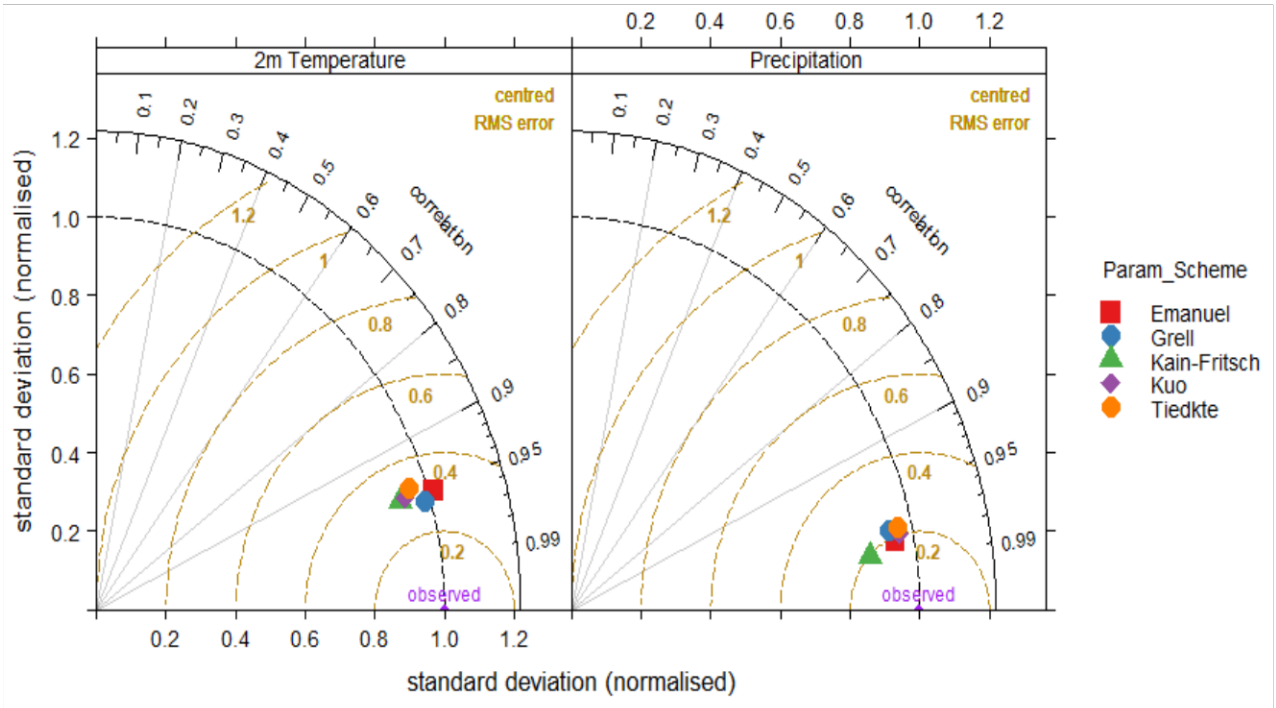

Figure 4.27: Taylor Diagram for 2m temperature and precipitation parametrization scheme with TRMM and CAMS as reference dataset.

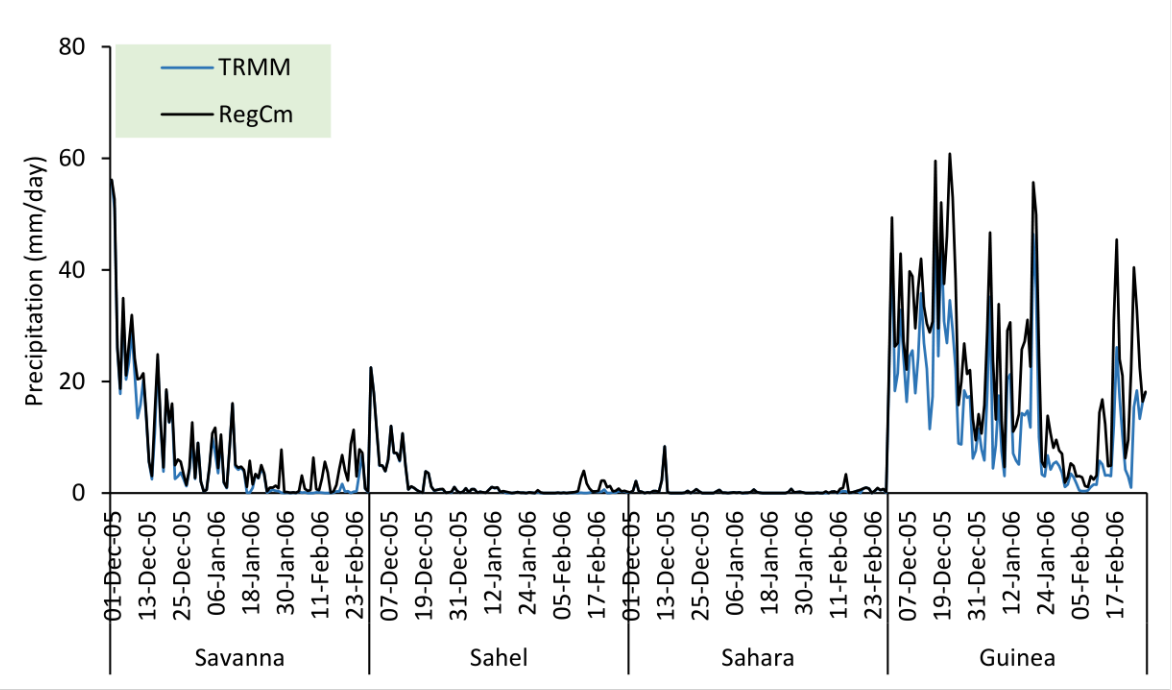

Figure 4.28: The comparison of the daily (mm/day) precipitation cycle for observations and simulated RegCM Kain-Fritsch cumulus precipitation convective scheme over the West African region.

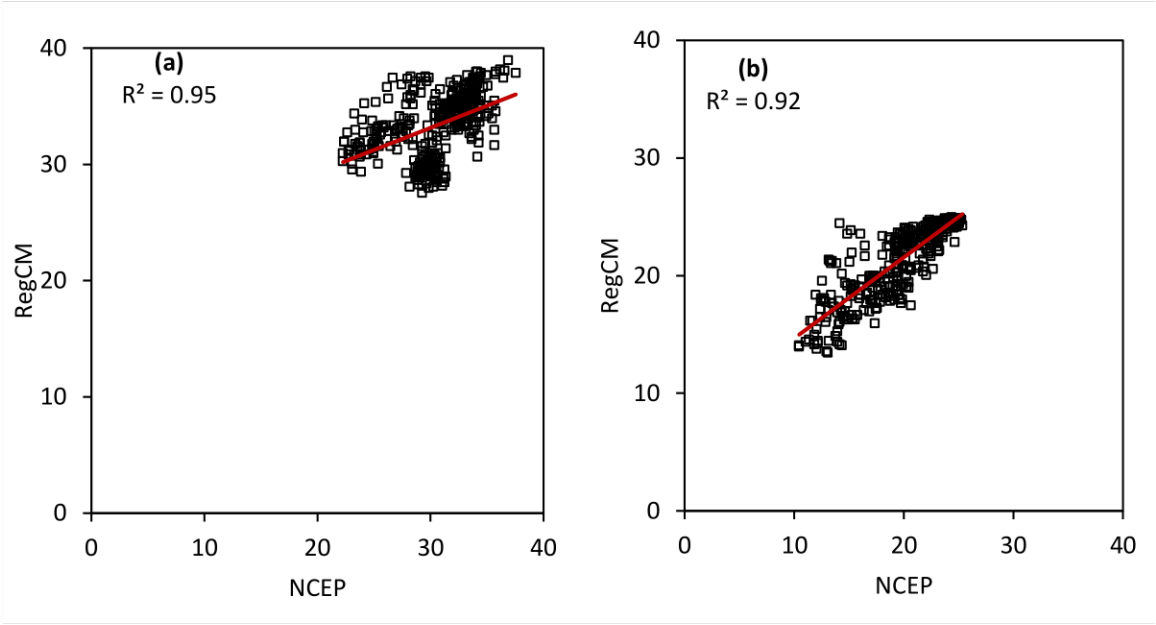

Figure 4.29: 2m near-surface temperature correlation plots for **a** Maximum Temperature and **b** Minimum Temperature for NCEP observations with simulated RegCM coupled with CLM4.5 over West African region.

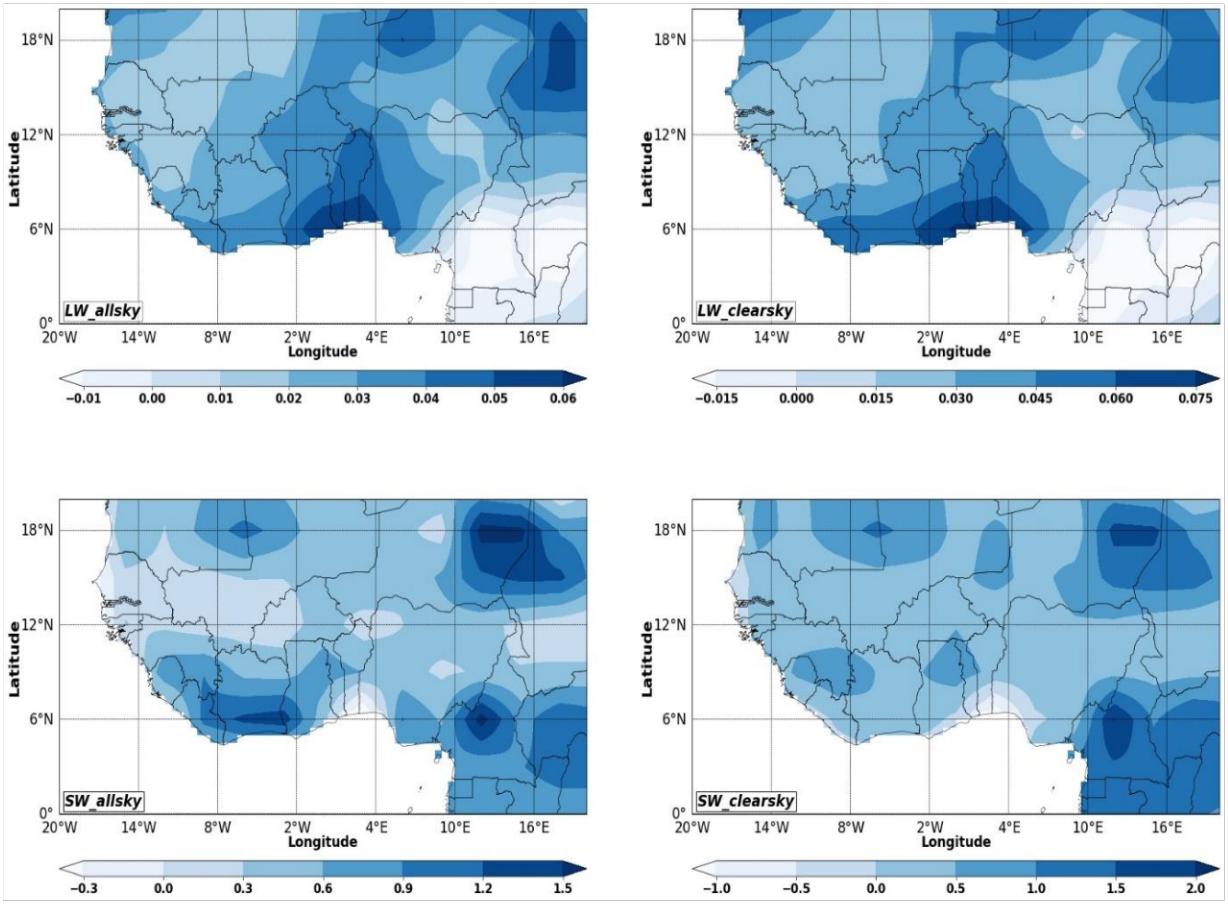

Figure 4.30: Direct radiative clear-sky and all-sky effects at the TOA without aerosols with blue colour indicating net-flux gains (warming) and grey colour indicating net-flux losses (cooling).

4.3 Simulation of Aerosol Radiative Properties

The aerosol radiative properties: aerosol optical depth (AOD), asymmetry factor (ASY) and single scattering albedo (SSA) for dust, black carbon, organic carbon and sea-salt are simulated over West Africa using RegCM 4..7.1 model coupled with CLM 4.5. In this simulation, I have considered K-F cumulus convective parameterization scheme, which is found to be the best schemes over the region as discussed above keeping all other parameters the same. Wet deposition is an important sink of aerosol that determines its lifetime and atmospheric burden (Bond et al. 2013). Appreciable differences in the absolute values of simulated precipitation with observations can significantly affect the wet scavenging of the aerosols (Srivastava and Sherin 2017, 2018). Hence, it is very important that the cumulus parameterization scheme is able to capture the variabilities in meteorological parameters over the study region. Similarly, the choice of PBL scheme generates high variability in atmospheric chemistry, diffusion, advection and deposition. Shallow wintertime atmospheric boundary layer is an important factor contributing to high surface aerosol concentrations in winter over West Africa by trapping pollutants near the surface. The nonlocal boundary layer scheme used in RegCM4 tends to overestimate vertical mixing in very stable conditions (Giorgi et al. 2012). RegCM4 with non-local boundary scheme failed to represent the very stable night-time conditions and therefore overestimates the vertical aerosol transport and underestimates the nocturnal aerosol (Nair et al. 2012). Therefore, the sensitivity with the advanced RegCM 4.7.1 version helps in the selection of cumulus and PBL scheme that has to be chosen wisely for aerosol simulations over West Africa. The analyses showed that use of Kain-Fritsch scheme as cumulus convective is closer to observed precipitation over the climatic sub-regions. Features like annual rainfall cycle, high monsoon rainfall and perfect rainfall pattern are simulated by the K-F scheme. This will aid in perfect wet scavenging/removal mechanism over source regions like the Bodele depression which even impacts the aerosol environment over the other parts of West Africa. I

have evaluated the simulated properties (AOD, ASY and SSA) with CAMS reanalysis over the four sub regions considered in this study.

4.3.1 Evaluation of RegCM Simulated Radiative Properties

Total extinction due to the existence of aerosols in the vertical column of atmosphere is determined by columnar spectral aerosol optical depth (AOD), which portrays the climate impact of aerosols. Hence in-depth understanding about the spatio-temporal variation of simulated AOD over West Africa is crucial. Studies for validating large-scale simulated aerosols are based on satellite/re-analysis observations due to their ability to provide aerosol information at regional to global scale with high temporal resolution. Figure 4.31 shows the spatio-temporal distribution of organic carbon AOD simulated by RegCM at 550 nm, CAMS AOD at 550 nm and the bias between CAMS and RegCM over West Africa. Spatio-temporal organic carbon AOD variation is well depicted by the model thereby simulation of the hotspots observed along the coasts of Nigeria to Ghana January, high organic carbon AOD over the Guinea coast during December and low black carbon over the Ocean in February can be associated with the partial decomposition of dead organic matter due to human activities. Simulated and CAMS reanalysis organic carbon AOD possess less discrepancy during the months, the bias being within ± 0.2. CAMS shows highest organic carbon AOD values (~ 0.4) over the Guinea sub region during January. This is associated with enhanced farm clearing activity over this region as also reported earlier (Ogunjobi and Awoleye 2019).

The strong north westerly advection of mineral dust is well represented by RegCM simulations (Figure 4.32), even though a small bias exists (Solmon et al. 2015). The extreme bias between the simulated and CAMS reanalysis AOD exists over the study domain during DJF, where RegCM underestimates CAMS by ~ 0.8. The primary reason for this might be the inadequacy of the emission inventories including the dominant burning events and other anthropogenic activities occurring over the region during DJF.

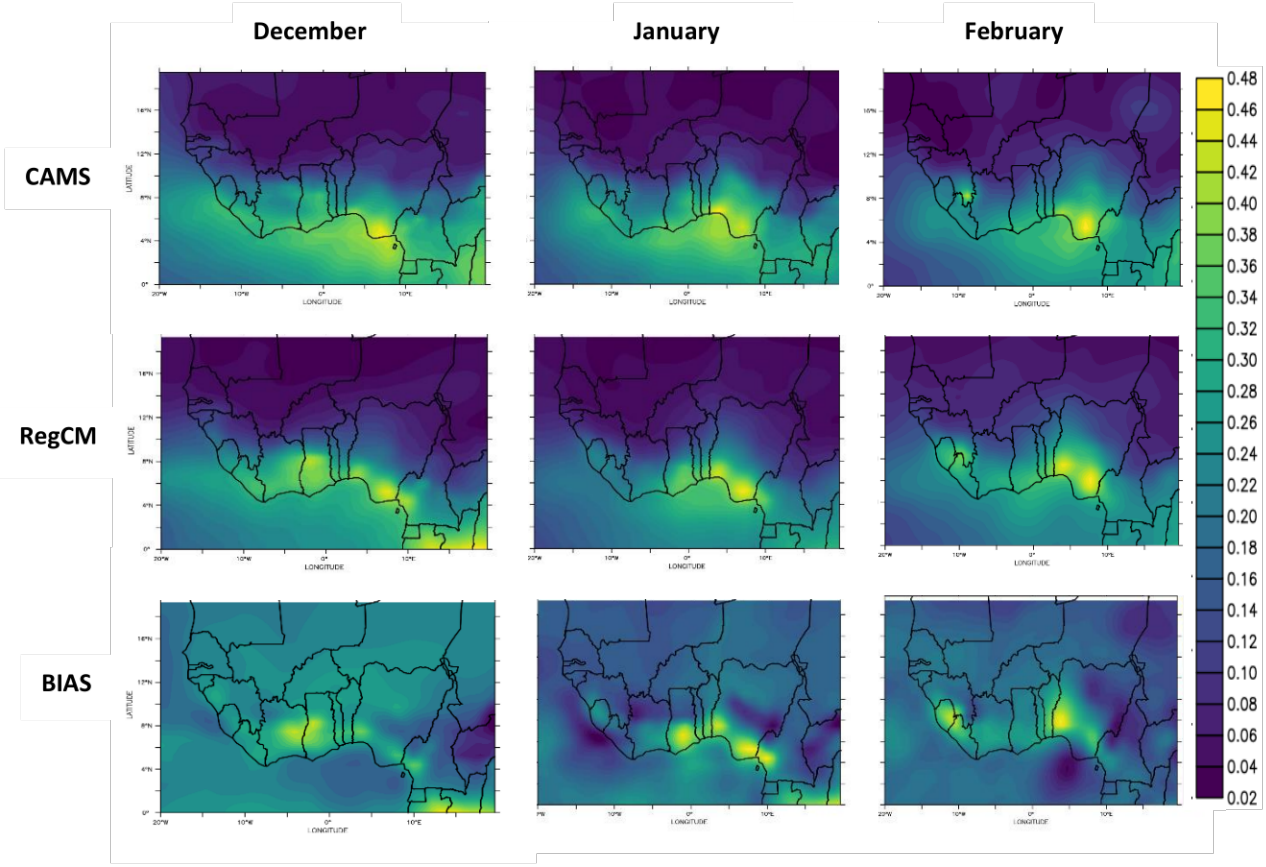

Figure 4.31: Simulated (RegCM4) and observed (CAMS) organic carbon AOD with bias

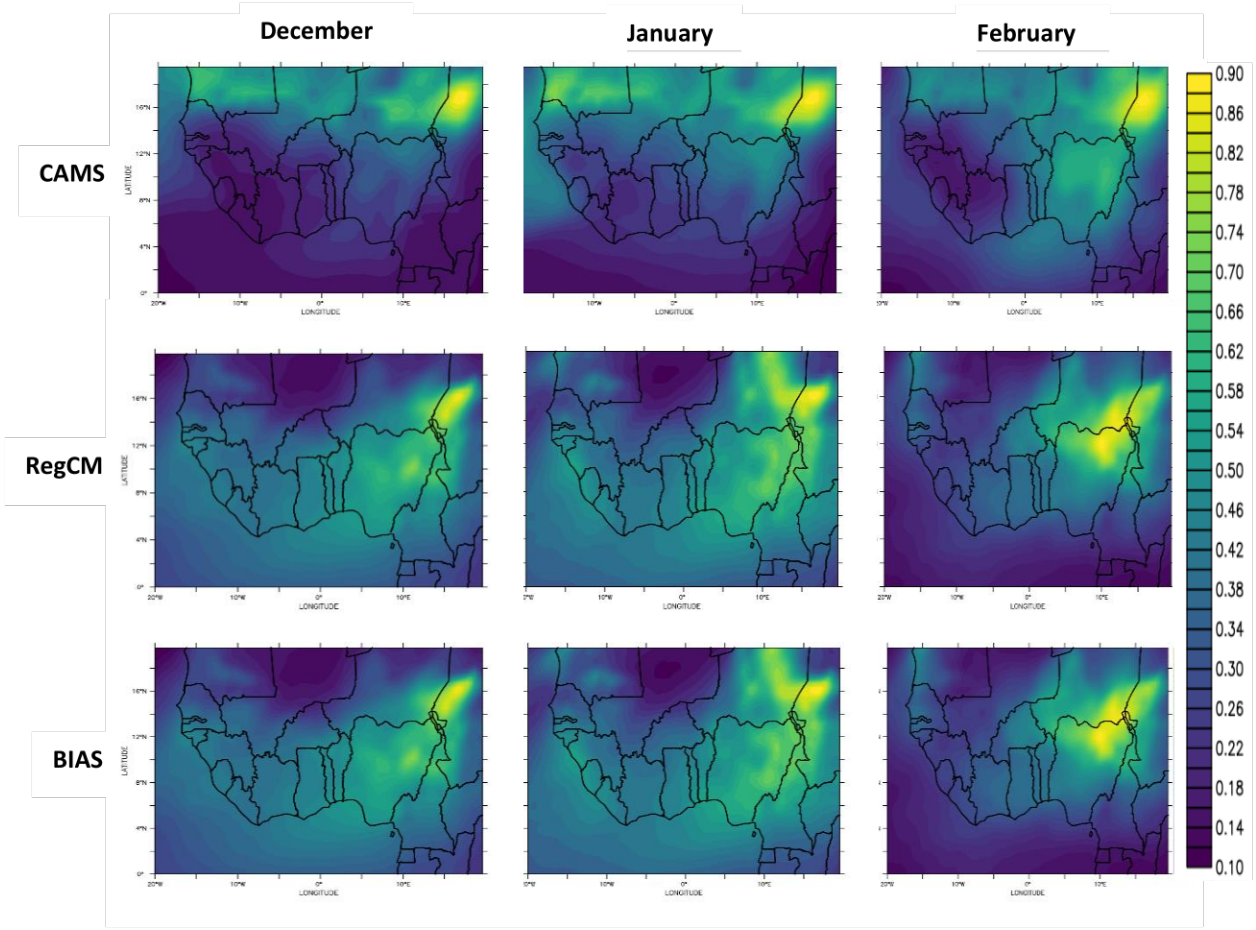

Figure 4.32: Simulated (RegCM4) and observed (CAMS) dust AOD with bias

This makes the DJF dust AOD underestimation high over regions, such as the Guinea climatic sub region where anthropogenic aerosol loading is higher than natural aerosols. Similar underestimation of AOD over the Sahara region during DJF was reported in earlier studies (Camara et al., 2010; Datchoh et al., 2018; Akinyoola et al., 2018, 2019) revealing the inadequacy of emission inventories. Also as stated by Korgo et al., (2021), imprecision of surface albedo representation in CAMS retrieval algorithm (Inness et al., 2019) over the West African region adds up to the AOD disagreement.

Black carbon (BC), one of the most tentative components of aerosols system over West Africa region (Ogunjobi et al., 2004) has strong radiative effects due to its high light absorbing nature. Many reports are available on spatiotemporal distribution of BC and its contribution to radiative forcing and thus to climate (Pathak and Bhuyan 2014; Subba et al., 2018; Boiyo et al., 2019). Also, BC measurements by satellites are non-existent. As such, models are the best tool to obtain regular information on spatio-temporal variability of BC. A few model-based studies on BC including validation against observation over the West Africa are available (Mallet et al., 2009; Malavelle et al., 2011; Zhao et al., 2011). Spatial and seasonal distribution of RegCM simulated BC reported in those studies are in agreement with the current simulations presented in Figure 4.33. The model is capable of capturing the BC hotspots in the study region, particularly during the dry season, thus revealing its capability of replicating the real BC seasonal scenario. However, there exists a difference in magnitude between observation and simulation. According to Korgo et al., (2021), absolute magnitudes of BC mass concentration were underestimated by RegCM by two to five times, with high underestimation in DJF. Model inability to replicate the diurnal variation of BC was found to be the foremost reason for this and is associated with the usage of non-local boundary layers in the model. Also the year average emission files lack the incorporation of local emission activities.

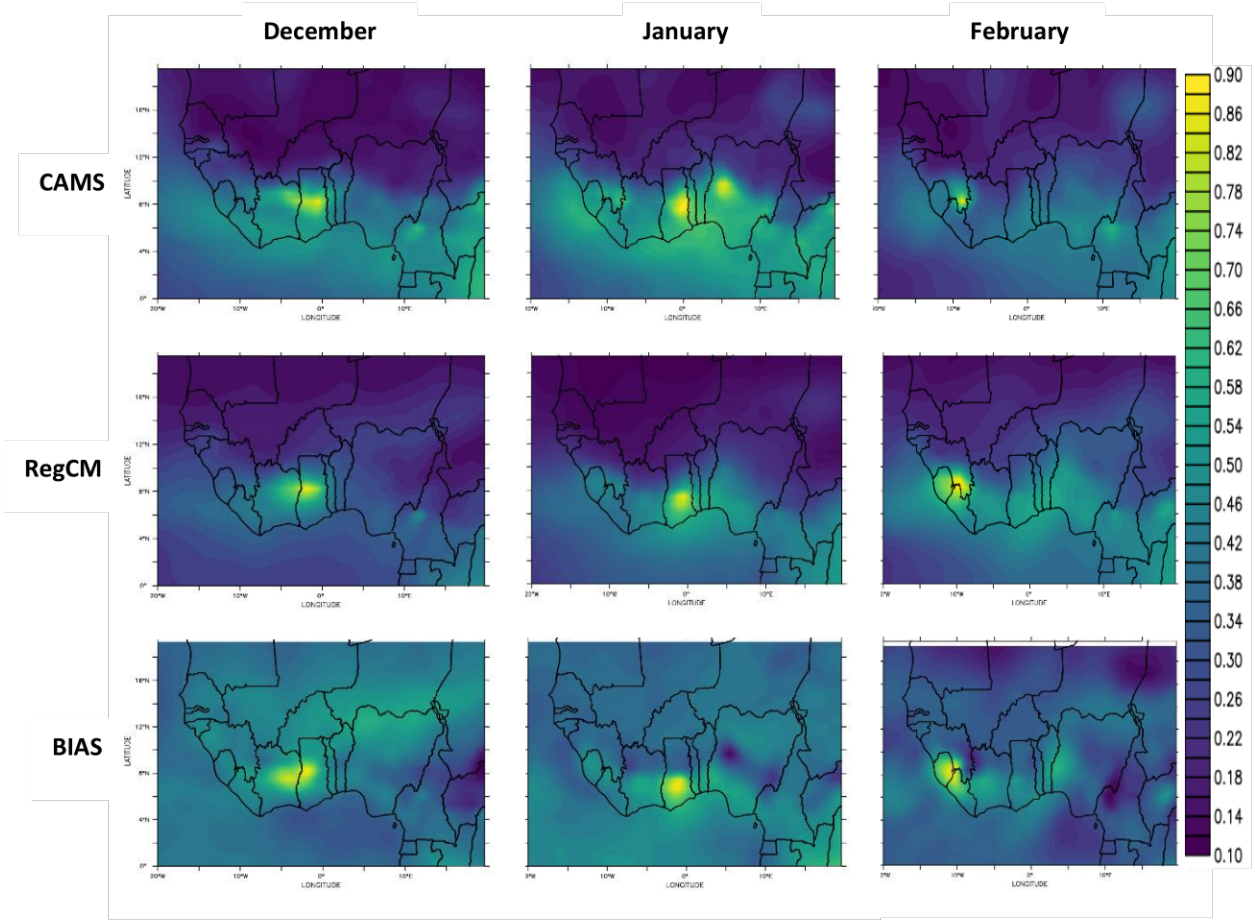

Figure 4.33: Simulated (RegCM4) and observed (CAMS) black carbon AOD with bias

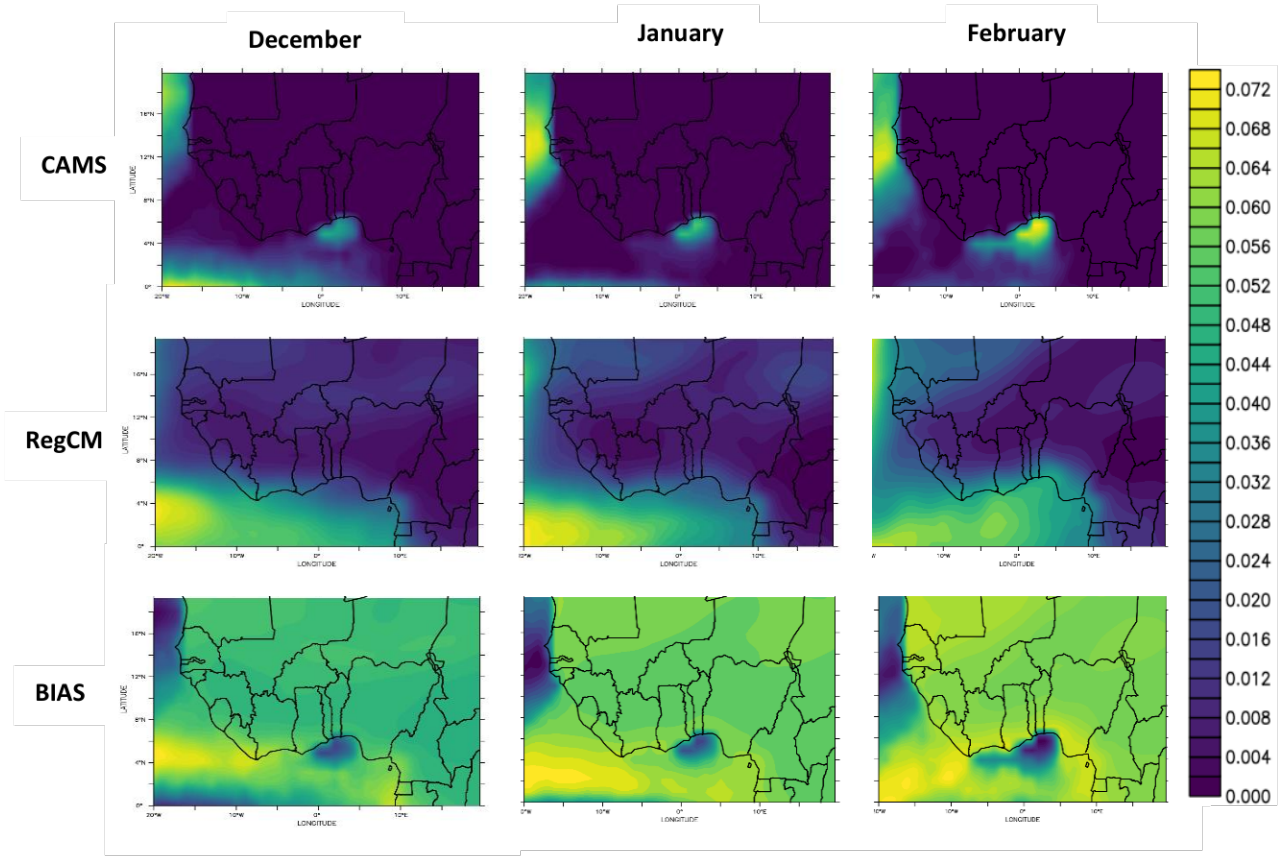

Figure 4.34: Simulated (RegCM4) and observed (CAMS) sea-salt AOD with bias

Figure 4.33 shows the spatio-temporal distribution of black carbon AOD simulated by RegCM at 550 nm, CAMS AOD at 550 nm and the bias over West Africa. Spatio-temporal black carbon AOD variation is well depicted by the model shows good agreement with observations in capturing the variation in BC AOD over time and space, including hotspots over Nigeria and Accra in January, high BC AOD over the Republic of Guinea in December, and low BC AOD over the ocean in February. The CAMS dataset also shows high organic carbon AOD values over the Guinea sub-region in December which can be associated with the intense farming activities and biomass burning. Adebiyi et al. (2020) explained that BC emissions from domestic cooking and heating using solid fuels contribute significantly to air pollution and human health impacts in rural communities in West Africa. Black carbon aerosol from biomass burning can impact cloud properties and precipitation, with implications for regional water resources and agriculture (Haywood et al., 2003). Emissions from West Africa can contribute also to the Saharan heat low and the West African monsoon, affecting rainfall patterns and agricultural productivity. Simulated and CAMS reanalysis black carbon AOD possess less discrepancy during the months, the bias being within ± 0.2. CAMS shows highest organic carbon AOD values (~ 1) over the Guinea sub region during December. This is associated with enhanced anthropogenic activities over this region as also reported earlier (Ogunjobi and Awoleye 2019).

Sea-salt aerosols are produced by the mechanical breakup of sea spray droplets and are a significant source of aerosols in marine environments. It can be noted in Figure 4.34 that the model overestimated sea-salt AOD over the ocean compared to CAMS observations. Sea-salt AOD values above 0.07 were noted across the Gulf of Guinea in the model simulations while values below 0.02 were observed by CAMS. AOD values are higher around the horn of Dakar in January which signifies intense emission of maritime aerosols from the North Atlantic Ocean.

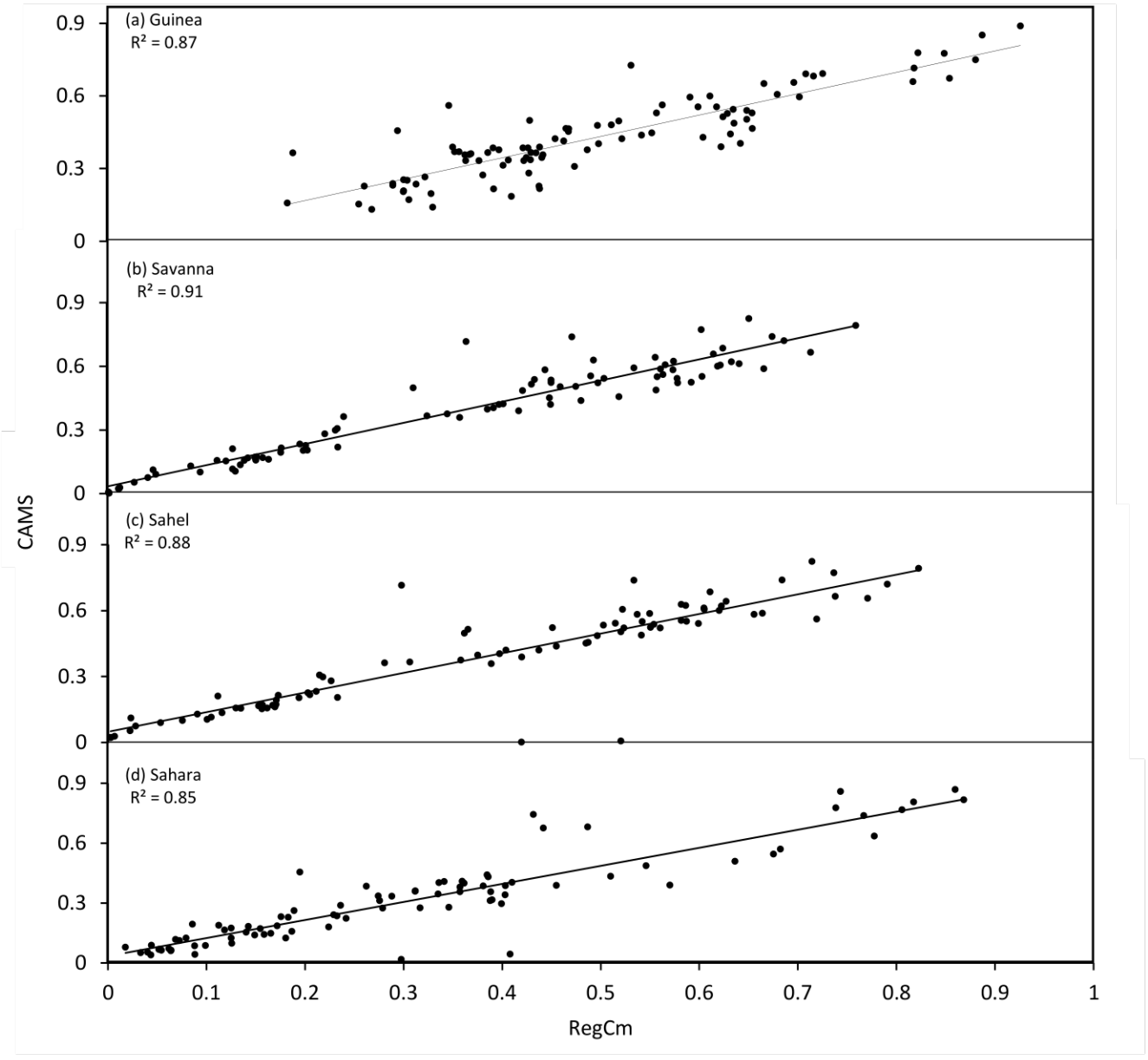

Figure 4.35: AOD correlation plots over (a) Guinea (b) Savana (c) Sahel (d) Sahara for observation (CAMS) with RegCM coupled with CLM 4.5.

Large Bias being within ± 0.8 range can be observed which is attributed to the low ability of the model simulating the maritime type of aerosols over the study domain, but was able to capture the inland flow of the particles. In West Africa, sea-salt aerosols can be transported far inland due to the strong winds associated with the Harmattan, a dry and dusty trade wind that blows southward from the Sahara across West Africa towards the Gulf of Guinea during the winter months (December to February). The transport of sea-salt aerosols can have important implications for regional climate and air quality, as they can contribute to atmospheric heating, affect cloud properties, and impact human health. Limited studies have investigated the characteristics of sea-salt aerosols over West Africa. For example, a study by Flamant et al. (2018) found that sea-salt aerosols can lead to a significant increase in atmospheric heating over West Africa, which can have important implications for regional climate. They also found that the concentration of sea-salt aerosols was highest during the Harmattan season, when the winds were strongest. Aerosols can be transported far inland, with concentrations highest over the Sahel region. The impact of sea-salt aerosols on regional climate can modify cloud properties and reduce precipitation over West Africa, which can have negative impacts on agriculture and water resources.

4.3.2 Intercomparison of Simulated and Observed AOD, ASY and SSA

Figures 4.35-4.37 and Table 4.2 present the correlation results between the daily simulated radiative properties and CAMS observed radiative properties at 550 nm for the four considered climatic zones over West Africa. The plots reveal AOD R^2 values of 0.87, 0.91, 0.88 and 0.85 for Guinea, Savanah, Sahel and Sahara regions, respectively, with the best correlation observed for Savanah. The corresponding statistical metrics of the comparison of each region as the parameters are of vital importance are presented in Table 4.2. The positive intercepts (0.00, 0.03, 0.04, 0.03) observed over the four climatic zones indicate a slight overestimation of surface reflectance (Oluleye et al., 2012, Bibi et al., 2015; Ogunjobi and Awoleye 2019).

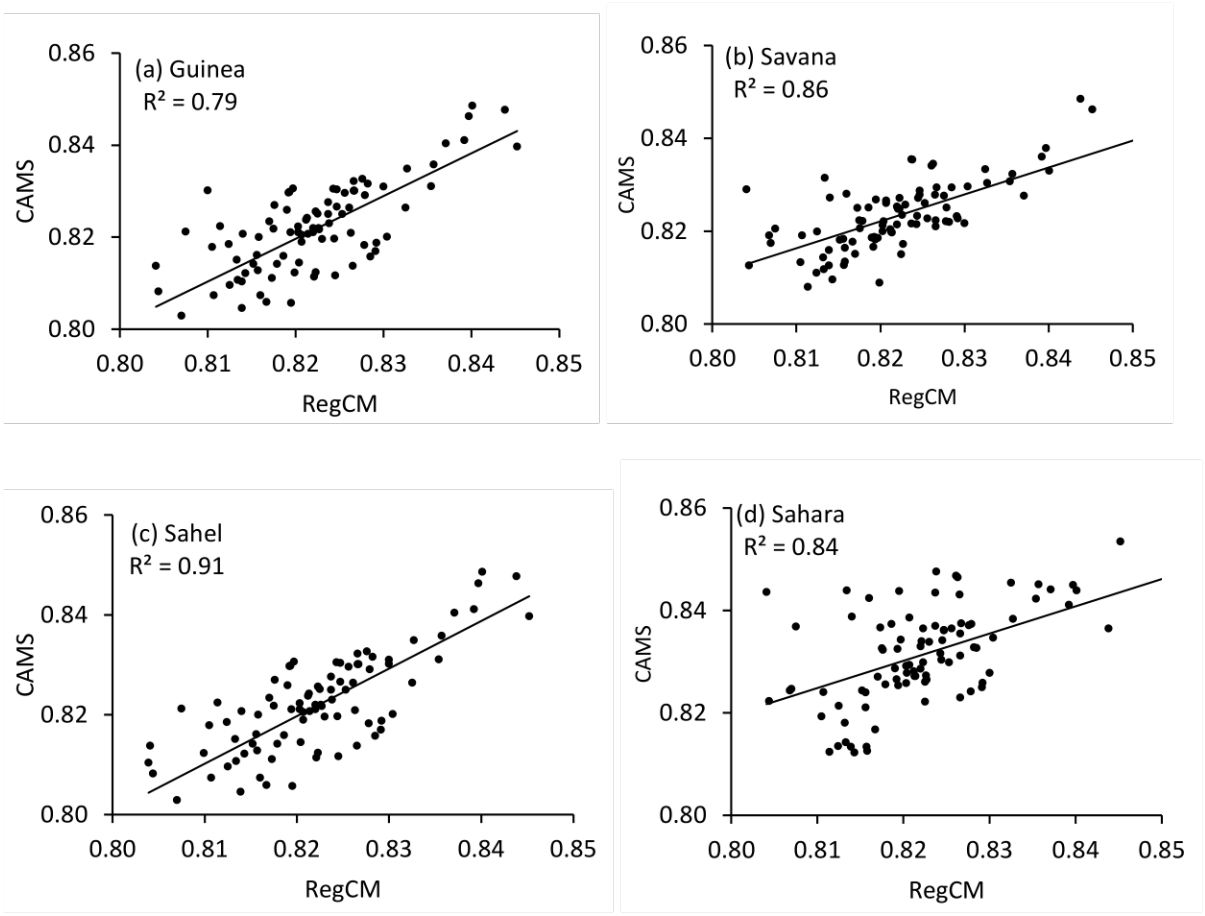

Figure 4.36: ASY correlation plots over (a) Guinea (b) Savana (c) Sahel (d) Sahara for observation (CAMS) with RegCM.

The slopes (m = 0.97, 1.10, 0.89, 0.90) deviated slightly from the ideal state (m = 1), except for the Savanah (1.10) which was underestimated when compared to the other locations. The observed results are an indication that the model underrated AODs over the four climatic zones. However, Anoruo (2023) observed a good correlation over Dakar during the wet season. The SSA from CAMS reanalysis was also compared with simulated AOD as shown in the same Table 4.2. The statistical implications show that correlation values for 550nm were 0.79, 0.74, 0.87, and 0.84 over Guinea, Savana, Sahel, and Sahara, respectively. There exists a strong correlation over the Sahel (0.87) and Sahara region (0.84). This explains that the model performs better than the Guinea and Savana regions. While the Guinea region exhibits the largest bias (5.2) of SSA, negative intercept was also noticed over the region (-0.02) shows an insignificant underestimation of SSA compared to other climatic zones. Also, the slope (m = 1.01) observed in the region confirms the underestimation of the single scattering albedo by the model. The intercepts are thus positive for the four zones having no negative intercept values, indicating a slight overcorrection of surface reflectance. The R^2 value for the Sahel is highest (0.91) compared to the other sites, while Guinea has lowest correlation comparatively (0.79). Even though the model performed well, but there still exists a higher bias, especially over the Guinea region (6.1). The model marginally underestimated the asymmetry parameter over all the locations with slope values ranging from 0.53 to 0.95 which is a deviation from the ideal state of unity. This agrees with the work of Korgo et al., (2021) reported a tendency for regional climate models to have lower asymmetry parameter than observations from reanalysis retrievals.

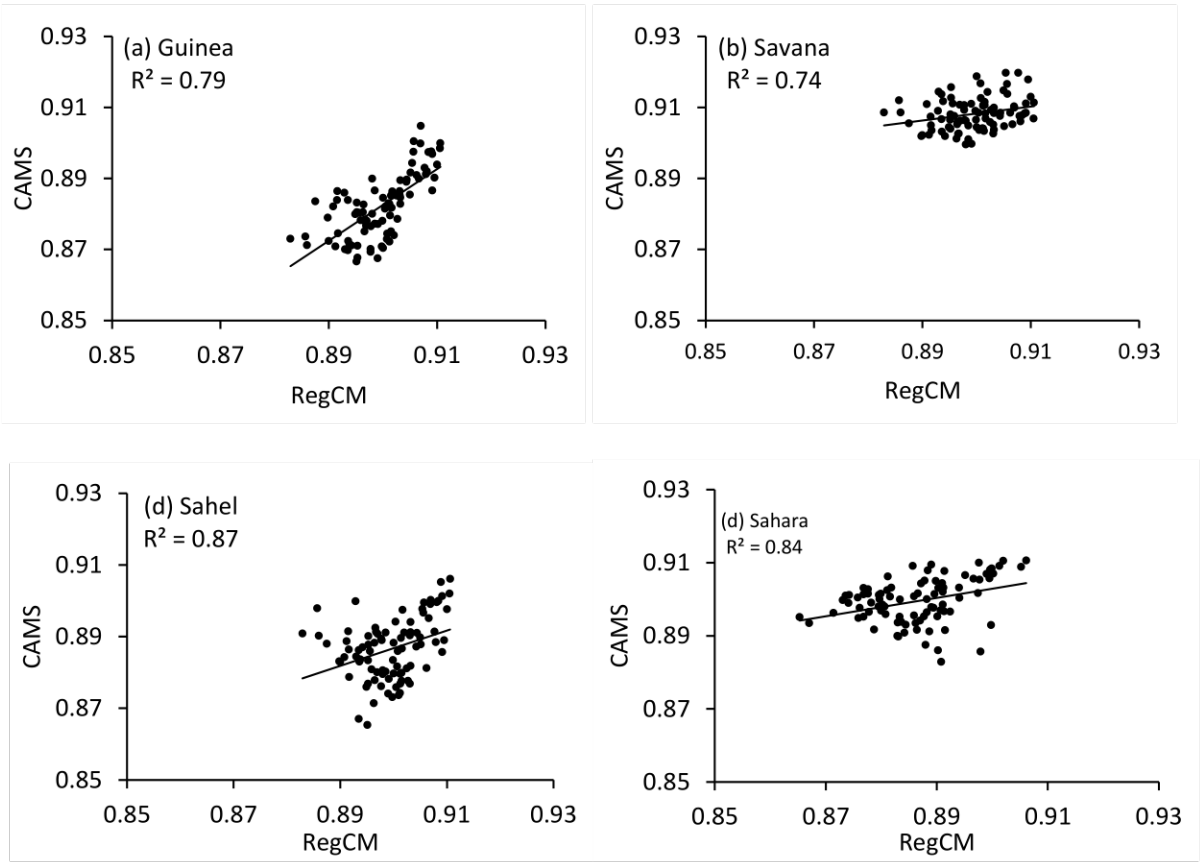

Figure 4.37: SSA correlation plots over (a) Guinea (b) Savana (c) Sahel (d) Sahara for observation (CAMS) with RegCM.

Table 4.2: Regression statistics and % bias of aerosol radiative forcing parameters observations against RegCM simulations over the climatic zones.

Climatic Zones	CAMS vs. RegCM											
	AOD				SSA				ASY			
	R^2	m	c	% Bias	R^2	m	c	% Bias	R^2	m	c	% Bias
Guinea	0.87	0.97	0.00	7.6	0.79	1.01	-0.02	5.2	0.79	0.92	0.05	6.1
Savana	0.91	1.10	0.03	8.5	0.74	0.19	0.73	3.4	0.86	0.53	0.38	5.1
Sahel	0.88	0.89	0.04	4.5	0.87	0.49	0.44	2.2	0.91	0.95	0.03	4.4
Sahara	0.85	0.90	0.03	4.1	0.84	0.25	0.67	2.1	0.84	0.53	0.39	4.4

Overall, RegCM is capable of simulating the real aerosol radiative properties features over the West African domain. Still, the inconsistencies in magnitude existing between the simulated and observed properties can mainly be assigned to the factors such as, (1) emission inventories: as the southern part of West Africa is highly influenced by the local burning and anthropogenic activities whereas emission scenario is not completely capable of recreating the real scenario. It should also be kept in mind that emission retrievals are yearly averaged. (2) As the southern part of West Africa is the highest rain receiving region, replicating observed precipitation with high reliability using model simulation is highly challenging. Wet deposition is one of the main aerosol removal processes and surface wetness is a controlling factor of aerosol production. Along with rainfall, other meteorological parameters also can influence the aerosol simulation (e.g., wind, planetary boundary layer). Hence, the model deficiency in simulating meteorology precisely can impose a bias in aerosol concentration and optical properties ultimately. Therefore, this inability to simulate same rainfall pattern and magnitude also adds to the model discrepancy.

4.4 Radiative Forcing Model Simulation Evaluation

The direct radiative forcing (DRF), which is the means to study the climate implication of aerosols, represents the perturbed radiation flux due to the presence of aerosols, at top of the atmosphere (TOA), in the atmosphere (ATM) and at the surface (SUR). These are estimated with the change in net solar flux considering with and without aerosol conditions. Direct atmospheric forcing (DRFATM) is the difference between the radiative forcing at the top of the atmosphere and at the surface:

$$DRF_{ATM} = DRF_{TOA} - DRF_{SUR} \quad (4.1)$$

These changes are measured by the amount of warming or cooling they can produce, which is called radiative forcing. Changes that have a warming effect are called positive forcing, while changes that have a cooling effect are called negative forcing.

Table 4.3: Regression and error statistics of observations (CAMS, NCEP, and TRMM) against RegCM simulations over the West African region.

Parameters	CAMS/NCEP/TRMM vs. RegCM						
	R^2	m	c	RMB	RMSE	MAE	% Bias
PRE	0.91	0.71	29.13	0.8421	0.0481	0.1764	3.6
MAX TEMP.	0.95	0.38	21.72	0.9605	0.0453	0.1943	3.5
MIN TEMP.	0.92	0.68	7.78	0.8902	0.0495	0.1118	3.4
AOD	0.89	0.79	0.01	0.9348	0.0865	0.0128	4.1
SSA	0.86	0.90	-0.02	0.6784	0.0157	0.1733	5.5
ASY	0.90	0.22	0.31	0.9833	0.0233	0.0193	4.6

Table 4.4: Regression statistics and % bias of observations (NCEP and TRMM) against RegCM simulations over the climatic zones.

Climatic Zones	NCEP/TRMM vs. RegCM											
	PRECIPITATION				MAXIMUM TEMPERATURE				MINIMUM TEMPERATURE			
	R^2	m	c	% Bias	R^2	m	c	% Bias	R^2	m	c	% Bias
Guinea	0.84	0.81	31.22	10.6	0.97	0.65	22.10	3.2	0.97	0.82	10.01	2.5
Savana	0.89	0.84	3.65	9.5	0.96	0.71	25.09	2.1	0.96	0.93	13.06	2.4
Sahel	0.87	0.86	1.12	5.5	0.96	0.68	28.11	2.3	0.96	0.88	18.11	2.1
Sahara	0.92	0.77	0.17	3.1	0.97	1.05	29.11	1.1	0.95	0.95	20.08	1.8

This study only focused on the radiative forcing at the top of the atmosphere and at the surface in order to effectively quantify the effects and dynamics associated with this forcing.

Earlier studies have revealed the importance of studying radiative forcing over the study domain as they contribute to the weakening of the monsoon system (Lau et al., 2006; Akinyoola et al., 2019; Korgo et al., 2021). The average daily mean anthropogenic aerosol-induced radiative forcing at the TOA and SUR from simulation and observation are shown in Figure 4.38. Over the Sahel and Sahara region, aerosols-induced radiative forcing at the TOA is almost 0 or less negative during DJF which exhibited relative cooling in the range -1 to 0 W/m^2 throughout DJF. This is due to low anthropogenic aerosol loading during DJF. On contrary, over the Savana and Guinea region, the forcing exhibits colder effects in the range of -4 to -13 which is induced due to the high surface albedo. The RegCM model was able to capture the cooling experienced over the Guinea climatic zone. During DJF the forcing at the TOA is less in the Sahel region, ranging from 0 to − 4 W/m^2, the TOA cooling increases in the Guinea (-5 to -16 W/m^2) compared to other regions, that can be attributed to the increasing black carbon mass fraction (Pathak et al. 2010). Slightly positive or negative TOA forcing over West Africa during winter is reported before which was correlated to the increase in dust and black carbon mass fraction (Oluleye et al., 2006). During DJF, radiative forcing at the surface over the Sahara and Sahel region domain ranges between 1 and -2 W/m^2 whereas over the rest of the climatic zones it is < -3 W/m2 (Figure 4.39). Radiative forcing at the surface increases northward throughout the study region, with highest over the Sahara. This may be assigned to the steady increase in simulated AOD during this season. Forcing effects reaches as high as >1 W/m^2 over the North Western region during when simulated AOD is also appreciable. The Savana region too experiences significant radiative forcing ranging from 1 to 3 W/m^2.

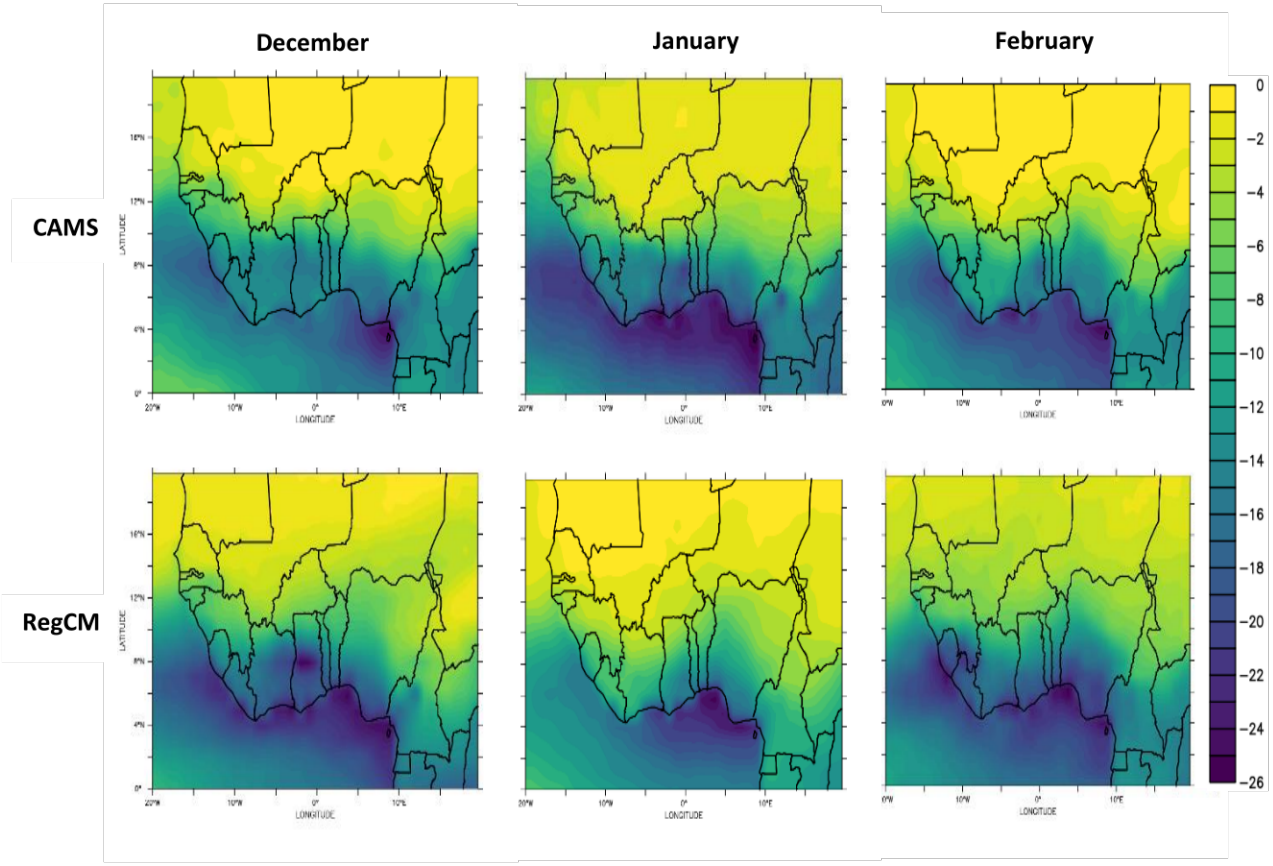

Figure 4.38: RegCM simulated and derived (CAMS) radiative forcing at the top of the atmosphere due to anthropogenic aerosol.

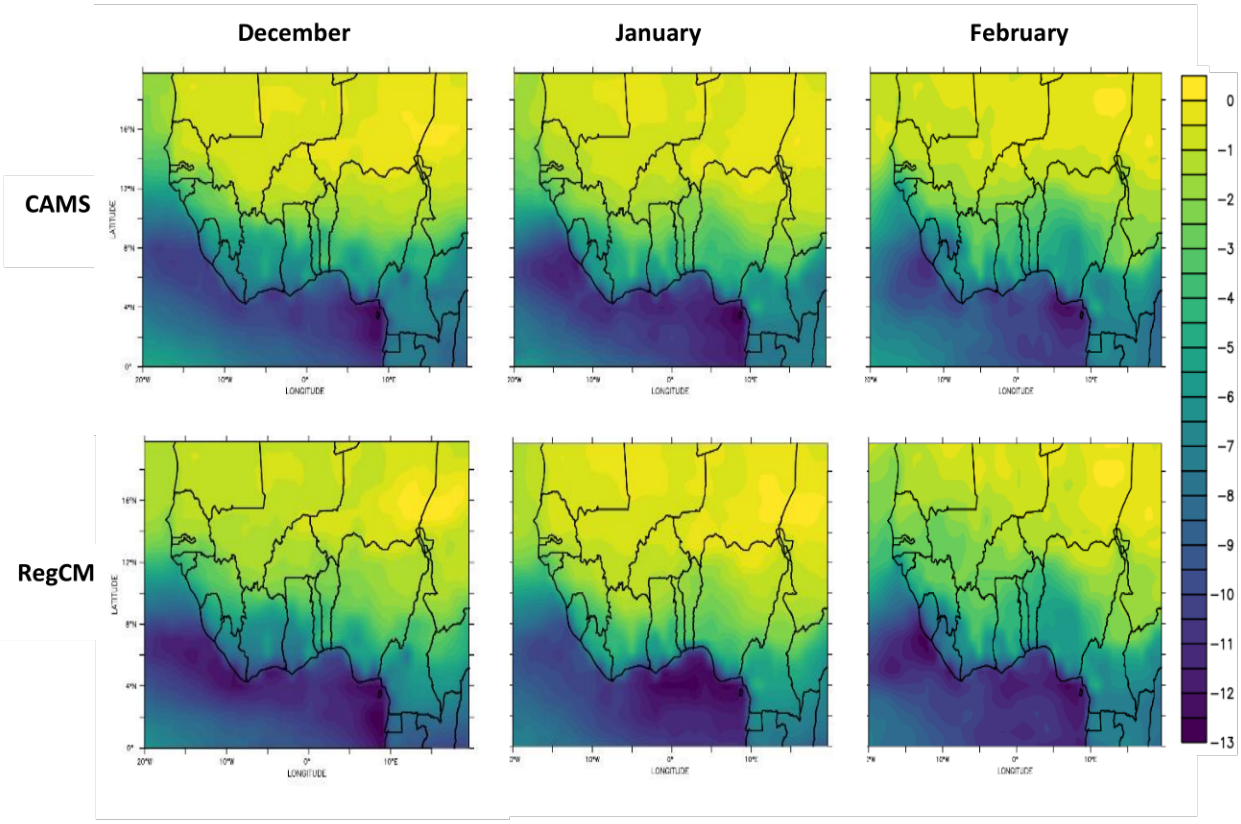

Figure 4.39: RegCM simulated and derived (CAMS) radiative forcing at the surface due to anthropogenic aerosols.

During DJF, anthropogenic aerosol-induced radiative forcing is comparatively less over all the aerosol hot spot regions. The model performed excellently well in its ability to capture the forcing due to anthropogenic aerosols when compared with the CAMS observation.

Figure 4.40 and 4.41 presents the forcing due to dust aerosol at the top of the atmosphere and surface from model simulation and observation. It can be observed that high cooling effect occurred during DJF, especially in February. Hypothetically mineral dust both scatter and absorb short and long-wave radiation energy. Previous analysis shows the mineral dust bands with coarse particles in the Sahel (Figure 4.2, 4.3). Smaller particles of aerosol are seen to be more prevalent in Sahel region, especially in Agoufou, Bodele, Banizoumbou, and Dakar with high single scattering albedo values. Figure 4.40 shows the that there was radiative forcing of about -2 to -4 W/m^2 over the dust band in the Sahel indicating high scattering potential of the dust in the region. There was another important observation at the shore of Mali and Mauritania where there were extension of dust through transportation to the ocean and this increases the water surface albedo which is responsible for the high negative radiation forcing of about -8 to -11 W/m^2 over the Ocean. This has been observed by Miller et al. (2004), Zakey et al. (2006a, b). The figure also shows decrease in radiative forcing at the top of atmosphere from the Guinea coast to between 12 and 14^oN in the Sahel and decrease in the same latitude in the model simulation.

Figure 4.41 shows the radiative forcing at the surface across the entire West Africa region with values ranging from 18 to 12 W/m^2 around Bodele source point region experiment. Increase in dust concentration induced short-wave radiative forcing of -1 W/m^2 at the surface across the Sahara and Sahel dust belt with the highest values at the dust source regions at Bodele and Banizoumbou. The latitudinal pattern of the surface radiative forcing is with simulated maximum value of > 8 W/m^2 between 16 and 18^oN and from 10 to 12 W/m^2 in CAMS observation.

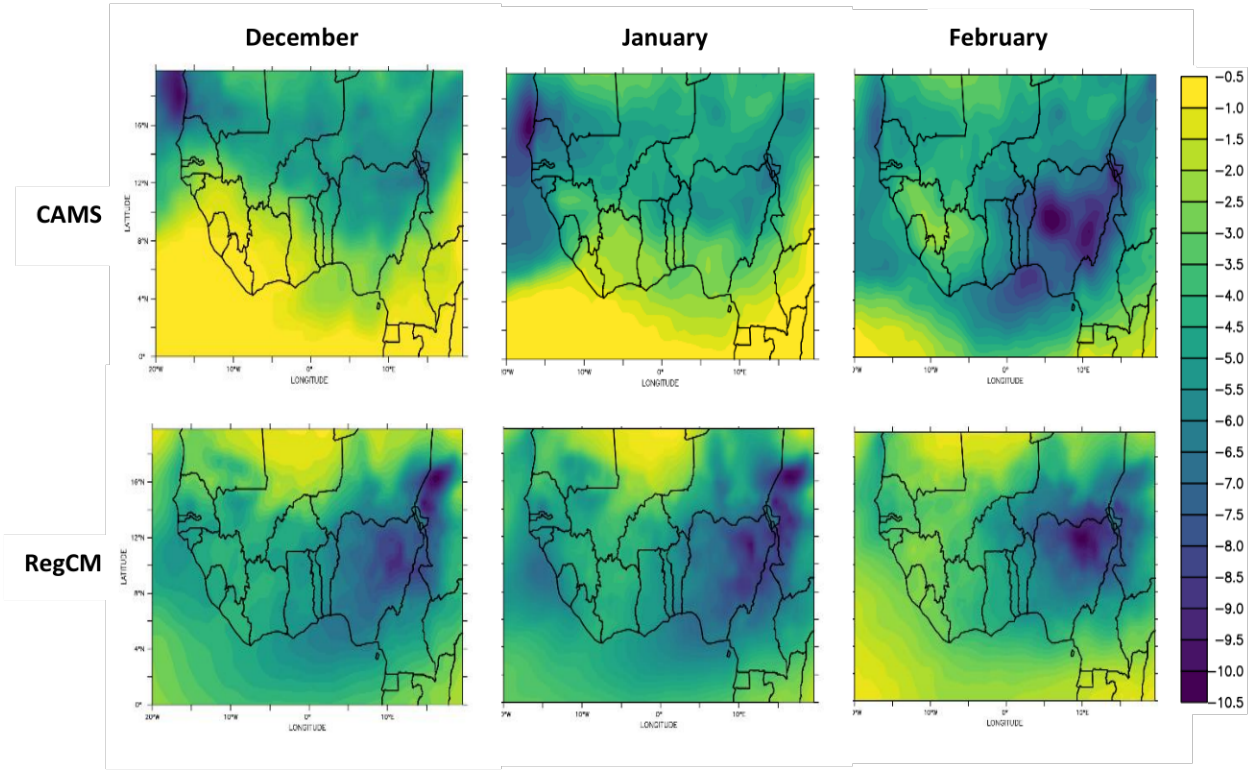

Figure 4.40: RegCM simulated and derived (CAMS) radiative forcing at the top of the atmosphere due to dust aerosol.

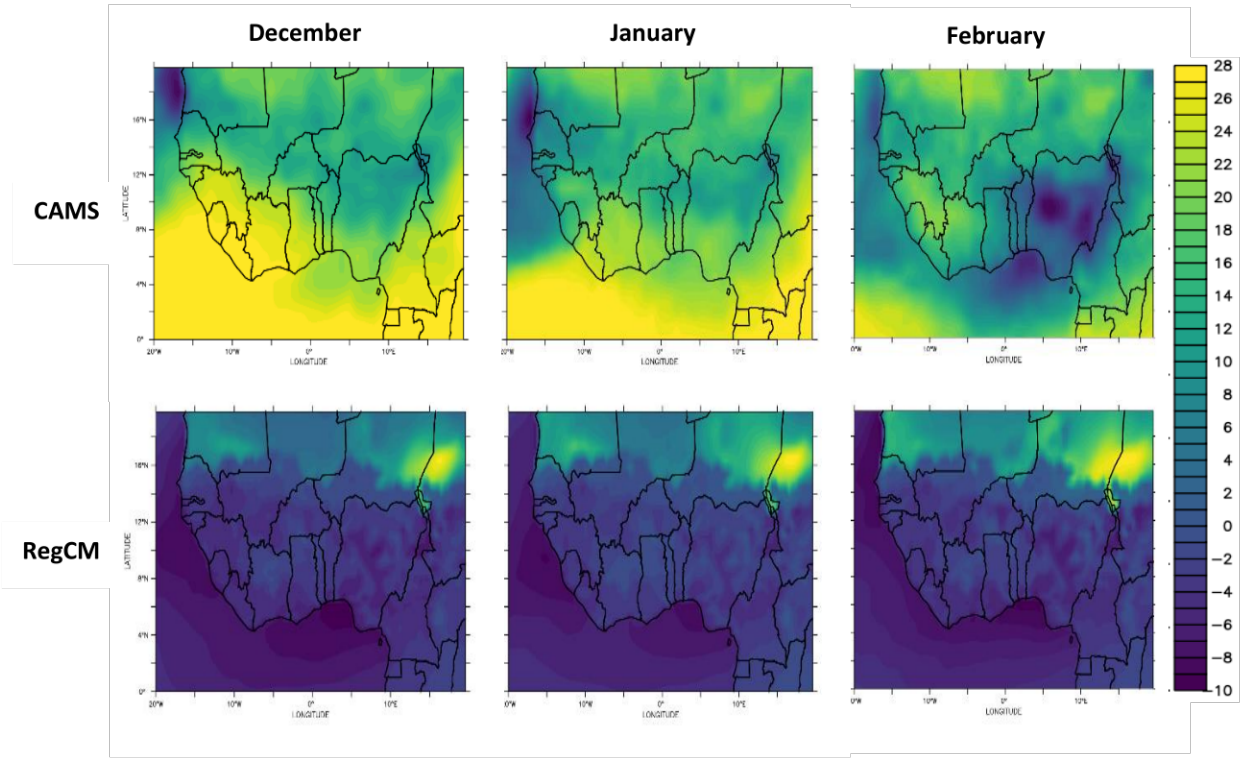

Figure 4.41: RegCM simulated and derived (CAMS) radiative forcing at the surface due to dust aerosol.

The surface short-wave reduction in the region is an indication of surface cooling which is a result of dust concentration variability in the Sahel. Radiative forcing at the surface follows the spatial distribution of AOD in the region. This was also noted by Konare et al. (2008a, b) and Solmon et al. (2008). As the dust concentration increases, there is an increase in the upward long-wave radiation flux across the entire region, thereby reducing potential of cloud formation even in the Guinea coast. The difference between the simulation and observation exerts an effect on the upward long-wave radiation flux, but has larger coverage in the Guinea coast which enhances cloud formation potential in the region.

In West Africa, marine aerosols have been found to play a key role in the region's climate system. Marine aerosols over the tropical Atlantic are transported westward over the region by the prevailing winds, and can have important implications for the timing and intensity of the West African monsoon. Marine aerosols can suppress precipitation over the region, leading to drought conditions, while their absence can enhance rainfall. Mallet et al. (2020) found that marine aerosols were primarily composed of sea salt and organic matter, with smaller contributions from mineral dust and combustion emissions from nearby urban areas over the Gulf of Guinea with significant seasonal and diurnal variations in the aerosol concentrations, driven by changes in wind patterns and other meteorological factors.

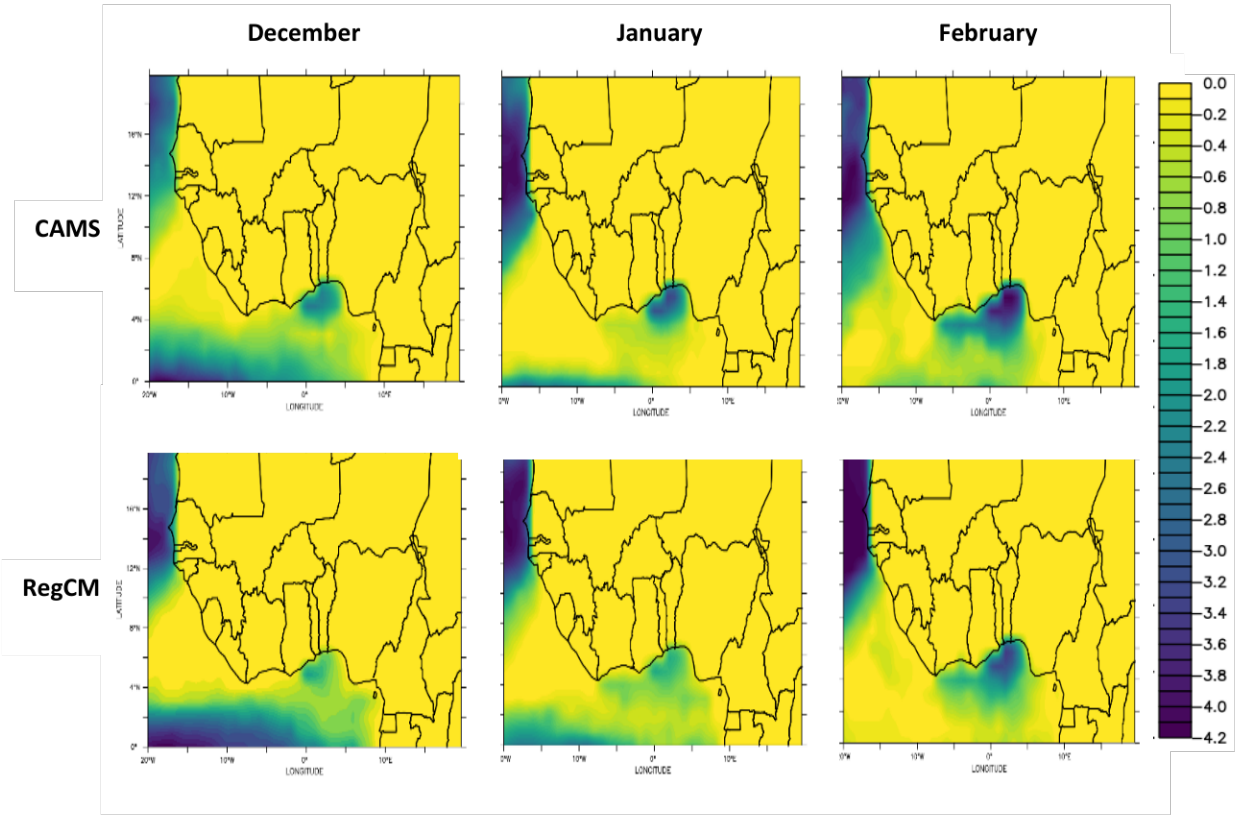

Figure 4.42: RegCM simulated and derived (CAMS) radiative forcing at the top of the atmosphere due to marine aerosol.

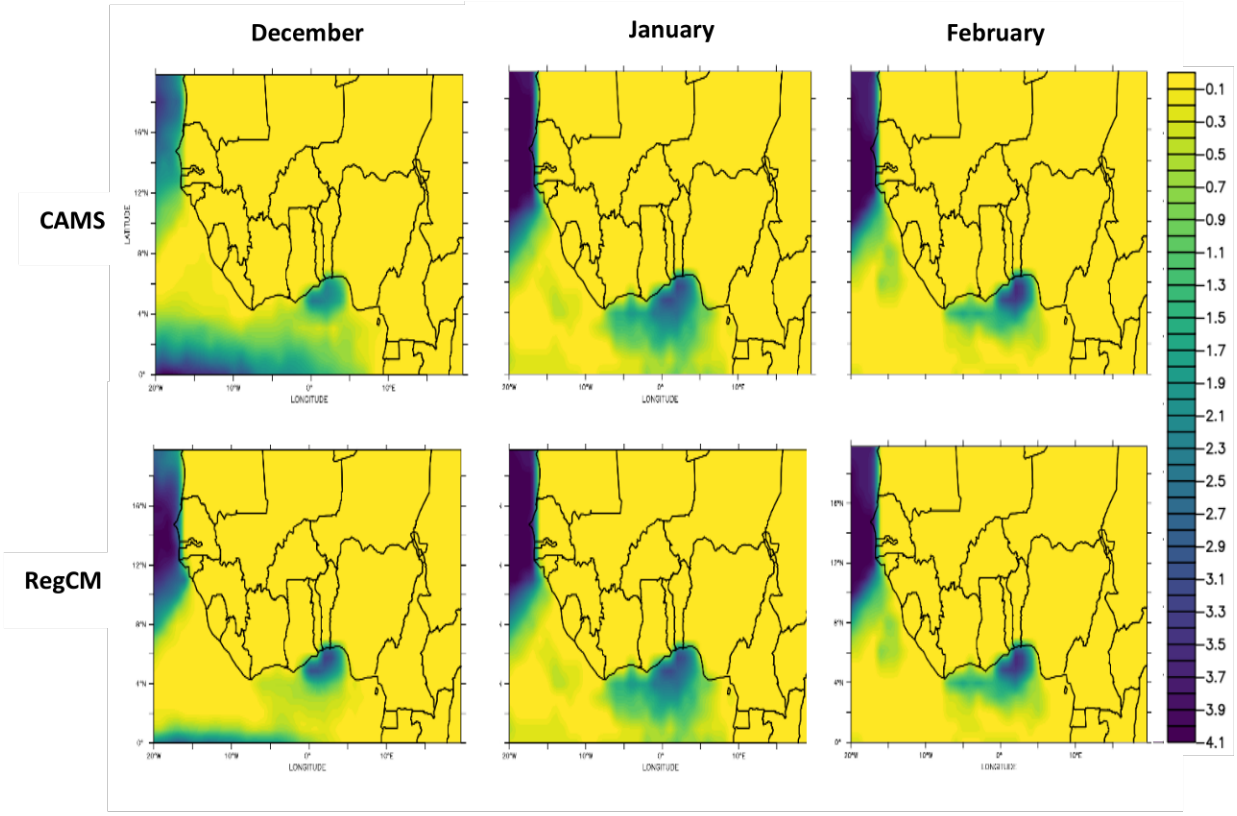

Figure 4.43: RegCM simulated and derived (CAMS) radiative forcing at the surface due to marine aerosol.

The model performs well in simulating the radiative forcing due to marine aerosols, but it underestimates the cooling effect across the Gulf of Guinea in December and January. It can be observed that marine aerosols over the tropical Atlantic have a cooling effect on the region, with a radiative forcing greater than -4 W/m² both at the TOA and SUR and also over the horn of Dakar and Mali. The aerosols' impact on cloud properties was a major contributor to this cooling effect, as the aerosols tended to promote the formation of low-level clouds that reflect more solar radiation back to space. The radiative forcing due to marine aerosols over the coast can also be attributed to widely varying factors such as wind patterns, and the location of nearby pollution sources. This cooling effect is primarily due to the aerosols' ability to scatter solar radiation and reduce the amount of energy that reaches the Earth's surface. It can therefore be noted in Table 4.6 that anthropogenic aerosols such as black carbon and organic carbon contribute significantly to the radiative forcing experienced during the study period. Dust-induced simulation shows a 43.5 and 47.4 for observation. Simulated BC-induced radiative forcing shows 40% contribution to the overall cooling radiative effect experienced during DJF, 2005-2006 while observation shows 42.1% contribution which implies that even though dust is a dominant aerosol type, black carbon emissions and the role it plays in modifying the climate of West Africa cannot be neglected. This result is in contrary to the AMMA-DABEX campaign in 2006, found that the cooling effect of the aerosols and dust particles was due to their ability to scatter and absorb solar radiation, which reduced the amount of energy reaching the Earth's surface. They also found that the aerosols and dust particles acted as cloud condensation nuclei, which affected the size and number of cloud droplets and ultimately influenced precipitation patterns where dust aerosol is being tagged as the aerosol responsible for the cooling radiative effect experienced during this period (Saha et al., 2008; Mallet et al., 2009), hence tagging the emission period as a period popularly known as the “dust episode”.

Table 4.5: Comparison of the CAMS reanalysis and RegCM 4.7.1 simulated (exp_STD and exp_DBL) AOD over the four climatic zones.

Area	DJF			MAM			JJA			SON		
	CAMS	exp_STD	exp_DBL	CAMS	exp_STD	exp_DBL	CAMS	exp_STD	exp_DBL	CAMS	exp_STD	exp_DBL
Guinea	0.50	0.12	0.21	0.48	0.25	0.35	0.56	0.30	0.47	0.39	0.21	0.38
Savana	0.43	0.14	0.26	0.44	0.30	0.41	0.70	0.41	0.59	0.45	0.27	0.47
Sahara	0.32	0.11	0.20	0.51	0.24	0.39	0.34	0.24	0.41	0.22	0.21	0.41
Sahel	0.35	0.15	0.27	0.53	0.24	0.40	0.46	0.21	0.34	0.34	0.25	0.45

Table 4.6: Influence of different types of aerosol on radiative forcing from simulated and derived aerosol variables

Aerosol	% Contribution					
	Savana sim|obs	Guinea sim|obs	Sahara sim|obs	Sahel sim|obs	Overall (Simulation)	Overall (Observation)
Organic Carbon	3.5|2	5|4.4	2.1|1.3	1.4|0.5	12	8.2
Sea-Salt	1|1	3.2|1.2	0.2|0	0.1|0.1	4.5	2.3
Dust	4|6.3	2|2.4	19|19.6	18|19.1	43.5	47.4
Black Carbon	11|10.1	15|20	6|7	8|5	40	42.1

4.5 Model Sensitivity to Enhanced Aerosol Emissions

Interactive coupling of chemistry/aerosol in regional climate models is a relevant topic over West African sub-continent as aerosols have significant effects on the monsoon. Several previous studies have also revealed significant underestimation of aerosols in emission inventories over West Africa in comparison with observations (Ogunjobi and Awoleye., 2019; Nicholson, 2013; Akinyoola et al., 2019; Boiyo et al., 2019). The accurate parameterization of aerosol emissions would help to decrease the uncertainty in aerosol concentrations over the domain and will enhance our understanding of the effects of aerosols, most especially anthropogenic aerosols on the climate over West Africa.

In the model simulation, anthropogenic emissions over the West Africa domain have been increased by 100% (exp_DBL) and are utilized to study the effect of enhancement in regional emissions. The results are compared with the standard experiment (exp_STD) as discussed in Table 4.5 and CAMS reanalysis AOD over the four climatic zones: Guinea, Sahel, Sahara and Savana. This result is in tandem with the observations from the AMMA-DABEX campaign which explained that the presence of aerosols and dust particles in the atmosphere had significant effects on the West African monsoon (Matsuki et al., 2010). The aerosols and dust particles had a cooling effect on the surface temperature, which in turn affected the formation of clouds and rainfall patterns. This led to a reduction in the amount of rainfall over the Sahel region of West Africa, which is already a semi-arid region (Raut and Chazette, 2008; Tanre et al., 2003; Gbobaniyi et al., 2013, 2014). The influence of enhancement in aerosol emission leads to an appreciable increase in AOD over entire West Africa with an increase of 38–97% seasonally over the four sub-regions. Despite the underestimation in comparison with CAMS AOD, significant improvement in model performance in simulating AOD is exhibited by exp_DBL than in exp_STD over all sub-regions during DJF and MAM. Noteworthy influence of enhanced emission is experienced over Guinea during JJA and SON with an increase of

AOD by 55% and 77% respectively. On the other hand, doubling emissions overestimate AOD over Sahara by 48% and 68% during JJA and SON. Simulated AOD in exp_DBL is also high over Savana and Sahel than CAMS retrieved AOD during SON. Overall, the results show that as simulated AOD is very sensitive to aerosol emissions, updating in emission inventory over the region will further improve model credibility. Though exp_DBL experiment reduced the underestimation, still the model underestimates the AOD over hot spots regions like Guinea, revealing that emission inventories miss few of the significant local sources over the domain. Also, the AOD bias with observation is not the same over all the four climatic zones during all the seasons. Hence, the exp_DBL simulated AOD overestimates the observed AOD from CAMS during SON over many sub-regions.

4.6 Impact of Land Use changes on Albedo, Radiative Forcing, and Land Surface Temperature

From the total land area of the study region (5,112,903 km^2) around 5% (128,249 km^2) experienced land cover changes between 2001 and 2006 (Figure 4.44). Of these, grassland to shrubland and savanna to mixed (crop/vegetation) conversions made up 58% of the total land cover change. The remaining land cover changes consisted of shrubland to grassland (15%), grassland to savanna (10.6%), savanna to grassland (8.3%), savanna to cropland (7.2%), and forest to cropland (1.3%) conversions (Table 4.7). Taller to shorter vegetation conversions (i.e., forest to cropland, savanna to grassland, and savanna to mixed crop/vegetation) all displayed consistent mean albedo increase in all seasons. The largest increase was observed in December, January, February (DJF), while the smallest was in September, October, November (SON) in all conversions. In terms of magnitude of change, forest to cropland conversion displayed the biggest mean albedo increase at 0.01 (SD 0.009), followed by savanna to grassland (mean 0.006 and SD 0.007), and savannah to mixed (crop/vegetation) (mean 0.003 and SD 0.005) conversions (Figure 4.45). These conversions generated a corresponding mean instantaneous shortwave radiative forcing (ISRF) of -2.6W/m^2, -1.5W/m^2, and -0.8W/m^2 (Figure 4.45), and

a subsequent average LST cooling of -0.12°K, -0.09°K, and -0.04°K, respectively, all during DJF (Figure 4.46a). Despite the cooling by radiative mechanisms, these conversions generated a substantial and consistent warming of 1.66°K, 0.58°K, and 0.57°K, respectively, from the non-radiative mechanisms (Figure 4.46b). Contrary to the rest of taller to shorter vegetation conversions, savanna to cropland conversion exhibited inconsistent patterns across seasons in the albedo, radiative forcing and change in LST. In land cover changes occurring in shorter vegetation types, grassland to shrubland and grassland to savanna showed relatively small yet consistent rise in albedo in all seasons (Figure 4.45). The maximum average albedo change was in DJF and the minimum in SON for both conversions. The maximum mean albedo increase of 0.005 (SD 0.008) in grassland to shrubland and a mean of 0.003 (SD 0.006) in grassland to savanna conversions resulted in an average ISRF of -1.38W/m^2 and -0.8W/m^2 (Figure 4.45).

In land cover changes occurring in shorter vegetation types, grassland to shrubland and grassland to savanna showed relatively small yet consistent rise in albedo in all seasons (Figure 4.45). The maximum average albedo change was in DJF and the minimum in SON for both conversions. The maximum mean albedo increase of 0.005 (SD 0.008) in grassland to shrubland and a mean of 0.003 (SD 0.006) in grassland to savanna conversions resulted in an average instantaneous shortwave radiative forcing of -1.38W/m^2 and -0.8W/m^2 (Figure 4.45), and a LST cooling of -0.08°K and -0.04°K, respectively (Figure 4.46b), whereas the corresponding ΔT_s due to non-radiative mechanisms showed inconsistent pattern across seasons (Figure 4.46a). In shrubland to grassland conversions, on the other hand, mean albedo showed a very small and inconsistent variation across seasons (i.e. albedo increased by 0.002 in DJF; decreased by the same magnitude (-0.002 in SON); and displayed a relatively small increase in June, July, August (JJA) (mean 0.0002) and March, April, May (MAM) (0.0007) (Figure 4.45). The DJF and SON albedo change has a radiative forcing of -0.4W/m^2 and

0.4W/m^2, respectively (Figure 4.45). The DJF albedo-increase caused -0.03^{o}K cooling while the SON albedo reduction brought warming of same magnitude (Figure 4.46b). Similar inconsistent patterns in ΔT_s were exhibited by the non-radiative mechanisms across seasons (i.e. cooling in DJF and warming in SON by the same magnitude) in shrubland to grassland conversions (Figure 4.46b). The average RISRF estimated from the relative contribution of each land cover conversion class showed negative forcing and considerable variation across seasons. The maximum mean regional instantaneous shortwave radiative forcing was in DJF (-0.056W/m^2) and the minimum in SON (-0.008W/m^2). Overall, land cover changes in the region exerted a mean annual instantaneous shortwave radiative forcing of -0.03W/m^2 ± 0.02 (Table 4.8).

Furthermore, the degree of agreement between T_s and ΔT_s across seasons was assessed in a scatterplot (Figure 4.47). The result showed that the observed and calculated LST difference had moderate agreement (Figure 4.47). The agreement was the best ($r^2 = 0.77$) in the dry season (DJF). Besides, the wet seasons (MAM and SON) demonstrated very similar results ($r^2 = 0.61$ and 0.62), while JJA displayed the lowest agreement ($r^2 = 0.50$), indicating higher uncertainty in the calculated LST changes during this period.

4.6.1 Impact of Land Use changes on Surface Radiation Balance, and Albedo Contribution to Land Surface Temperature change

Land cover change showed a consistent increase in mean albedo and a corresponding negative radiative forcing across all seasons, except for shrubland to grassland and savanna to cropland conversions. Despite the average increase in albedo, significant within-class variability was observed, with albedo change ranging from -0.04 to 0.04. The biggest impact on the surface radiative balance and surface temperature through radiative changes is caused by taller vegetation conversions (forest to cropland and savanna to grassland). In these conversion classes, unlike others, around 75% of the total pixels had an increase in albedo, and exhibited

the biggest local impact on mean ISRF (-2.6W/m^2) and surface temperature cooling by radiative mechanisms of up to -0.12^{o}K.

The overall increase in albedo resulting from the replacement of taller vegetation can be explained by the smaller albedo of taller vegetation compared with brighter shorter vegetation (Betts and Ball, 1997; Hollinger et al., 2010). Despite the average increase, however, up to 25% of the pixels showed decrease in albedo. This likely indicates that albedo is influenced not only by the vegetation structure but also by the underlying local conditions (such as soil albedo, rainfall, soil colour and moisture, etc.) (Bright et al., 2015). In other words, when the background surface is brighter, albedo can increase in taller to shorter vegetation conversions. The maximum influence of albedo increase on LST occurred in the dry season (DJF) and the smallest in the wet season (SON). This is likely owing to soil moisture content enhancement that increases the amount of incident solar radiation absorbed by the soil system and reduces background surface albedo, leading to a small difference in albedo values compared with the dry period (Wallace et al., 1990). The inconsistencies observed in shrubland to grassland conversions can be attributed to the small difference in their albedo values together with the influence of background surface albedo, which can be strong in determining the overall albedo in such open-canopy ecosystems (Campbell and Norman, 1998). Furthermore, grassland to savanna conversion, which was expected to show a decrease in albedo compared with savanna to grassland conversion, displayed an opposite result (i.e., an increase in albedo). The conversion classes do not occupy the same geographic location or pixel (i.e. they do not share exactly same background material) and hence the influence of background material can vary depending on the soil colour and moisture condition of that location or pixel. This likely can affect and determine the sign and magnitude of albedo change and may lead to an overall average increase in albedo in this conversion class (Campbell and Norman, 1998).

(a)

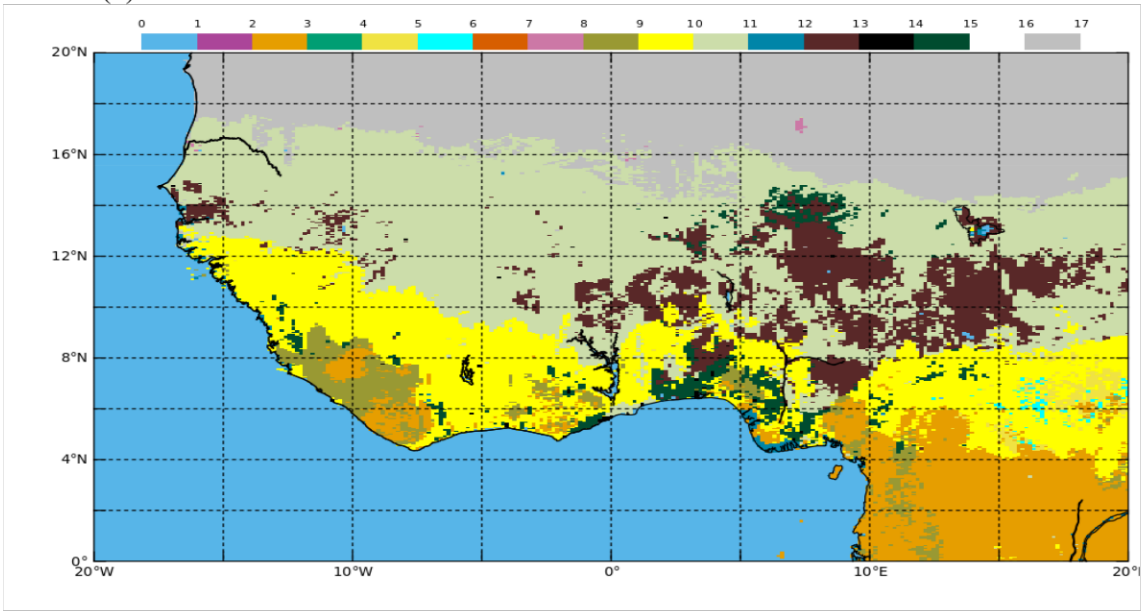

(b)

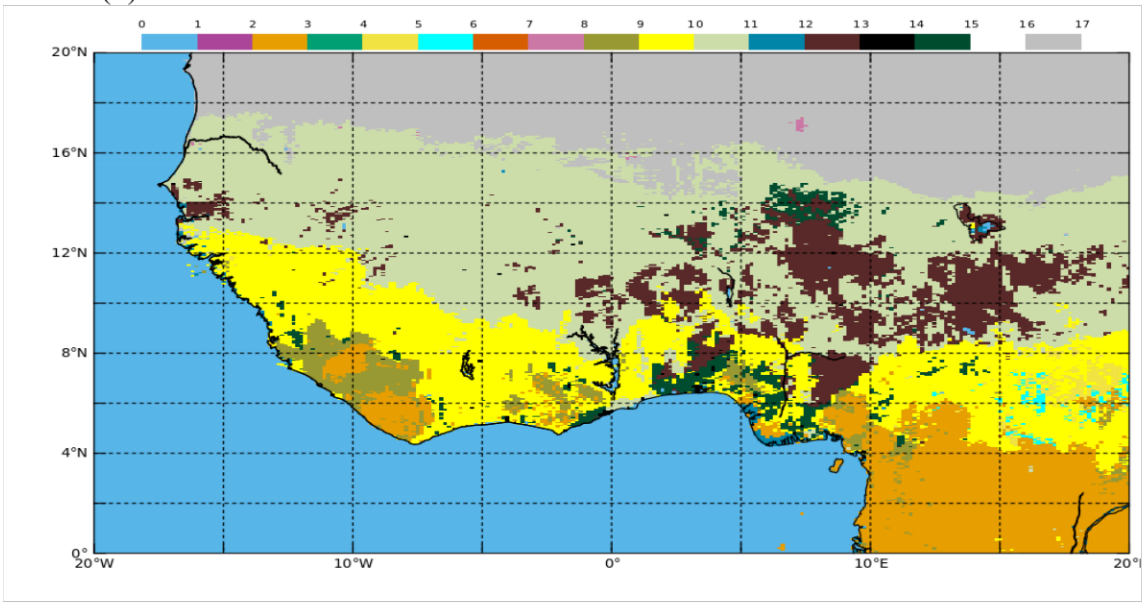

Figure 4.44: Moderate Resolution Imaging Spectro-radiometer (MODIS) (a) 2001 (b) 2006 land cover map.

Classifications: (0) Water bodies; (1) Evergreen Needle leaf Forests; (2) Evergreen Broadleaf Forests; (3) Deciduous Needle leaf Forests; (4) Deciduous Broadleaf Forests; (5) Mixed Forests; (6) Closed Shrub lands; (7) Open Shrub lands; (8) Woody Savannahs; (9) Savannahs; (10) Grasslands; (11) Wetlands; (12) Croplands; (13) Urban and Built; (14) Natural Vegetation; (15) Snow and Ice; (16) Barren Lands.

Savanah to cropland change can similarly be affected by the background albedo. Moreover, the difficulty in accurately separating small-scale croplands, which often occur mixed with other vegetation at 1 km resolution (Zhang et al., 2005), can cause inconsistencies in the observed results. Further studies using high resolution land cover and soil data are needed to better quantify the actual albedo changes in such conversion areas.

Overall, when the radiative impacts from all land cover changes is considered, the regional instantaneous shortwave radiative forcing obtained (-0.03W/m^2) was smaller than the global radiative forcing estimate (-0.09W/m^2) (Myhre et al., 2013). This is due to three reasons. First, the total area affected by land cover changes in the region during 2001-2006 was around 5%. Second, the biggest local radiative forcing was obtained from forest to cropland and savanna to grassland conversions, which constitute only 1% and 8% of the total land cover change area, respectively. Third, the global estimate represents the period since pre-industrial times (i.e., radiative forcing reported using 1750 as the reference time (Myhre et al., 2013)), and hence compared with this time, the change in land cover over 13 years (2001-2006) can be small. Although land cover changes dominantly increased albedo in the region, the net LST displayed mainly warming in taller vegetation conversions. This opposing result indicates that the radiative cooling effects of land cover change are less influential (maximum -0.12^{o}K in forest to cropland conversions) and are largely outweighed by warming impacts from non-radiative processes (e.g., ET and surface roughness) by a maximum of >10 times (1.66^{o}K) (Figure 4.46). As a result, an overall warming of up to 1.2^{o}K occurred in the study region from forest to cropland changes. This result supports earlier findings of observational (Li et al., 2016; Cabral and Costa, 2017), and modelling studies (Zhang et al., 2017; Ding et al., 2022) in the tropics, which all reported warming after deforestation. The warming in forest to cropland conversion in the region is related to a decrease in ET efficiency following leaf area decline and a shift to a shallow rooting system (Claussen et al., 2001; Davin and de Noblet-Ducoudre, 2010; Bonan,

2008). The larger warming during dry period, in comparison with the rainy seasons, can be explained by the enhanced soil moisture and ET, a reduction in the radiation loading due to clouds, and the strong rainfall-vegetation interaction in wet periods (Abera et al., 2018). Moreover, the forests tend to maintain their higher ET efficiency during the dry period through their deep rooting system unlike croplands, and this further increases the difference in warming during dry period (Li et al., 2015).

Savanah to grassland conversions also showed warming across all seasons over West Africa. The warming in this conversion can be explained by the decline in the woody cover, which can affect the structural and functional properties of the savanna (Hoffmann and Jackson, 2000). Moreover, the consistent warming by non-radiative mechanisms in the region further suggests a decline in ET and surface roughness due to the decrease in woody cover (Fig 4.46). Savannahs, compared with grasslands, have higher surface roughness (Miranda et al., 1997), rooting depths (Jackson et al., 1997), as well as LAI, and hence their conversion to grassland leads to warming. Although the impact of savanna to grassland conversion on LST using observational data is rare in the region, modelling studies showed a 0.5°C mean increase in air temperature in the tropics (Hoffmann and Jackson, 2000). Although land surface temperature and air temperature are different in their meaning and magnitude (Jin and Dickinson, 2010), the impact of land cover changes is likely to have similar patterns in these two variables. For instance, several studies have indicated that changes in woody vegetation (e.g., forest) to grassland/cropland increases both surface and air temperature in the tropics (Alkama and Cescatti (2016), Ge et al., (2021), and Duveiller et al., (2020) for an extensive review of the literature). A consistent cooling across seasons was observed when the conversion was the other way around (i.e., grassland to savanna). Such a result further indicates the importance of woody-cover change in determining temperature shift.

Table 4.7: Land Cover Conversions and their Area Coverage

Conversion type	Area (km^2)	Percentage change (%)
Grassland to shrubland	47,881	37.3
Savanah to mixed (crop/vegetation)	26.046	20.3
Shrubland to grassland	19,202	15
Grassland to savanna	13,580	10.6
Savanah to grassland	10,634	8.3
Savanah to cropland	9,249	7.2
Forest to cropland	1657	1.3
Total area	**128,249**	

Table 4.8: Seasonal regional radiative forcing metrics for all land cover change classes over West Africa during 2001−2006.

Land cover category	Mean Instantaneous Shortwave Surface Radiative Forcing ($-SW_{in} * \Delta\alpha$) in W/m^2				Mean Regional Instantaneous Shortwave Surface Radiative Forcing ($-SW_{in} * \Delta\alpha) * A_i/A_t$ in W/m^2			
	DJF	MAM	JJA	SON	DJF	MAM	JJA	SON
Grassland to shrubland	-1.400	-1.000	-0.800	-0.300	-0.027	-0.019	-0.015	-0.006
Savanah to mixed (crop/vegetation)	-0.800	-0.400	-0.100	-0.020	-0.008	-0.004	-0.001	0.000
Shrubland to grassland	-0.400	-0.200	0.040	0.400	-0.003	-0.002	0.000	0.003
Grassland to savanna	-0.800	-0.900	-0.500	-0.090	-0.004	-0.005	-0.003	0.000
Savanah to grassland	-1.500	-1.200	-0.900	-0.600	-0.006	-0.005	-0.004	-0.003
Savanah to cropland	-1.200	-0.500	0.200	-0.200	-0.004	-0.002	0.001	-0.001
Forest to cropland	-2.600	-1.900	-1.700	-1.700	-0.002	-0.001	-0.001	-0.001
Total	**-8.700**	**-6.100**	**-3.760**	**-2.510**	**-0.056**	**-0.038**	**-0.023**	**-0.008**
Annual mean	**-5.268**				**-0.031**			

When the impacts of the different land cover change classes on observed LST compared, forest to cropland and savanna to grassland conversions generated more warming than others. Furthermore, the conversion of natural vegetation to cropland (i.e., forest to cropland, savanna to cropland, and savanna to cropland/vegetation) alone constitute 28.8% of the land cover changes in the region. This can cause a considerable anthropogenic impact on the climate through generating a cooling radiative forcing. Hence, owing to their stronger impact on climate, future anthropogenic pressure on forests and savannas through cropland land expansion will cause further warming in the study domain. Besides, when such anthropogenic pressure is coupled with the increasing trends of drought intensity in the region (Nicholson, 2017), climate change impacts can be amplified through additional warming from land cover changes.

In forest and savanna, albedo increased during the vegetation growing period (Figure 4.48a, b). In forest, BSA increased by 8%, and in savanna it increased by 27%, between winter minima and growing season maxima. Both displayed an offset with LAI seasonality in the growing period (i.e., albedo reached a peak value before LAI by up to two weeks in forest and four weeks in savanna, and sharply decreased afterwards). The albedo increments in forest and savanna, during the growing period, caused a -2.47 W/m^2 and -10 W/m^2 decrease in available energy, respectively (Table 4.9). In grassland and shrubland, albedo and LAI had opposite seasonal patterns (Fig. 2c, d). In the growing period, albedo decreased by 18% in grassland and by 10% in shrubland between the maximum and minimum values in winter and the growing season, respectively. The negative relationship between albedo and LAI seasonality had an offset of ~1–2 weeks in grassland and a small offset (~1 week maximum) in shrubland. The decline in albedo during the growing period in grassland and shrubland resulted in a rise in available energy of 7.11 W m^{-2} and 5.04 W m^{-2}, respectively (Table 4.9).

The Spearman correlation between albedo and LAI seasonality across the study region showed a similar pattern, i.e., deciduous forest and savanna displayed a mainly positive correlation ($r > 0.7$), while shrubland and grassland of a significant albedo-LST relation. However, albedo and LST dominantly had a non-significant ($P > 0.05$) relation for large parts of the study region. Overall, the results showed that the radiative impact of albedo change on LST seasonality, either in the growing period or during land cover transitions, was relatively small in comparison with the influence of non-radiative processes (e.g., ET). Hence, our results highlight the importance of accounting for non-radiative mechanisms for a better quantification and understanding of the impacts of land cover change on climate, as well as for setting effective land use policies and mitigation strategies in the region.

Finally, it should be noted that our assessments carry uncertainties associated with the inherent limitations of the data sources used. For example, in land cover change analysis, although we have attempted to minimize the impact of land cover classification accuracy (~75%) on the results by focusing on changes between stable pixels in the first and last five years of 2001-2006, incorrectly identified pixels can exist in the analysis and this might introduce uncertainty in the results. However, the impact of such uncertainty has been minimized by taking the average value in each land cover change class. Also, the use of the empirical method of Lee et al. (2011) to calculate LST change from individual contribution by radiative and non-radiative processes using satellite observation data can be affected by the inherent limitations of the data (i.e., LST changes within 1 km^2 pixels were assumed homogeneous due to a limitation of the spatial resolution, but in reality LST change can vary as long as land cover type differs within the 1 km^2 pixels). Furthermore, in quantifying the uncertainty in our LST estimation, despite the unavailability of in-situ flux data in the region, we tested and showed the robustness of the method by comparing the calculated LST change from the model with the observed LST change from the MODIS LST. The results (Figure 4.47) showed reasonably good agreement

(r^2 = 0.77), particularly during the dry period (DJF). Nonetheless, the future availability of ground flux tower data across different land cover types in the region will help improve quantification of the uncertainty in such a method.

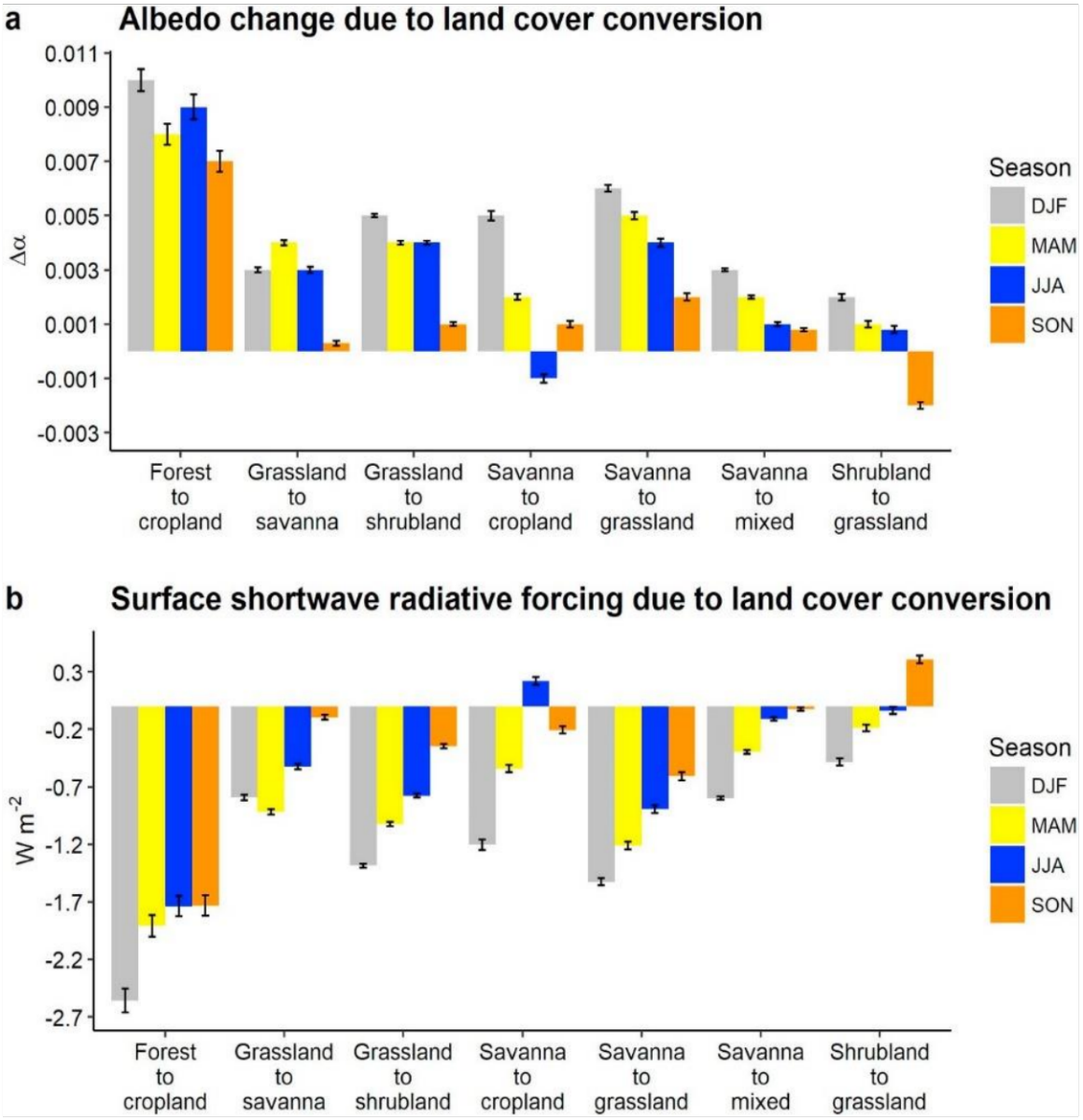

Figure 4.45: (a) Seasonal mean albedo change and (b) instantaneous surface radiative forcing (ISRF) associated with land cover conversions during 2001–2006 over West Africa. All land change pixels were considered for each conversion class in four seasons (DJF, MAM, JJA, and SON). Error bars show the 95% confidence interval. DJF =December, January, February; JJA = June, July, August; MAM =March, April, May; SON = September, October, November.

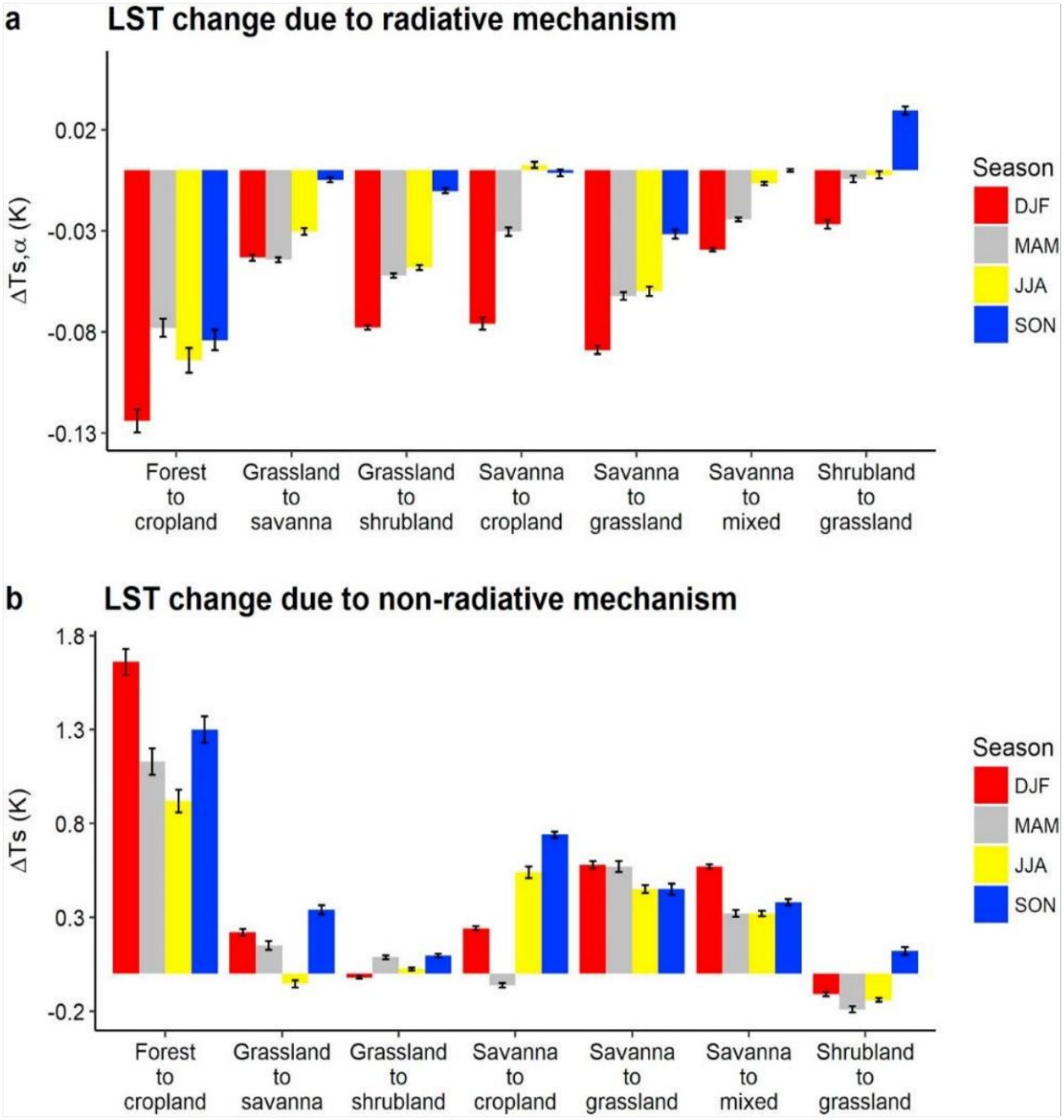

Figure 4.46: Contribution to average observed land surface temperature (LST) change by (a) radiative and (b) non-radiative mechanisms following land cover conversions over West Africa between 2001 and 2006 in four seasons. Error bars show the 95% confidence interval. DJF =December, January, February; JJA = June, July, August; MAM = March, April, May; SON =September, October, November.

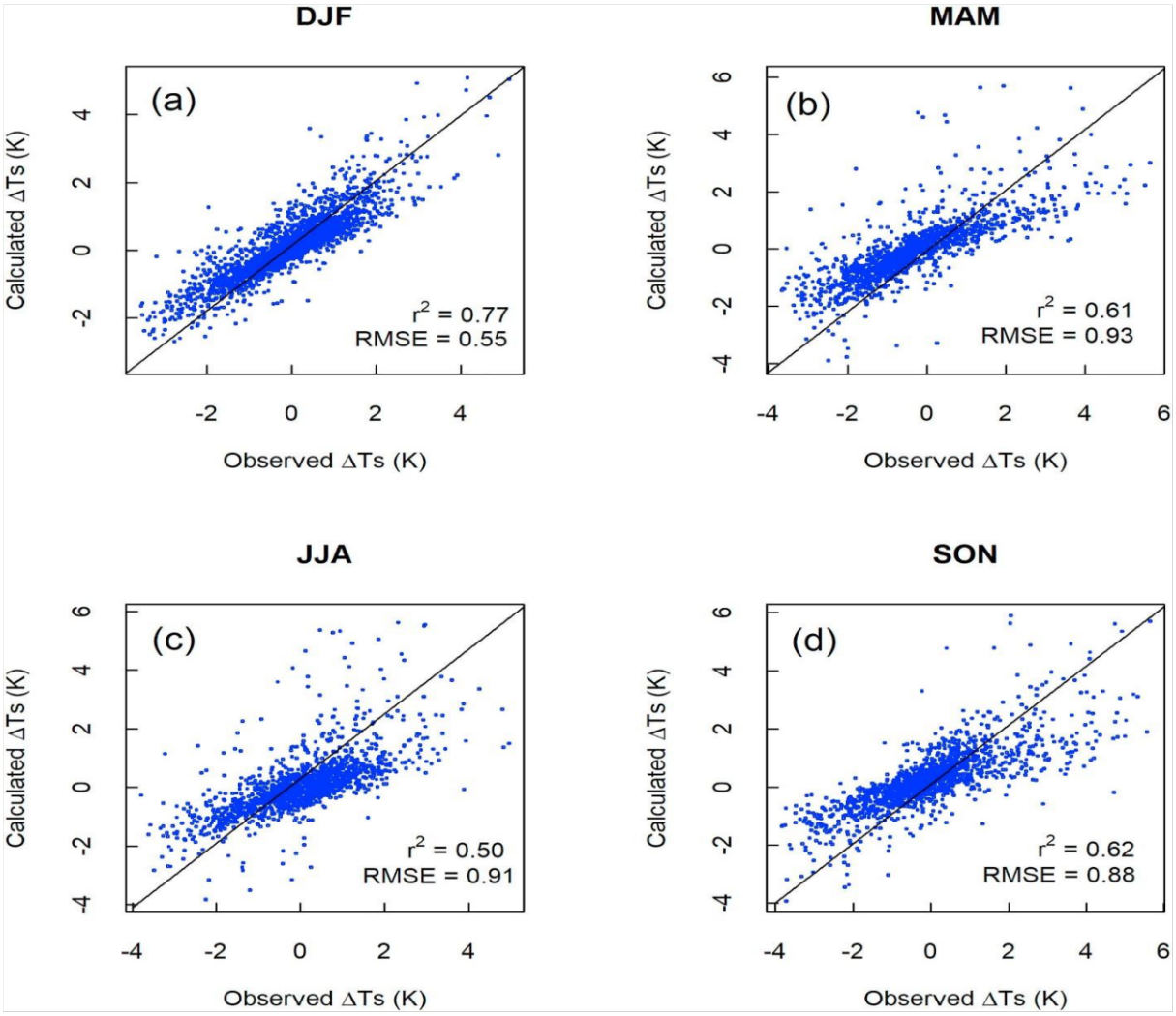

Figure 4.47: Comparison of the observed and calculated land surface temperature change due to land cover conversion across four seasons over West Africa during 2001–2013 based on Moderate Resolution Imaging Spectroradiometer (MODIS) data and the empirical method of Lee et al. (2011). DJF = December, January, February; JJA = June, July, August; MAM = March, April, May; RMSE = root-mean-square error; SON =September, October, November.

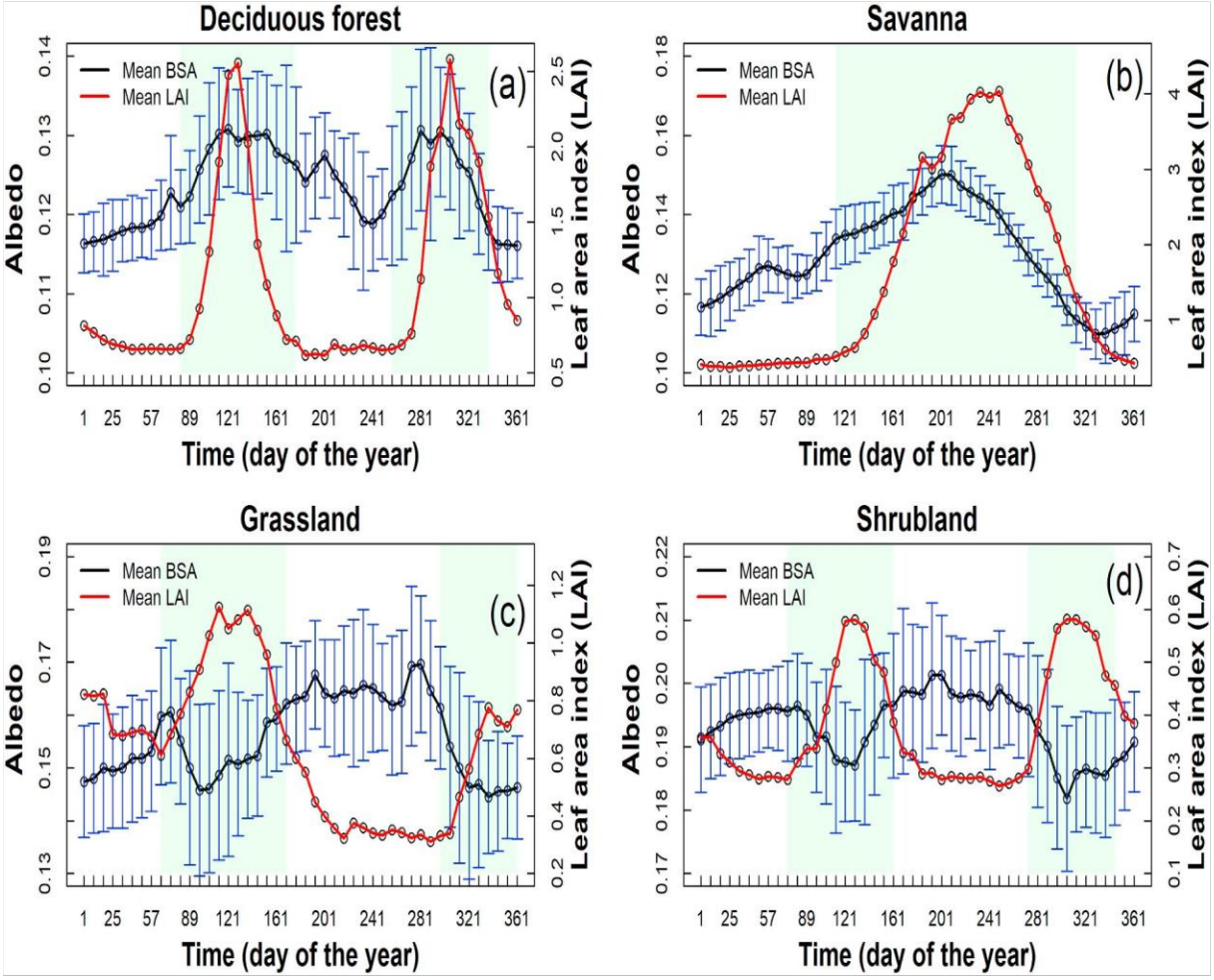

Figure 4.48: Seasonality of average 8-day composite leaf area index (LAI) and shortwave broadband black sky albedo (SBSA) over 2001–2013 in the Horn of Africa in (a) deciduous forest, (b) savanna, (c) grassland, and (d) shrubland. Error bars show mean ± standard deviation of SBSA. Shaded area shows growing period.

Table 4.9: Qualitative metrics on impact of growing period albedo dynamics on net shortwave radiation.

Land cover	α_{gs}	α_{ng}	$\Delta\alpha$	$\Delta S_{(\alpha)}(W/m^2)$
Forest	0.13	0.12	0.01 (8%)	−2.47
Savanah	0.15	0.11	0.04 (27%)	−10
Grassland	0.14	0.17	−0.03 (18%)	7.11
Shrubland	0.18	0.20	−0.02 (10%)	5.04

α_{gs} = growing season albedo; α_{ng} = non-growing season albedo; $\Delta\alpha$ =albedo change; $\Delta S_{(\alpha)}$ = net shortwave radiation changes due to albedo dynamics.

CHAPTER FIVE

5.0 CONCLUSION

5.1 Radiative Forcing due to Aerosol-Radiation Interaction

Over West African climatic zones (Sahara, Sahel, Savannah, and the coast of Guinea) between December 2005 and January 2006, the daily average of aerosol radiative property parameters like AOD, SSA, AF, and the angstrom exponent characterized the interaction of aerosols with solar radiation to cause a radiative forcing effect. The direct effects of radiative forcing at the top of the atmosphere and the surface under clear-sky conditions were characterized. This study has observed negative forcing over all the four climatic zones in West Africa during the study period. Consequently, this study critically analyses the dynamics of various aerosol sources and types and their contribution to the forcing effect observed.

This study reports variations in high load of anthropogenic and dust aerosols in the climatic zones. While anthropogenic aerosols such as black carbon and organic matter and marine aerosols were reportedly high in the Guinea and Savanah zones, contributing to the high cooling forcing observed, dust aerosol was reportedly observed in the Sahara and Sahel climatic zones, also contributing to the unusual cooling forcing observed during the study period. The study also noted that the early days in February are notably days of dust episodes as the study effectively analyses the fact. This observation doesn't necessarily agrees with the report of the DABEX AMMA-SOP campaign over West Africa in 2006.

The following conclusions can be deducted from this study;

i. Radiative forcing of aerosols is a major function of the aerosol single scattering albedo, aerosol asymmetry factor, aerosol optical depth and the aerosol angstrom exponent
ii. The following distinguishing characteristics of the aerosol radiative property parameters are present: (a) High AOD causes high atmospheric absorption and low surface net radiation fluxes; (b) when the angstrom exponent is low, a greater amount

of radiation is absorbed at the top of the atmosphere; (c) the radiative properties vary with changing aerosol concentration and distribution in the atmosphere; and (d) an increase in anthropogenic aerosols lead to increase in the SSA.

iii. The daily average analyses of the aerosols show a high concentration of dust in the Sahara and Sahel with a high concentration of black carbon and organic matter in the Guinea and Savanah region, but little sea-salt aerosols in the region.

iv. Medium and small dust particles are easily transported while large particles have slow mobilization. Black carbon and organic matter aerosols are heavily deposited in the coastal region of West Africa during the study period.

v. A substantial amount of anthropogenic and non-dust aerosols, apart from the predominant dust aerosol in this region, could cause and boost the radiative forcing of aerosols which was observed in the early days of February

vi. Fine and coarse mode particles were significantly present as substantial coarse-mode particles were deposited in all the climatic zones.

This research study utilized the regional climate model RegCM 4.7.1 to conduct a sensitivity study over West Africa through coordinated Regional climate Downscaling Experiment domain, with the aim of identifying the optimal cumulus convective precipitation scheme, planetary boundary layer (PBL), and land-surface scheme. Through sensitivity experiments, it was determined that the community land model version 4.5 (CLM 4.5) provided the best performance over the biosphere-atmosphere transfer scheme, while the Kain-Fritsch scheme for cumulus convective precipitation and the University of Washington (UW) scheme for PBL were the most effective. The resulting simulation with these parameterization schemes demonstrated a strong correlation with observed precipitation patterns over West Africa, as well as well-simulated temperatures.

Further utilizing RegCM 4.7.1 with these optimized parameterization schemes, the study then simulated aerosol fields and aerosol direct radiative forcing (DRF) over the same domain for the period 2005-2006, with a specific focus on the four climatic zones (Guinea, Sahara, Sahel and Savana. The model successfully captured the daily variation in aerosol radiative properties (AOD, ASY and SSA) and chemistry (dust, black carbon, organic carbon and sae-salt aerosols) over the climatic zones with source regions. The observed to simulated BC ratio over the Guinea zone was found to be improved, however, the model underestimated the radiative forcing significantly in January, which was likely due to the lack of consideration for burning over the region in emission inventories.

Overall, this study presents important findings regarding the optimization of parameterization schemes for regional climate modelling, as well as the successful simulation of aerosol fields and radiative forcing over West Africa, further research is needed to address the limitations identified in this study, particularly with regard to the inclusion of burning in emission inventories in order to more accurately simulate radiative forcing. The best agreement with observational data over entire West Africa is obtained considering the Kain-Fritsch as cumulous convective precipitation scheme. It can also be observed that climate change issue is strongly related to atmospheric constituent change. The study also shows how increase in aerosol concentration can enhance rainfall in the Guinea coast, but aid drought in the Sahel region. Reduction of anthropogenic activities that increase black and organic carbon emissions in the region must be reduced to reduce the drought occurrence in Sahel region of West Africa. With further detail study, the experiment can serve as a feasibility study for field campaign experiment as a mitigation strategy of climate change in West Africa region.

5.2 Land use Change Radiative Forcing Effects

In this study, we investigated how radiative mechanisms associated with seasonal dynamics in natural vegetation and abrupt land cover changes caused by anthropogenic activities may affect

the climate system. In taller vegetation (forest and savanna), albedo increased during the growing period, causing a decline in net shortwave radiation of -10W/m^2; whereas in shorter vegetation (grassland and shrubland), albedo decreased, resulting in an increase in net shortwave radiation of 7W/m^2. The albedo cooling and warming impact during the growing period in taller and shorter vegetation, respectively, were however highly outweighed by ET cooling, which had a dominating influence on LST seasonality in West Africa. Land cover changes caused an average increase in albedo, with a maximum surge observed in the dry period (DJF). The albedo changes from all land cover changes together generated a regional instantaneous shortwave surface radiative forcing of -0.03W/m^2. Regardless of the small regional forcing, the mean instantaneous local surface radiative forcing in forest to cropland (-2.6W/m^2) and savanna to grassland (-1.5W/m^2) conversions and their contributions to LST cooling (-0.12^{o}K and -0.09^{o}K) were bigger than other conversion classes, respectively. Despite such LST cooling, however, these conversion classes displayed the largest average observed LST warming of up to 1.2^{o}K and 0.4^{o}K, respectively. These warming impacts are due to the dominant influence of non-radiative mechanisms through a reduction in ET and surface roughness following woody cover decline, which largely offset the albedo cooling effect. The increase or decrease in woody cover was shown to largely determine the observed LST change in the region as indicated in the savanna to grassland and grassland to savanna conversions that displayed consistent average warming and cooling across seasons, respectively.

Much of the uncertainty arises from the simulation of aerosol–cloud interactions and the indirect effect for which very little model consensus exists on a global scale (Forster et al., 2007). In addition to these uncertainties, the perturbations of natural aerosol emissions by land use activities (mineral dust, SOA, wildfire smoke) are only beginning to be better understood on a global scale (Ganzeveld et al., 2010; Ginoux et al., 2012;). Further research into the sources and lifetimes of natural aerosols, as well as anthropogenic impacts on their emissions,

could efficiently reduce our uncertainty in the contribution of land use changes to global and regional radiative forcing, especially over West Africa.

While it is likely that advances in, and proliferation of, agricultural technologies will be sufficient to meet global food demand without such an extreme increase in crop and pasture area, investment in foreign lands for agriculture, as a cost-effective alternative to intensification of existing agriculture, may be hastening the conversion of unprotected natural lands (Rulli et al., 2013). Given the huge potential for climate impacts from land use changes in this century, estimated to be at the maximum, similar to some estimates of future climate impacts from fossil fuels (e.g., van Vuuren et al., 2011), this study substantiates that not only energy usage but also land use change need to remain a focus of climate change mitigation.

Overall, this study underscores the complex interactions between aerosols, land-use change and climate in the West Africa region and the need for continued research and data collection to better understand these interactions and their impacts. The findings from this study can inform policy decisions and guide future climate change mitigation and adaptation strategies in the region.

5.3 Contribution to knowledge

The effective integration of aerosols into future climate models depends on a comprehensive understanding of the processes that govern aerosol properties. This requires improved research efforts to enhance our understanding of the forcing effects of aerosols and its interaction with radiation. The results of these studies will be significant in informing the development of climate models that accurately capture the interaction between aerosols and radiation. Additionally, they will contribute to the knowledge of aerosol-cloud interactions and their response to changes in land use. Moreover, the research findings will be useful in the comprehensive characterization of aerosols, including closure studies of CCN, inter-comparison of models and measurements, and evaluation of satellite retrieval methods.

Furthermore, this research will provide valuable information on land-use practices that promote sustainable climate change mitigation techniques. The outcomes of the study will also support policymakers in making informed decisions regarding land-use policies.

In summary, an improved understanding of aerosol properties and their interactions with radiation and clouds will enable better integration into climate models, more comprehensive aerosol characterization, and more informed land-use policies for sustainable climate change mitigation.

5.4 Stakeholder's commitment and beneficiaries of the Research

The West African Science Service Centre on Climate and Adapted Land-Use (WASCAL) is been funded by the Federal Ministry of Education and Research, Germany (BMBF), a collaboration with 11 West African countries. The centre is designed to address various challenges in climate change and adaptation, climate change effects and mitigation policies, through quality research and capacity building. Therefore capacities and expertise are drawn from 11 different West African countries such as Benin, Burkina-Faso, Capo Verde, Cote d'Ivoire, The Gambia, Ghana, Niger, Nigeria, Mali, Senegal and Togo. This present study is therefore being supervised by WASCAL and expected to meet the goals and vision of WASCAL.

The effects of land-use and aerosol radiative properties over West Africa cannot be over emphasized. This is due to the major role aerosols play in modifying and determining the climate and weather pattern of West Africa, especially in the issues surrounding climate change. Hence, this study will explain various land-use processes and the associated interaction with aerosol radiative properties which affects the West African Climate System. This study will also emphasize on different radiative properties of aerosols and how they interact with the climate system, as this will help in better understanding and more accurate forecasting of the West African climate system. This study seeks to help the various meteorological and

environmental agencies across West Africa in further advancing the fight against climate change by providing more efficient climate services to end-users in the region. This study will directly give climate service users, such as farmers, corporate organisations and individuals the information they need on seasonal variability of climate variables due to the radiative properties atmospheric aerosols possess. Also, policy makers in the region will be able to provide adequate policies for mitigation and adaptation techniques through better land-use practices for a climate resilient environment and economic boosts. This study will be able to directly suggest some land-use policies policy makers can adopt for a climate resilient environment. Some of which may include;

i. Controlled emission of particles through the burning of biomass, farm wastes and other urban types.
ii. Vegetation practices, in terms of types and species of climate resilient trees required for planting, more adequate forest reserves and sustaining plant biodiversities.
iii. Reduction of bare surfaces which enhances the raising of dust particles, especially in the Sahelian region of West Africa.
iv. De-congestion of urban centres to reduce the concentration of aerosols.
v. Development of efficient renewable energy schemes to reduce aerosol concentrations and modification of the radiative forcing capabilities of aerosols for a more climate friendly environment.

REFERENCES

Abera, T.A., Heiskanen, J., Pellikka, P.K., Maeda, E.E., (2018). Rainfall-vegetation interaction regulates temperature anomalies during extreme dry events in the horn of Africa. Glob. Planet. Chang. 167, 35–45. https://doi.org/10.1016/j.gloplacha.2018. 05.002.

Abiodun, B. J., Adeyewa, Z. D., Oguntunde, P. G., Salami, A. T., & Ajayi, V. O. (2012). Modelling the impacts of reforestation on future climate in West Africa. Theoretical and Applied Climatology, 110, 77-96.

Agusti-Panareda, A. S., Massart, F., Chevallier, G., Balsamo, S., Boussetta, E. Dutra, and Beljaars, A., (2016). A biogenic CO2 flux adjustment scheme for the mitigation of large-scale biases in global atmospheric CO2 analyses and forecasts, Atmos. Chem. Phys., 16, 10399–10418, https://doi.org/10.5194/acp-16-10399-2016.

Ajay, P., Pathak, B., Solmon, F., Bhuyan, P. K., and Giorgi, F. (2019). Obtaining best parameterization scheme of RegCM 4.4 for aerosols and chemistry simulations over the CORDEX South Asia. Climate dynamics, 53, 329-352.

Akinyoola, J. A., Ajayi, V. O., Abiodun, B. J., Ogunjobi, K. O., Gbode, I. E., and Ogungbenro S. B., (2019). Dynamic response of monsoon precipitation to mineral dust radiative forcing in the West Africa region. Modeling Earth Systems and Environment (2019) 5:1201–1214; https://doi.org/10.1007/s40808-019-00620-z.

Akinyoola, J. A., Eresanya, E. O., Orimoogunje, O. O. I., and Oladosu, K., (2018). Monitoring the spatio-temporal aerosol loading over Nigeria. Modeling Earth Systems and Environment, 4, 1365-1375.

Alkama, R., and Cescatti, A., (2016). Biophysical climate impacts of recent changes in global forest cover. Science 351 (6273), 600–604. https://doi.org/10.1126/science. aac8083.

Alkama, R., and Cescatti, A., (2016). Biophysical climate impacts of recent changes in global forest cover. Science 351 (6273), 600–604. https://doi.org/10.1126/science. aac8083.

Allen, S.J., Wallace, J.S., Gash, J.H.C., Sivakumar, M.V.K., (1994). Measurements of albedo variation over natural vegetation in the Sahel. Int. J. Climatol. 14 (6), 625-636. https://doi.org/10.1002/joc.3370140603.

Andrea, M. O., (1996). Atmospheric aerosols: Composition, transformation, climate and health effects. John Wiley & Sons.

Andreae, M.O., Jones, C.D., Cox P.M., (2005). Strong present-day aerosol cooling implies a hot future. Nature 435:1187–1190

Anoruo, C. M., (2023). Variations of aerosol optical depth over the West Africa Sahel region. International Journal of Environmental Science and Technology, 20(2), 1997-2008.

Ansmann, A., Mamouri, R. E., Baars, H., & Nisantzi, A., (2011). Potential of polarization lidar to provide profiles of CCN- and INP-relevant aerosol parameters. Atmospheric Chemistry and Physics, 11(2), 543-554.

Antje Inness, Melanie Ades, Anna Agustí-Panareda, Jérôme Barré, Anna Benedictow, Anne-Marlene Blechschmidt, Juan Jose Dominguez, Richard Engelen, Henk Eskes, Johannes Flemming, Vincent Huijnen, Luke Jones, Zak Kipling, Sebastien Massart, Mark

Parrington, Vincent-Henri Peuch, Miha Razinger, Samuel Remy, Michael Schulz, and Martin Suttie, (2019). The CAMS reanalysis of atmospheric composition. Atmospheric Chemistry and Physics.19, 3515–3556, 2019.

Arola, A., Schuster, G., Myhre, G., Kazadzis, S., Dey, S., Tripathi, S.N., (2010). Inferring absorbing organic carbon content from AERONET data. Atmos. Chem. Phys. Discuss, 10, 215–225.

Bala, G., Caldeira, K., Wickett, M., Phillips, T. J., Lobell, D. B., Delire, C., and Mirin, A., (2007). Combined climate and carbon-cycle effects of large-scale deforestation, P. Natl. Acad. Sci.

Bartok, B., (2016). Recent advances in solid-state lighting. Optik, 127(11), 4838-4843.

Bauer, S. E., Menon, S., Koch, D. M., Bond, T. C., and Tsigaridis, K., (2007). A global modelling study on carbonaceous aerosol microphysical characteristics and radiative forcing. Atmospheric Chemistry and Physics, 7(5), 1185-1204.

Beauchemin, C., (2005). Pour une relecture des tendances migratoires entre villes et campagnes: une étude comparée Burkina Faso-Côte d'Ivoire: Etudes de la Population Africaine/African Population Studies, v. 20, no. 1, p. 141-165.

Bellouin, N., Quaas, J., Gryspeerdt, E., Kinne, S., Stier, P., Watson-Parris, D., and Schulz, M., (2020). Bounding global aerosol radiative forcing of climate change. Reviews of Geophysics, 58(4), e2019RG000660.

Bellouin, N., Quaas, J., Gryspeerdt, E., Kinne, S., Stier, P., Watson-Parris, D., and Schulz, M., (2013). Bounding aerosol radiative forcing of climate change. Reviews of Geophysics, 51(4), 123-149.

Bennouna, Y. S., Singh, R. P., & Kogan, F. N., (2011). Drought and heat wave monitoring and forecasting using remotely sensed data. In remote sensing of drought (pp. 193-224). Springer, Dordrecht. doi: 10.1007/978-90-481-8737-4_9.

Betts, A.K., and Ball, J.H., (1997). Albedo over the boreal forest. J. Geophys. Res.-Atmos. 102 (D24), 28901–28909. https://doi-org.libproxy.helsinki.fi/10.1029/96JD03876.

Betts, A.K., and Ball, J.H., (1997). Albedo over the boreal forest. J. Geophys. Res.-Atmos. 102 (D24), 28901–28909. https://doi-org.libproxy.helsinki.fi/10.1029/96JD03876.

Betts, R. A., (2000). Offset of the potential carbon sink from boreal forestation by decreases in surface albedo. Nature, 408(6809), 187-190.

Betts, R. A., Boucher, O., Collins, M., Cox, P. M., Falloon, P. D., Gedney, N., and Webb, M. J., (2007). Projected increase in continental runoff due to plant responses to increasing carbon dioxide. Nature, 448(7157), 1037-1041.

Bhatla, R., Ghosh S, Mandal, B., Mall, R. K., and Sharma, K., (2016). Simulation of Indian summer monsoon onset with different parameterization convection schemes of RegCM-4.3. Atmos Res 176–177:10–18. https: //doi.org/10.1016/j.atmos res.2016.02.010

Bibi, H., Alam, K., Chishtie, F., Bibi, S., Shahid, I., and Blaschke, T., (2015). Intercomparison of MODIS, MISR, OMI, and CALIPSO aerosol optical depth retrievals for four locations on the Indo-Gangetic plains and validation against AERONET data. Atmospheric Environment, 111, 113-126.

Bindoff, N. L., Stott, P. A., AchutaRao, K. M., Allen, M. R., Gillett, N., Gutzler, D., & Zhou, G., (2013). Detection and attribution of climate change: from global to regional. In Climate change 2013: the physical science basis. Contribution of Working Group I to the

Fifth Assessment Report of the Intergovernmental Panel on Climate Change (pp. 867-952). Cambridge University Press.

Boiyo, R., Adeyemi, B., and Maduekwe, A., (2019). Assessment of the impact of atmospheric aerosols on surface insolation over Nigerian environment. Environmental Science and Pollution Research, 26(2), 1466-1479.

Boiyo, R., Kumar, K. R., Zhao, T., and Guo, J., (2019). A 10-year record of aerosol optical properties and radiative forcing over three environmentally distinct AERONET sites in Kenya, East Africa J. Geophys. Res. Atmos. 124 1596–617

Bonan, G. B., (2008). Ecological climatology: concepts and applications. Cambridge University Press. doi: 10.1017/CBO9780511754829.

Bond, T. C., Doherty, S. J., Fahey, D. W., Forster, P. M., Berntsen, T., DeAngelo, B. J., and Zender, C. S., (2013). Bounding the role of black carbon in the climate system: a scientific assessment. Journal of Geophysical Research: Atmospheres, 118(11), 5380-5552.

Boucher, O., Randall, D., Artaxo, P., Bretherton, C., Feingold, G., Forster, P., and Zhang, X. Y., (2014). Clouds and aerosols. Climate Change 2013: The Physical Science Basis. Contribution of Working Group I to the Fifth Assessment Report of the Intergovernmental Panel on Climate Change, 571-658.

Boucher, O., Randall, D., Artaxo, P., Bretherton, C., Feingold, G., Forster, P., and Wood, R., (2013). Clouds and aerosols. In Climate change 2013: The physical science basis. Contribution of Working Group I to the Fifth Assessment Report of the Intergovernmental Panel on Climate Change (pp. 571-658).

Bozzo, A., Kirchengast, G., von Clarmann, T., and Raspollini, P., (2020). Improved precision of climate change projections enabled by the refined overlap analysis of satellite and ground based measurements. Remote Sensing, 12(1), 136. doi: 10.3390/rs12010136.

Bretherton, C. S., McCaa, J. R., Grenier, H., (2004). A new parameterization for shallow cumulus convection and its application to marine subtropical cloud-topped boundary layers. I. Description and 1D results. Mon Weather Rev 132:864–882.

Bright, Ryan M., Zhao, Kaiguang, Jackson, Robert B., Cherubini, and Francesco, (2015). Quantifying surface albedo and other direct biogeophysical climate forcing of forestry activities. Glob. Chang. Biol. 3246–3266. https://doi.org/10.1111/gcb.12951.

Bright, Ryan M., Zhao, Kaiguang, Jackson, Robert B., Cherubini, Francesco, (2015). Quantifying surface albedo and other direct biogeophysical climate forcing of forestry activities. Glob. Chang. Biol. 3246–3266. https://doi.org/10.1111/gcb.12951.

Brovkin, V., Boysen, L., Raddatz, T., Gayler, V., Loew, A., and Claussen, M., (2013). Evaluation of vegetation cover and land-surface albedo in MPI-ESM CMIP5 simulations. Journal of Advances in Modeling Earth Systems, 5(1), 48-57.

Brovkin, V., Claussen, M., Driesschaert, E., Fichefet, T., Kicklighter, D., Loutre, M. F., and Sokolov, A., (2006). Biogeophysical effects of historical land cover changes simulated by six Earth system models of intermediate complexity. Climate Dynamics, 26, 587 600.

Brovkin, V., Sitch, S., von Bloh, W., Claussen, M., Bauer, E., and Cramer, W., (2004). Role of land cover changes for atmospheric CO2 increase and climate change during the last 150 years, Global Change Biol., 10, 1253–1266, doi:10.1111/j.1365- 2486.2004.00812.

Cabral, A. I., & Costa, F. L. (2017). Land cover changes and landscape pattern dynamics in Senegal and Guinea Bissau borderland. Applied Geography, 82, 115-128.

Camara, M., (2010). Interactive comment on “Impacts of dust on West African climate during 2005 and 2006” by M. Camara et al.

Campbell, G.S., and Norman, J.M., (1998). An Introduction to Environmental Biophysics. Springer, New York (286 pp).

Chaibou, A. I., Gao, Y., Marijnissen, J. C., and Peters, E. A. J. F., (2020). Direct numerical simulation of turbulence in the gas phase of a turbulent liquid jet in cross-flow: Effect of sub grid-scale modelling. Chemical Engineering Science, 214, 115406.

Chandra, S., Satheesh, s. k., and Srinivasan, J., (2004). Can the state of mixing of black carbon aerosols explain the mystery of ‘excess’ atmospheric absorption? Geophys. Res. Lett., 31, L19109, doi:10.1029/2004GL020662.

Chung, C. E., (2012). Aerosol Direct Radiative Forcing: A Review. In (Ed.), Atmospheric Aerosols, Regional Characteristics, Chemistry and Physics. IntechOpen. https://doi.org/10.5772/50248

Chung, S. H., and Seinfeld, J. H., (2002). Global distribution and climate forcing of carbonaceous aerosols. Journal of Geophysical Research: Atmospheres, 107(D19), ACH 7-1-ACH 7-21.

Church, R.J., (1966). West Africa: a study of the environment and of man’s use of it: Longman’s, Green and Co., Ltd.

Claussen, M., Brovkin, V., and Ganopolski, A., (2001). Biogeophysical versus biogeochemical feedbacks of large-scale land cover change, Geophys. Res. Lett., 28, 1011-1014, doi:10.1029/2000gl012471.

Cleugh, H.A., Leuning, R., Mu, Q., and Running, S.W., (2007). Regional evaporation estimates from flux tower and MODIS satellite data. Remote Sens. Environ. 106 (3), 285–304. https://doi.org/10.1016/j.rse.2006.07.007.

Coakley Jr, J. A., and Bretherton, F. P., (1982). Cloud cover from high-resolution scanner data: Detecting and allowing for partially filled fields of view. Journal of Geophysical Research: Oceans, 87(C7), 4917-4932.

Davin, E. L., and de Noblet-Ducoudré, N., (2010). Climatic impact of global-scale deforestation: Radiative versus nonradiative processes. Journal of Climate, 23(1), 97-112.

Davin, E. L., de Noblet-Ducoudré, N., & Friedlingstein, P., (2007). Impact of land cover change on surface climate: Relevance of the radiative forcing concept. Geophysical research letters, 34(13).

Davin, E.L., de Noblet-Ducoudre, N., (2010). Climatic impact of global-scale deforestation: radiative versus nonradiative processes. J. Clim. 23 (1), 97-112. https://doi.org/10.1175/2009JCLI3102.1.

de Noblet-Ducoudré, N., Boisier, J. P., Pitman, A., Bonan, G. B., Brovkin, V., Cruz, F., and Voldoire, A., (2012). Determining robust impacts of land-use-induced land cover changes on surface climate over North America and Eurasia: results from the first set of LUCID experiments. Journal of Climate, 25(9), 3261-3281.

Després, V. R., Nowoisky, J. F., Klose, M., Conrad, R., Andreae, M. O., and Pöschl, U., (2012). Characterization of primary biogenic aerosol particles in urban, rural, and high-alpine air by DNA sequence and restriction fragment analysis of ribosomal RNA genes. Atmospheric Chemistry and Physics, 12(18), 9419-9433. doi: 10.5194/acp-12-9419-

2012.Remy, S., Flamant, C., Derrien, S., Dabas, A., Chaboureau, J. P., Jordan, A., ... & Faloona, I., (2019). Observation of clear-air turbulence at cruising altitude and en-route descent. Atmospheric Chemistry and Physics, 19(17), 11337-11350. doi: 10.5194/acp-19-11337-2019.

Dickinson, R., Henderson-Sellers, A., and Kennedy, P., (1993) Biosphere- Atmosphere Transfer Scheme (BATS) Version 1eas Coupled to the NCAR Community Climate Model, NCAR Technical Note.

Dickinson, R.E., and Kennedy, P., (1992). Impacts on regional climate of Amazonian deforestation. Geophys. Res. Lett. 19 (19), 1947–1950. https://doi.org/10.1029/92GL01905.

Ding, Q., Pan, T., Lin, T., & Zhang, C. (2022). Urban Land-Cover Changes in Major Cities in China from 1990 to 2015. International Journal of Environmental Research and Public Health, 19(23), 16079.

Druyan, L. M., Fulakeza, M., Lonergan, P., and Noble, E. (2009). Regional climate model simulation of the AMMA Special Observing Period# 3 and the pre-Helene easterly wave. Meteorology and atmospheric physics, 105, 191-210.

Duveiller, G., Caporaso, L., Abad-Viñas, R., Perugini, L., Grassi, G., Arneth, A., & Cescatti, A. (2020). Local biophysical effects of land use and land cover change: towards an assessment tool for policy makers. Land Use Policy, 91, 104382.

Eddy, C., (2012). Aerosol Direct Radiative Forcing: A Review. Atmospheric Aerosols - Regional Characteristics - Chemistry and Physics. doi: 10.5772/50248.

Emanuel, K. A., and Zivkovic-Rothman, M., (1999) Development and evaluation of a convection scheme for use in climate models, J. Atmos. Sci., 56, 1766–1782.

Emanuel, K., (1991). A Scheme for Representing Cumulus Convection in Large-Scale Models, J. Atmos. Sci., 48, 2313–2329.

Eresanya, E.O., Oluleye, A., Daramola, M.T., (2017). The influence of rainfall and temperature on total column ozone over West Africa. Adv Res 10(2):1–11 (Article no. AIR.34312)

Esteve, A. R., Vázquez, M., and De La Rosa, J. D., (2016). A review of atmospheric mercury emissions, pollution and control in Spain. Atmospheric Pollution Research, 7(3), 471-492.

Facchini, M. C., Mircea, M., Fuzzi, S., Charlson, R. J., and Ceburnis, D., (2008). Cloud albedo enhancement by surface-active organic solutes in growing droplets. Nature, 417(6887), 429-432. doi: 10.1038/nature00775.

Flamant, C., Knippertz, P., Fink, A. H., Akpo, A., Brooks, B., Chiu, C. J., and Yoboué, V. (2018). The dynamics–aerosol–chemistry–cloud interactions in West Africa field campaign: Overview and research highlights. Bulletin of the American Meteorological Society, 99(1), 83-104.

Foley, J. A., Defries, R., Asner, G. P., Barford, C., Bonan, G., Carpenter, S. R., Chapin, F. S., Coe, M. T., Daily, G. C., Gibbs, H. K., Helkowski, J. H., Holloway, T., Howard, E. A., Kucharik, C. J., Monfreda, C., Patz, J. A., Prentice, I. C., Ramankutty, N., and Snyder, P. K., (2005). Global consequences of land use, Science, 309, 570-574, doi:10.1126/science.1111772.

Foley, J. A., Ramankutty, N., Brauman, K. A., Cassidy, E. S., Gerber, J. S., Johnston, M., Mueller, N. D., O/'Connell, C., Ray, D. K., West, P. C., Balzer, C., Bennett, E. M., Carpenter, S. R., Hill, J., Monfreda, C., Polasky, S., Rockstrom, J., Sheehan, J., Siebert,

S., Tilman, D., and Zaks, D. P. M., (2011). Solutions for a cultivated planet, Nature, 478, 337-342, 2011.

Forster, P. M., Ramaswamy, V., Artaxo, P., Berntsen, T., Betts, R., Fahey, D. W., and Slingo, J. M., (2007). Changes in atmospheric constituents and in radiative forcing. In Climate Change 2007: The Physical Science Basis. Contribution of Working Group I to the Fourth Assessment Report of the Intergovernmental Panel on Climate Change (pp. 129-234).

Forster, P., Ramaswamy, V., Artaxo, P., Berntsen, T., Betts, R., Fahey, D. W., Haywood, J., Lean, J., Lowe, D. C., Myhre, G., Nganga, J., Prinn, R., Raga, G., Schulz, M., and Dorland, R. V., (2007). Changes in Atmospheric Constituents and in Radiative Forcing, in: Climate Change 2007: The Physical Science Basis. Contribution of Working Group I to the Fourth Assessment Report of the Intergovernmental Panel on Climate Change, edited by: Tubiello, F. N., Salvatore, M., Rossi, S., Ferrara, A., Fitton, N., and Smith, P.: The FAOSTAT database of greenhouse gas emissions from agriculture, Environ. Res. Lett., 8, 015009.

Friedl, M.A., Sulla-Menashe, D., Tan, B., Schneider, A., Ramankutty, N., Sibley, A., and Huang, X., (2010). MODIS collection 5 global land cover: algorithm refinements and characterization of new datasets. Remote Sens. Environ. 114 (1), 168–182. https://doi. org/10.1016/j.rse.2009.08.016.

Fritsch, J. M., and Chappell, C. F., (1980). Numerical prediction of convectively driven mesoscale pressure systems. Part I: convective parameterization. J Atmos Sci 37:1722-1733

Ganzeveld, L., Bouwman, L., Stehfest, E., van Vuuren, D. P., Eickhout, B., and Lelieveld, J., (2010). Impact of future land use and land cover changes on atmospheric chemistry climate interactions, J. Geophys. Res., 115, D23301, doi:10.1029/2010jd014041, 2010.

Gautam, R, Liu, Z., Singh, R. P., and Hsu, N. C., (2009). Two contrasting dust dominant periods over India observed from MODIS and CALIPSO data. Geophys Res Lett 36:L06813. org/10.1029/2008G L0369 67

Gautam, R., Hsu, N. C., and Lau, K. M., (2010). Premonsoon aerosol characterization and radiative effects over the Indo-Gangetic Plains: implications for regional climate warming. J Geophys Res 115:D17208. https ://doi.org/10.1029/2010J D0138 19

Gbobaniyi, E. O., Abiodun, B. J., Tadross, M. A., Hewitson, B. C., Gutowski, W. J., (2011). The coupling of cloud base height and surface fluxes: a trans-ferability intercomparison. Theor. Appl. Climatol. 106: 189–210.

Ge, J., Qiu, B., Chu, B., Li, D., Jiang, L., Zhou, W., & Guo, W. (2021). Evaluation of coupled regional climate models in representing the local biophysical effects of afforestation over continental China. Journal of Climate, 34(24), 9879-9898.

Ginoux, P., Prospero, J. M., Gill, T. E., Hsu, N. C., and Zhao, M., (2012). Global-scale attribution of anthropogenic and natural dust sources and their emission rates based on MODIS Deep Blue aerosol products. Reviews of Geophysics, 50(3), RG3005. doi: 10.1029/2012RG000388.

Ginoux, P., Prospero, J. M., Gill, T. E., Hsu, N. C., and Zhao, M., (2012). Global-scale attribution of anthropogenic and natural dust sources and their emission rates based on MODIS Deep Blue aerosol products, Rev. Geophys., 50, RG3005, doi:10.1029/2012RG000388.

Giorgi, F., Coppola, E., Solmon, F., Mariotti, L., Sylla, M. B., Bi, X., Elguindi, N., Diro, G. T., Nair, V., Giuliani, G., Cozzini, S., Guettler, I., O'Brien, T., Tawfik, A., Shalaby, A., Zakey, A. S., Steiner, A., Stordal, F., Sloan, L., and Brankovic, C., (2012). RegCM4: model description and preliminary tests over multiple CORDEX domains, Clim. Res., 52, 7–29, https://doi.org/10.3354/cr01018.

Giorgi, F., Mearns, L. O., (2003). Probability of regional climate change based on the reliability ensemble averaging (REA) method. Geophys Res Lett 30:1629. https ://doi.org/10.1029/2003G L0171 30

Granier, C., Bessagnet, B., Bond, T., D'Angiola, A., Denier van der Gon, H., Frost, G. J., Heil, A., Kaiser, J. W., Kinne, S., Klimont, Z., Kloster, S., Lamarque, J.-F., Liousse, C., Masui, T., Meleux, F., Mieville, A., Ohara, R., Raut, J.-C., Riahi, K., Schultz, M. G., Smith, S. G., Thompson, A., van Aardenne, J., van der Werf, G. R., and van Vuuren, D. P., (2011). Evolution of anthropogenic and biomass burning emissions of air pollutants at global and regional scales during the 1980–2010 period, Climatic Change, 109, 163–190, https://doi.org/10.1007/s10584-011-0154-1.

Granier, C., Bessagnet, B., Bond, T., D'Angiola, A., Denier van der Gon, H., Frost, G. J., Heil, A., Kaiser, J. W., Kinne, S., Klimont, Z., Kloster, S., Lamarque, J.-F., Liousse, C., Masui, T., Meleux, F., Mieville, A., Ohara, R., Raut, J.-C., Riahi, K., Schultz, M. G., Smith, S. G., Thompson, A., van Aardenne, J., van der Werf, G. R., and van Vuuren, D. P., (2011). Evolution of anthropogenic and biomass burning emissions of air pollutants at global and regional scales during the 1980–2010 period, Climatic Change, 109, 163–190, https://doi.org/10.1007/s10584-011-0154-1.

Grell, G., (1993). Prognostic evaluation of assumptions used by cumulus parameterizations. Mon Weather Rev 121:764–787

Grell, G., Dudhia, J., and Stauffer, D. R., (1994). A description of the fifth generation Penn State/NCAR Mesoscale Model (MM5), National Center for Atmospheric Research Tech Note.

Grenier, H., Bretherton, C. S., (2001). A moist PBL parameterization for large-scale models and its application to subtropical cloud topped marine boundary layers. Mon Weather Rev 129:357– 377.

Hahmann, A.N., and Dickinson, R.E., (1997). RCCM2-BATS model over tropical South America: applications to tropical deforestation. J. Clim. 10, 1944–1964. https://doi.org/10. 1175/1520-0442(1997)010.

Haywood, J. M., Johnson, B. T., Osborne, S. R., and Shine, K. P., (2003). Radiative forcing by aerosol particles and their uncertainty: A review. Meteorologische Zeitschrift, 12(4), 271-287.

Haywood, J.M., Boucher, O., (2000). Estimates of the direct and indirect radiative forcing due to tropospheric aerosols: a review. Rev Geophys 38(4):513–543 16.

Heald, C. L., Henze, D. K., Horowitz, L. W., Feddema, J., Lamarque, J. F., Guenther, A., Hess, P. G., Vitt, F., Seinfeld, J. H., Goldstein, A. H., and Fung, I., (2008). Predicted change in global secondary organic aerosol concentrations in response to future climate, emissions, and land use change, J. Geophys. Res., 113, D05211, doi:10.1029/2007jd009092.

Hoffmann, W.A., and Jackson, R.B., (2000). Vegetation–climate feedbacks in the conversion of tropical savanna to grassland. Am. Meteorol. Soc. 13 (9), 1593–1602. https://doi. org/10.1175/1520-0442.

Holben, B. N., Tanré, D., Smirnov, A., Eck, T. F., Slutsker, I., Abuhassan, N., Newcomb, W. W., Schafer, J.S., Chatenet, B., Lavenu, F., Kaufman, Y. J., Castle, J. V., Setzer A.,

Markham, B., Clark, D., Frouin, R., Halthore, R., Karneli, A., O'Neill, N. T., Pietras, C., Pinker, R., Voss, T., K., Zibordi, G., (2001). An emerging ground-based aerosol climatology: Aerosol optical depth from AERONET, Journal of Geophysical Research, 106D111206712097.

Hollinger, D. Y., Ollinger, S. V., Richardson, A. D., Meyers, T. P., Dail, D. B., Martin, M. E., Verma, S. V., (2010). Albedo estimates for land surface models and support for a new paradigm based on foliage nitrogen concentration. Glob. Chang. Biol. 16, 696–710. https://doi.org/10.1111/j.1365-2486.2009.02028.

Holtslag, A. A. M., Brujin E. E., Pan, H. L., (1990). A high-resolution air mass transformation model for short-range weather forecasting. Mon Weather Rev 118:1561–1575.

Huffman, G. J., Adler, R. F., Bolvin, D. T., Gu, G., Nelkin, E. J., Bowman, K. P., Hong, Y, Stocker, E. F., and Wolff, D. B., (2007). The TRMM multisatellite precipitation analysis: quasi-global, multiyear, combined-sensor precipitation estimates at fine scale, J. Hydrometeorol., 8, 38–55.

Hurtt, G. C., Chini, L. P., Frolking, S., Betts, R. A., Feddema, J., Fischer, G., Fisk, J. P., Hibbard, K., Houghton, R. A., Janetos, A., Jones, C. D., Kindermann, G., Kinoshita, T., Klein Goldewijk, K., Riahi, K., Shevliakova, E., Smith, S., Stehfest, E., Thomson, A., Thornton, P., Vuuren, D. P., and Wang, Y. P., (2011). Harmonization of land-use scenarios for the period 1500–2100: 600 years of global gridded annual land-use transitions, wood harvest, and resulting secondary lands, Climatic Change, 109, 117–161, doi:10.1007/s10584-011-0153-2.

Inness, A., Ades, M., Agustí-Panareda, A., Barré, J., Benedictow, A., Blechschmidt, A.-M., Dominguez, J. J., Engelen, R., Eskes, H., Flemming, J., Huijnen, V., Jones, L., Kipling, Z., Massart, S., Parrington, M., Peuch, V.-H., Razinger, M., Remy, S., Schulz, M., and

Suttie, M., (2019). The CAMS reanalysis of atmospheric composition, Atmos. Chem. Phys., 19, 3515–3556, https://doi.org/10.5194/acp-19-3515.

Intergovernmental Panel on Climate Change (IPCC) (2007), Climate Change 2007: The Scientific Basis. Contribution of Working Group I to the Fourth Assessment Report of the Intergovernmental Panel on Climate Change, edited by S. Solomon et al., Cambridge Univ. Press, New York.

IPCC (2013). In Stocker T. F., Qin, D., Plattner, G. K., Tignor, M., Allen S. K., Boschung, J., Nauels, A., Xia, Y., Bex, V., and Midgley, P. M., (Eds.), Climate change (2013). The physical science basis. Contribution of Working Group I to the Fifth 4 assessment report of the intergovernmental panel on climate change (p. 1535). Cambridge, United Kingdom and New York, NY, USA: Cambridge University Press. https://doi.org/10.1017/CBO9781107415324

Jackson, R.B., Mooney, H.A., and Schulze, E.D., (1997). A global budget for fine root biomass, surface area, and nutrient contents. Proc. Natl. Acad. Sci. 94 (14), 7362–7366. https://doi.org/10.1073/pnas.94.14.7362.

Jacobson, M. Z., (2001). Global direct radiative forcing due to multicomponent anthropogenic and natural aerosols. Journal of Geophysical Research: Atmospheres, 106(D2), 1551-1568.

Jin, M., and Dickinson, R.E., (2010). Land surface skin temperature climatology: benefitting from the strengths of satellite observations. Environ. Res. Lett. 5 (4), 44004. https:// doi.org/10.1088/1748-9326/5/4/044004.

Jin, Y., and Roy, D. P., (2005). Fire-induced albedo change and its radiative forcing at the surface in northern Australia. Geophys. Res. Lett. 32 (13). https://doi.org/10.1029/2005GL022822.

Johnson, B. T., Haywood, J. M., Langridge, J. M., Darbyshire, E., Morgan, W. T., Szpek, K., and Coe, H., (2008). Direct observations of aerosol radiative forcing over the tropical Indian Ocean during the aerosol-99 experiment. Geophysical Research Letters, 35(12), L12810.

Jonas Witthuhn, Anja Hünerbein, Florian Filipitsch, Stefan Wacker, Stefanie Meilinger, and Hartwig Deneke, (2021). Aerosol properties and aerosol–radiation interactions in clear sky conditions over Germany. Atmos. Chem. Phys., 21, 14591-14630; https://doi.org/10.5194/acp-21-14591.

Kain, J. S., and Fritsch, J. M., (1993). Convective parameterization for mesoscale models: the kain-fritsch scheme. In: Emanuel, K. A., Raymond, J., (eds) The representation of cumulus convection in numerical models. Meteorological Monographs. American Meteorological Society, https ://doi.org/10.1007/978-1-93570 4-13-3_16.

Kalnay, E., and Cai, M., (2003). Impact of urbanization and land-use change on climate. Nature 423:528–531. doi:10.1038/nature01675.

Kanamitsu, M., Ebisuzaki, W., Woollen, J., Yang, S-K., Hnilo, J. J., Fiorino, M., and Potter, G. L., (2002) NCEP-DOE AMIP-II reanalysis (R-2). Bull Am Meteorol Soc 83(11):1631-1643.

Kang, N., Kumar, K. R., Yu, X., & Yin, Y. (2016). Column-integrated aerosol optical properties and direct radiative forcing over the urban-industrial megacity Nanjing in the

Yangtze River Delta, China. Environmental Science and Pollution Research,23. 17532-17552. https://doi.org/10.1007/s11356-016-6953-1.

Kaufman, Y. J., Tanré, D., Remer, L. A., Vermote, E. F., Chu, A., & Holben, B. N., (2002). Operational remote sensing of tropospheric aerosol over land from EOS moderate resolution imaging spectroradiometer. Journal of Geophysical Research: Atmospheres, 107(D22), AER 2-1 - AER 2-14. doi: 10.1029/2002JD002238.

Kiehl, J. T., Hack, J. J., Bonan, G. B., Boville, B. A., Breigleb, B. P., Williamson, D., Rasch, P., (1996). Description of the NCAR community climate model (CCM3). NCAR Technical note NCAR/TN-420 + STR, p 152

Kinne, S., (2019) The MACv2 Aerosol Climatology, Tellus B, 71, 1–21.

Kinne, S., O'Donnel, D., Stier, P., Kloster, S., Zhang, Z., Schmidt, H., Rast, S., Giorgetta, M., Eck, T., and Stevens, B., (2013). MAC-v1: A new global aerosol climatology for climate studies, J. Adv. Model. Earth Sy., 5, 704–740, 2013.

Kloster, S., Mahowald, N. M., Randerson, J. T., and Lawrence, P. J., (2012). The impacts of climate, land use, and demography on fires during the 21st century simulated by CLM-CN, Biogeosciences, 9, 509–525, doi:10.5194/bg-9-509-2012.

Konare, A., Zakey, A. S., Solmon, F., Giorgi, F., Rauscher, S., Ibrah, S., and Bi, X., (2008a). A regional climate modelling study of the effect of desert dust on the West African monsoon. J Geophys Res 113:D12206. https ://doi.org/10.1029/2007J D0093 22,

Konare, A., Zakey, A. S., Solmon, F., Giorgi, F., Rauscher, S., Ibrah, S., and Bi, X., (2008b). A regional climate modelling study of the effect of desert dust on the West African monsoon. J Geophys Resv113:D12206. https ://doi.org/10.1029/2007j d0093 22.

Koné, B., Diedhiou, A., Sylla, M. B., Giorgi, F., Anquetin, S., Bamba, A., and Kobea, A. T., (2018). Sensitivity study of the regional climate model RegCM4 to different convective schemes over West Africa. Earth System Dynamics, 9(4), 1261-1278.

Korgo, B., (2014). Optical and Microphysical Characterization of Atmospheric Aerosol in West African Urban Areas: Application to Radiative Forcing Calculations in Ouagadougou. PhD Thesis, University Blaise Pascal, Clermont Ferrand, France/University of Ouagadougou, Burkina Faso.

Korgo, B., Kafando, P., Zouma, B., Bado, N., Zerbo, I., Roger, J., and Bathiebo, J., (2021). The Radiative Forcing of Aerosols in a West Africa Sahelian Urban City: Case Study of Ouagadougou. Atmospheric and Climate Sciences, 11, 73-85. doi:10.4236/acs.2021.111005.

Kouassi, A. A., Kone, B., Silue, S., Dajuma, A., N'datchoh, T. E., Adon, M., and Yoboue, V. (2022). Sensitivity Study of the RegCM4's Surface Schemes in the Simulations of West Africa Climate.

Lal, R., (2004). Soil carbon sequestration impacts on global climate change and food security, Science, 304, 1623–1627, doi:10.1126/science.1097396

Lau, K.M., Kim, M. K., and Kim, K. M., (2006). Asian summer monsoon anomalies induced by aerosol direct forcing: the role of the Tibetan Plateau. Clim Dyn 26:855–864. https ://doi.org/10.1007/s0038 2-006-0114-z

Lawrence, P. J., Feddema, J. J., Bonan, G. B., Meehl, G. A., O'Neill, B. C., Oleson, K. W., Levis, S., Lawrence, D. M., Kluzek, E., Lindsay, K., and Thornton, P. E., (2012). Simulating the Biogeochemical and Biogeophysical Impacts of Transient Land Cover

Change and Wood Harvest in the Community Climate System Model (CCSM4) from 1850 to 2100, J. Climate, 25, 3071–3095, doi:10.1175/jcli-d-11-00256.

Leck, C., and Bigg, E. K., (2008). Biogenic particles in the surface microlayer and overlaying atmosphere in the central Arctic Ocean during summer. Tellus B: Chemical and Physical Meteorology, 60(1), 110-122. doi: 10.1111/j.1600-0889.2007.00328.

Lee, X., Goulden, M. L., Hollinger, D. Y., Barr, A., Black, T. A., Bohrer, G., and Zhao, L., (2011). Observed increase in local cooling effect of deforestation at higher latitudes. Nature 479 (7373), 384–387. https://doi.org/10.1038/nature10588.

Legrand, M., Plana-Fattori, A., and N'doumé C., (2001). Satellite detection of dust using IR imagery of Meteosat: 1. Infrared difference dust index, J. Geophys. Res., 106(D16), 18,251– 18,274, doi:10.1029/2000JD900749.

Levy, R. C., Remer, L. A., Kleidman, R. G., Mattoo, S., Ichoku, C., Kahn, R., and Eck, T. F., (2010). Global evaluation of the collection 5 MODIS dark target aerosol products over land. Atmos Chem Phys Discuss 10:14815–14873.

Li, Y., Zhao, M., Mildrexler, D.J., Motesharrei, S., Mu, Q., Kalnay, E., and Wang, K., (2016). Potential and actual impacts of deforestation and afforestation on land surface temperature. J. Geophys. Res.-Atmos. https://doi.org/10.1002/2016JD024969.

Li, Y., Zhao, M., Motesharrei, S., Mu, Q., Kalnay, E., and Li, S., (2015). Local cooling and warming effects of forests based on satellite observations. Nat. Commun. 6, 6603. https://doi.org/10.1038/ncomms7603.

Liao, H., and Seinfeld, J., (1998). Radiative forcing by mineral dust aerosol: sensitivity to key variables. J Geophys Res 103(31):637–646.

Lin, G., Penner, J. E., Flanner, M. G., Sillman, S., Xu, L., Zhou, C., and Wang, X. (2014). Radiative forcing of organic aerosol in the atmosphere and on snow: Effects of SOA and brown carbon. Journal of Geophysical Research: Atmospheres, 119(10), 6122-6139.

Lu, Z., Zhang, Q., and Streets, D. G., (2010). Sulfur dioxide and primary carbonaceous aerosol emissions in China and India, 1996-2010. Atmospheric Chemistry and Physics, 10(14), 6863-6879. doi: 10.5194/acp-10-6863-2010.

Lubin, D., Satheesh, S. K., McFarquar, G and Heymsfield, A. J., (2002). Longwave radiative forcing of Indian Ocean tropospheric aerosol, J. Geophys. Res., 107(D19), 8004, doi:10.1029/2001JD001183.

Luyssaert, S., et al., (2014). Land management and land-cover change have impacts of similar magnitude on surface temperature. Nat. Clim. Chang. 4, 389–393. https:// doi.org/10.1038/NCLIMATE2196.

Malavelle, F., Pont, V., Mallet, M., Solmon, F., Johnson, B., Léon, J., and Liousse, C., (2011). Simulation of Aerosol Radiative Effects over West Africa during DABEX and AMMA SOP-0. Journal of Geophysical Research: Atmospheres, 116, Article ID: D08205. 17

Mallet, M., Solmon, F., Nabat, P., Elguindi, N., Waquet, F., Bouniol, D., and Formenti, P., (2020). Direct and semi-direct radiative forcing of biomass-burning aerosols over the southeast Atlantic (SEA) and its sensitivity to absorbing properties: a regional climate modelling study. Atmospheric Chemistry and Physics, 20(21), 13191-13216.

Mallet, M., Tulet, P., Serça, D., Solmon, F., Dubovik, O., Pelon, J., and Thouron, O., (2009). Impact of dust aerosols on the radiative budget, surface heat fluxes, heating rate profiles and convective activity over West Africa during March 2006. Atmospheric Chemistry and Physics, 9(18), 7143-7160.

Marticorena, B., Bergametti, G., Aumont, B., Callot, Y., N'Doume, C., and Legrand, M., (2010). Modeling the atmospheric dust cycle: Design of a soil-derived dust emission scheme. Journal of Geophysical Research: Atmospheres, 115(D12), D12202.

Matsuki, A., Schwarzenboeck, A., Venzac, H., Laj, P., Crumeyrolle, S., and Gomes, L., (2010). Cloud processing of mineral dust: direct comparison of cloud residual and clear sky particles during AMMA aircraft campaign in summer 2006. Atmospheric Chemistry and Physics, 10(3), 1057-1069.

Matthews, H. D., Weaver, A. J., Meissner, K. J., Gillett, N. P., and Eby, M., (2004) Natural and anthropogenic climate change: incorporating historical land cover change, vegetation dynamics and the global carbon cycle, Clim. Dynam., 22, 461–479, doi:10.1007/s00382-004-0392-2.

Michalsky, J. J., Harrison, L. C., Berkheiser Jr, W. E., Richardson, S. J., and Michalsky, S. P., (2006). The multi-filter rotating shadow band radiometer: an instrument for optical depth and radiation measurements. Metrologia, 43(4), S51.

Michalsky, J. J., Harrison, L. C., Kiedron, P. W., Berndt, J. L., Min, Q., and Cebula, R. P., (2006). Aerosol optical depth measurements by the US Department of Agriculture UV-B Monitoring and Research Program: 1992 to 2001. Journal of Geophysical Research: Atmospheres, 111(D14).

Middleton, N., (2017). Climate hazards and disaster resilience in coastal cities: challenges and opportunities for Ho Chi Minh City and other rapidly urbanizing regions. Sustainability Science, 12(6), 923-937. doi: 10.1007/s11625-017-0449-z.

Miller, J. M., and Tegen, I., (1998). Climate response to soil dust aerosols. Journal of Climate, 11(12), 3247-3267.

Miller, R. L., Schmidt, G. A., Nazarenko, L. S., Tausnev, N., Bauer, S. E., Del Genio, A. D., and Yao, M. S., (2004). Present-day atmospheric simulations using GISS Model: Comparison to in-situ, satellite, and reanalysis data. Journal of Climate, 17(24), 4668 4687.

Ming, Y., Ramaswamy, V., (2011). A model investigation of aerosol induced changes in tropical circulation. J Clim 24(19):5125–5133.

Miranda, A.C., Miranda, H.S., Lloyd, J., Grace, J., Francey, R.J., Mcintyre, J.A., and Brass, J.B., (1997). Fluxes of carbon, water, and energy over Brazilian cerrado: an analysis using eddy covariance and stable isotopes. Plant Cell Environ. 20 (3), 315–328. https://doi.org/10.1046/j.1365-3040.1997.d01-80.x.

Moore, K.E., Fitzjarrald, D.R., Sakai, R.K., (1996). Seasonal variation in radiative and turbulent exchange at a deciduous forest in Central Massachusetts. J. Appl. Meteorol. 35 (1), 122–134. https://doi.org/10.1175/1520-0450.

Mukherjee, T., Vinoj, V., (2021). The Sub-Daily Variability of Aerosol Loading and Associated Radiative Forcing Over the Indian Region: Frontiers in Earth Science, 10.3389/feart.2021.727169:2296-6463.

Myhre, G., Samset, B. H., Schulz, M., Balkanski, Y., Bauer, S., Berntsen, T. K., and Stier, P., (2014). Radiative forcing of the direct aerosol effect from AeroCom Phase II simulations. Atmospheric Chemistry and Physics, 13(4), 1853-1877.

Myhre, G., Shindell, D., Bréon, F. M., Collins, W., Fuglestvedt, J., Huang, J., and Zhang, R., (2013). Anthropogenic and natural radiative forcing. In Climate Change 2013: The Physical Science Basis. Contribution of Working Group I to the Fifth Assessment Report

of the Intergovernmental Panel on Climate Change (pp. 659-740). Cambridge University Press.

Myhre, G., Shindell, D., Bréon, F.-M., Collins, W., Fuglestvedt, J., Huang, J., Zhang, D. Koch… H., 2013. Anthropogenic and natural radiative forcing. In: Stocker, T.F., Qin, D., Plattner, G.-K., Tignor, M., Allen, S.K., Boschung, J., Nauels, A., Xia, Y., Bex, V., Midgley, P.M. (Eds.), Climate Change (2013). The Physical Science Basis. Contribution of Working Group I to the Fifth Assessment Report of the Intergovernmental Panel on Climate Change. Cambridge University Press, Cambridge, United Kingdom and New York, NY, USA.

Myneni, R., Knyazikhin, Y., and Park, T., (2015). MCD15A2H MODIS/Terra+Aqua Leaf Area Index/FPAR 8-day L4 Global 500m SIN Grid V006. NASA EOSDIS Land Processes DAAChttps://doi.org/10.5067/MODIS/MCD15A2H.006.

Nabat, P., Somot, S., Mallet, M., Sanchez-Lorenzo, A., and Wild, M., (2014). Contribution of anthropogenic sulphate aerosols to the changing Euro-Mediterranean climate since 1980. Geophysical Research Letters, 41(2), 560-565.

NASA LP DAAC, 2016b. MCD43B3 Black-sky and white-sky albedo 8-Day L3 Global 1 km SIN Grid. Version 6. NASA EOSDIS Land Processes DAAC, USGS Earth Resources Observation and Science (EROS), Center, Sioux Falls, South Dakota. https://lpdaac. usgs.gov.

N'Datchoh, E. T., Diallo, I., Konaré, A., Silué, S., Ogunjobi, K. O., Diedhiou, A., and Doumbia, M., (2018). Dust induced changes on the West African summer monsoon features. International Journal of Climatology, 38(1), 452-466.

Nicholson, S. E., (2013). The west African Sahel: a review of recent studies on the rainfall regime and its inter-annual variability. ISRN Meteorol 2013:453521.

Nicholson, S.E., (2017). Climate and climatic variability of rainfall over eastern Africa. Rev. Geophys. 55, 590–635. https://doi.org/10.1002/2016RG000544.

O'Brien, T. A., Chuang, P. Y., Sloan, L. C., Faloona, I. C., Rossiter, D. L., (2012). Coupling a new turbulence parametrization to RegCM adds realistic stratocumulus clouds. Geosci Mod Dev 5:989–1008.

O'Halloran, T. L., Law, B. E., Goulden, M. L., Wang, Z., Barr, J. G., Schaaf, C., Brown, M., Fuentes, J. D., Göckede, M., Black, A., and Engel, V., (2011). Radiative forcing of natural forest disturbances, Global Change Biol., 18, 555–565, doi:10.1111/j.1365-2486.2011.02577.

Ogunjobi, K. O., and Awoleye, P.O., (2019). Intercomparison and Validation of Satellite and Ground-Based Aerosol Optical Depth (AOD) Retrievals over Six AERONET Sites in West Africa. Aerosol Sci Eng 3(1):32–47. https: //doi.org/10.1007/s4181 0-019-00040 - 7 (ISSN 2510-375X).

Ogunjobi, K. O., He, Z., Kim, K. W., & Kim, Y. J. (2004). Aerosol optical depth during episodes of Asian dust storms and biomass burning at Kwangju, South Korea. Atmospheric Environment, 38(9), 1313-1323.

Ogunjobi, K. O., Kim, Y. J., & He, Z. (2003). Aerosol optical properties during Asian dust storm episodes in South Korea. Theoretical and Applied Climatology, 76, 65-75.

Ohneiser, C., Chang, K. L., and Voulgarakis, A. (2020). Evaluating the impact of land use and land cover change on global climate through atmospheric energy budgets. Journal of Climate, 33(4), 1351-1365. doi: 10.1175/JCLI-D-19-0295.1.

Oleson, K. W., Lawrence, D. M., Bonan, G. B., Drewniak, B., Huang, M., Koven, C. D., Levis, S., Li, F., Riley, W. J., Subin, Z. M., Swenson, S. C., Thornton, P. E., Bozbiyik, A., Fisher, R., Heald, C. L., Kluzek, E., Lamarque, J.-F., Lawrence, P. J., Leung, L. R., Lipscomb, W., Muszala, S., Ricciuto, D. M., Sacks, W., Sun, Y., Tang, J., and Yang Z.-L., (2013) Technical description of version 4.5 of the Community Land Model (CLM). NCAR technical note NCAR/TN-503CSTR, National Center for Atmospheric Research.

Oluleye, A., Ogunjobi, K. O., Bernard, A., Ajayi, V. O., and Akinsanola, A. A., (2012). Multiyear analysis of ground-based sun photometer (AERONET) aerosol optical properties and its comparison with Satellite Observations over West Africa. Global Journal of Human Social Science. Geography & Environmental GeoSciences. 12-10-1.0, 2249-460x

Paeth, H., and Feichter, J., (2006) Greenhouse-gas versus aerosol forcing and African climate response. Climate Dyn., 26 , 35–54.

Paeth, H., and Hense, A., (2006). On the linear response of tropical African climate to SST changes deduced from regional climate model simulations. Theor. Appl. Climatol., 83, 1–19.

Papadimas, C. D., Hatzianastassiou, N., Mihalopoulos, N., Matsoukas, C., Vardavas, I., and Kanakidou, M., (2012). Aerosol and cloud microphysical characteristics of rift and surrounding regions during ASTEX over western Mediterranean. Atmospheric Chemistry and Physics, 12(22), 10831-10849.

Patel, P. N., Dumka, U. C., Kaskaoutis, D. G., Babu, K. N., and Mathur, A. K., (2017). Optical and radiative properties of aerosols over Desalpar, a remote site in western India; Source identification, modification processes and aerosol type discrimination. Science of the Total Environment, 575, 612-627. https://doi.org/10.1016/j.scitotenv.2016.09.023.

Pathak, B., and Bhuyan, P. K., (2014). Absorbing and scattering properties of boundary layer aerosols over Dibrugarh, Northeast India. Int J Remote Sens 35:5527–5543. https ://doi.org/10.1080/01431 161.2014.92642 4

Peng, S.-S., Piao, S., Zeng, Z., Ciais, P., Zhou, L., Li, L.Z.X., and Zeng, H., (2014). Afforestation in China cools local land surface temperature. Proc. Natl. Acad. Sci. 111 (8), 2915-2919. https://doi.org/10.1073/pnas.1315126111.

Penner, J. E., (1995). Effects of anthropogenic aerosols on the budget of radiative forcing. Climate Change, 31(2-4), 195-236.

Penner, J. E., Dong, X., and Chen, Y., (2004). Observational evidence of a change in radiative forcing due to indirect aerosol effect, Nature, 427, 231–234.

Pielke Sr, R. A., Adegoke, J., BeltraáN-Przekurat, A., Hiemstra, C. A., Lin, J., Nair, U. S., and Nobis, T. E., (2007). An overview of regional land-use and land-cover impacts on rainfall. Tellus B: Chemical and Physical Meteorology, 59(3), 587-601.

Pitman, A. J., Avila, F. B., Abramowitz, G., Wang, Y. P., Phipps, S. J., and de Noblet-Ducoudré, N., (2011). Importance of background climate in determining impact of land-cover change on regional climate. Nature Climate Change, 1(9), 472-475.

Podgorny, I. A., Ramanathan, V., (2001a). Modeling study of the direct effect of aerosols over the tropical Indian Ocean, Journal of Geophysical Research, 106D202409724105.

Prospero, J. M., Ginoux, P., Torres, O., Nicholson, S. E., and Gill, T. E., (2002). Environmental characterization of global sources of atmospheric soil dust identified with the Nimbus 7 Total Ozone Mapping Spectrometer (TOMS) absorbing aerosol product. Reviews of Geophysics, 40(1), 1002.

Quaas, J., Boucher, O., Bellouin, N., and Kinne, S., (2013). Satellite-based estimate of the direct and indirect aerosol climate forcing. Journal of Geophysical Research: Atmospheres, 118(18), 10,700-10,720.

Quijano, J. C., Sánchez, A., Hoyos, C. D., & Hernández, M. E., (2000). Optical properties of atmospheric aerosols during a dust storm in northern Mexico. Journal of Geophysical Research: Atmospheres, 105(D19), 24435-24444.

Randerson, J. T., Liu, H., Flanner, M. G., Chambers, S. D., Jin, Y., Hess, P. G., Pfister, G., Mack, M. C., Treseder, K. K., Welp, L. R., Chapin, F. S., Harden, J. W., Goulden, M. L., Lyons, E., Neff, J. C., Schuur, E. A., and Zender, C. S., (2006). The impact of boreal forest fire on climate warming, Science, 314, 1130-1132, doi:10.1126/science.1132075

Raut, J. C., and Chazette, P., (2008). Radiative budget in the presence of multi-layered aerosol structures in the framework of AMMA SOP-0, Atmos. Chem. Phys., 8, 6839–6864, https://doi.org/10.5194/acp-8-6839-2008.

Ricchiazzi, P., Yang, S., Gautier, C., and Sowle, D., (1998). SBDART: A research and software tool for plane-parallel radiative transfer in the Earth's atmosphere. Bulletin of the American Meteorological Society, 79, 2101–2114. https://doi.org/10.1175/1520-0477 079%3c2101.

Rosenfeld, D., Lohmann, U., Raga, G. B., O'Dowd, C. D., Kulmala, M., Fuzzi, S., and Snider, J. R., (2008). Flood or drought: how do aerosols affect precipitation?. Science, 321(5894), 1309-1313.

Rulli, M. C., Saviori, A., and D'Odorico, P., (2013). Global land and water grabbing, P. Natl. Acad. Sci. USA, 110, 892–897, doi:10.1073/pnas.1213163110, 2013.

Running, S., Mu, Q., Zhao, M., (2017). MOD16A2 MODIS/Terra Net Evapotranspiration 8Day L4 Global 500m SIN Grid V006. NASA EOSDIS Land Processes DAAChttps://doi. org/10.5067/MODIS/MOD16A2.006.

Russell, L. M., Clarisse, L., Deuzé, J. L., and Remer, L. A., (2002). Smoke aerosol properties and radiative effects during extreme fire event over Europe during summer 2003. Journal of Geophysical Research: Atmospheres, 107(D23), LAC 8-1-LAC 8-9.

Schroedter-Homscheidt, M., Renné, D., Geuder, N., and Meyer, R., (2012). Assessment of solar resource assessment data sources. Solar Energy, 86(5), 1289-1304.

Schwartz, M.D., (1992). Phenology and springtime surface-layer change. Mon. Weather Rev. 120, 2570-2578. https://doi.org/10.1175/1520-0493(1992).

Seinfeld, J. H., et al., (2004). ACE-ASIA regional climatic and atmospheric chemical effects of Asian dust and pollution, Bull. Am. Meteorol. Soc., 85, 367-380, doi:10.1175/BAMS-85-3-367.

Sherwood, S. C., Bony, S., Boucher, O., Bretherton, C., Forster, P. M., Gregory, J. M., and

Singh, R. P., Dey, S., Tripathi, S. N., Tare, V., and Holben, B. N., (2004). Variability of aerosol parameters over Kanpur city, northern India, J. Geophys. Res., 109, D23206, doi:10.1029/2004JD004966.

Singh, S., Nath, S., Kohli, R., and Singh, R., (2005). Aerosol over Delhi during pre-monsoon months: Characteristics and effect on surface radiative forcing, Geophys. Res. Lett., 32, L13808, doi:10.1029/2005GL023062

Singh, S., Soni, K., Bano, T., Tanwar, R. S., Nath, S., and Arya, B. C., (2010). Clear-sky direct aerosol radiative forcing variations over mega-city Delhi. Ann. Geophys., 28, 1157-1166, 2010; www.ann-geophys.net/28/1157/2010; doi:10.5194/angeo-28-1157-2010.

Sitch, S., Brovkin, V., von Bloh, W., van Vuuren, D., Eickhout, B., and Ganopolski, A., (2005). Impacts of future land cover changes on atmospheric CO2 and climate, Global Biogeochem. Cy. 19, GB2013, doi:10.1029/2004gb002311, 2005.

Solomon, S., Qin, D., Manning, M., Chen, Z., Marquis, M., Averyt, K. B., and Miller, H. L. (2007). Climate change 2007: the physical science basis. Contribution of Working Group I to the Fourth Assessment Report of the Intergovernmental Panel on Climate Change. Cambridge University Press.

Song, J., (1999). Phenological influences on the albedo of prairie grassland and crop fields. Int. J. Biometeorol. 42 (3), 153–157. https://doi.org/10.1007/s004840050099.

Srivastava, A. K., Yadav, V., Pathak, V., Singh, S., Tiwari, S., Bisht, D. S., and Goloub, P., (2014). Variability in radiative properties of major aerosol types: A year-long study over Delhi - An urban station in Indo-Gangetic Basin. Science of the Total Environment, 473-474,659–666. https://doi.org/10.1016/j.scitotenv.2013.12.064.

Srivastava, R., and Sherin, S. H., (2017). Spatio-temporal variations of black carbon and optical properties in a regional climate model. Int J Climatol 37:1432–1443. https ://doi.org/10.1002/joc.4787.

Srivastava, R., and Sherin, S. H., (2018). Impact of dynamical and microphysical schemes on black carbon prediction in a regional climate model over India. Environ Sci Pollut Res 25:14844. https ://doi. org/10.1007/s1135 6-018-1607-0

Steiner, A., Pal, J., Rauscher, S., Bell, J., Diffenbaugh, N., Boone, A., Sloan, L., and Giorgi, F., (2009). Land Surface Coupling in Regional Climate Simulations of the West African Monsoon, Clim. Dynam., 33, 869–892.

Stevens, B., (2015). Adjustments in the forcing-feedback framework for understanding climate change. Bulletin of the American Meteorological Society, 96(2), 217-228.

Stier, P., Seinfeld, J. H., Kinne, S., Boucher, O., (2007). Aerosol absorption and radiative forcing, Atmospheric Chemistry and Physics, 71952375261.

Stöckli, R., Vermote, E., Saleous, N., Simmon, R., and Herring, D., (2005). The Blue Marble Next Generation—a true colour earth dataset including seasonal dynamics from MODIS (NASA Earth Observatory): NASA Earth Observatory at http://earthobservatory.nasa. gov/Newsroom/BlueMarble.

Subba, T., Gogoi, M. M., Pathak, B., Ajay, P., Bhuyan, P. K., Solmon, F., (2018). Assessment of 1D and 3D model simulated radiation flux based on surface measurements and estimation of aerosol forcing and their climatological aspects. Atmos Res 204:110–127. https :// doi.org/10.1016/j.atmos res.2018.01.012

Sussmann, R., Retalis, A., Hadjimitsis, D., Michaelides, S., and Chrysoulakis, N., (2016). Estimating aerosol optical depth in the atmosphere with use of a satellite-based neural network approach. Remote Sensing, 8(4), 330.

Sylla, M. B., Giorgi, F., Coppola, E., and Mariotti, L. (2013). Uncertainties in daily rainfall over Africa: assessment of gridded observation products and evaluation of a regional climate model simulation. International Journal of Climatology, 33(7), 1805-1817.

Sylla, M. B., Giorgi, F., Coppola, E., and Mariotti, L. (2013). Uncertainties in daily rainfall over Africa: assessment of gridded observation products and evaluation of a regional climate model simulation. International Journal of Climatology, 33(7), 1805-1817.

Tanré, D., Haywood, J., Pelon, J., Léon, J. F., Chatenet, B., Formenti, P., and Myhre, G., (2003). Measurement and modelling of the Saharan dust radiative impact: Overview of

the Saharan Dust Experiment (SHADE). Journal of Geophysical Research: Atmospheres, 108(D18).

Tegen, I., Heinold, B., Todd, M. C., Helmert, J., Washington, R., Dubovik, O., and Eck, T. F., (2004). Modelling soil dust aerosol in the Bodélé depression during the BoDEx campaign. Atmospheric Chemistry and Physics, 4(5), 1315-1330.

Tiedtke, M., (1989). A comprehensive mass-flux scheme for cumulus parameterization in large-scale models. Mon Weather Rev 117:1779–1800. https ://doi.org/10.1175/1520-0493.

Titos, G., Cazorla, A., Zieger, P., Andrews, E., Lyamani, H., Granados-Muñoz, M.J., Olmo, F. J., and Alados-Arboledas, L., (2016). Effect of hygroscopic growth on the aerosol light-scattering coefficient: a review of measurements, techniques and error sources. Atmos Environ 1:1. https: //doi.org/10.1016/j.atmos env.2016.07.021.

Unger, N., Bond, T. C., Wang, J. S., Koch, D. M., Menon, S., Shindell, D. T., and Bauer, S., (2013). Attribution of climate forcing to economic sectors, P. Natl. Acad. Sci. USA, of the United States of America, 107, 3382–3387, doi:10.1073/pnas.0906548107, 2010.1748-9326/8/1/015009.

Vachaspati, C. V., Begam, G. R., Ahammed, Y. N., Kumar, K. R., and Reddy, R. R., (2018). Characterization of aerosol optical properties andmodel computed radiative forcing over a semi-arid region, Kadapa in India. Atmospheric Research, 209, 36-49. https://doi.org/10.1016/j.atmosres.2018.03.013.

van Vuuren, D. P., Edmonds, J., Kainuma, M., Riahi, K., Thomson, A., Hibbard, K., Hurtt, G. C., Kram, T., Krey, V., Lamarque, J.- F., Masui, T., Meinshausen, M., Nakicenovic, N.,

Smith, S. J., and Rose, S. K., (2011). The representative concentration pathways: an overview, Climatic Change, 109, 5–31, doi:10.1007/s10584-011- 0148-z.

Wallace, J.S., Gash, J.H.C., and Sivakumar, M.V.K., (1990). Preliminary measurements of net radiation and evaporation over bare soil and fallow bushland in the Sahel. Int. J. Climatol. 10 (2), 203–210. https://doi.org/10.1002/joc.3370100207.

Wan, Z., Hook, S., and Hulley, G., (2015). MOD11A2 MODIS/Terra Land Surface Temperature/ Emissivity 8-Day L3 Global 1km SIN Grid V006. NASA EOSDIS LP DAAChttps://doi. org/10.5067/modis/mod11a2.006.

Wan, Z., Zhang, Y., Zhang, Q., and Li, Z., (2002). Validation of the land surface temperature products retrieved from Terra Moderate Resolution Imaging Spectroradiometer data. Remote Sens. Environ. 83 (1), 163–180. https://doi.org/10.1016/S0034-4257(02) 00093-7.

Wang, X., Yang, M., and Pang, G., (2015). Influences of two land-surface schemes on RegCM4 precipitation simulations over the Tibetan Plateau. Adv Meteorol. https ://doi.org/10.1155/2015/10689 1

Ward, P. J., Jongman, B., Weiland, F. S., Bouwman, A., van Beek, R., Bierkens, M. F., and Winsemius, H. C., (2014). Assessing flood risk at the global scale: model setup, results, and sensitivity. Environmental Research Letters, 8(4), 044019. doi: 10.1088/1748-9326/8/4/044019.

Weinzierl, B., Sauer, D., Esselborn, M., Petzold, A., Veira, A., Rose, M., and Wirth, M., (2017). Volcanic particle properties and ash/cloud discrimination: results from the Eyjafjallajökull eruption. Atmospheric Chemistry and Physics, 10(4), 1545-1564. doi: 10.5194/acp-10-1545-2010.

Williamson, Scott N., Barrio, Isabel C., Hik, David S., Gamon, John A., (2016). Phenology and species determine growing-season albedo increase at the altitudinal limit of shrub growth. Glob. Chang. Biol. 3621–3631. https://doi.org/10.1111/gcb.13297.

Winckler, J., Lejeune, Q., Reick, C. H., and Pongratz, J., (2019). Nonlocal effects dominate the global mean surface temperature response to the biogeophysical effects of deforestation. Geophysical Research Letters, 46(2), 745-755.

Winckler, J., Reick, C. H., & Pongratz, J., (2017). Robust identification of local biogeophysical effects of land-cover change in a global climate model. Journal of Climate, 30(3), 1159-1176.

Wolfgang, M. J., Haywood, J. M., Abel, S. J., Barrett, P. A., Boucher, O., Charlson, R. J., and Warren, S. G., (2007). Radiative forcing by aerosols. In Climate Change 2007: The Physical Science Basis. Contribution of Working Group I to the Fourth Assessment Report of the Intergovernmental Panel on Climate Change (pp. 129-234).

Xue, Y., Hall, A., and Bonfils, C., (2010). Observed and simulated changes in atmospheric boundary layer height over the continental United States. Journal of Geophysical Research: Atmospheres, 115(D22), D22106.

Yu, H., Kaufman, Y. J., Chin, M., Feingold, G., Remer, L. A., Anderson, T. L., and Livingston, J. M., (2006). A review of measurement-based assessments of the aerosol direct radiative effect and forcing. Atmospheric Chemistry and Physics, 6(3), 613-666.

Yu, X. N., Lu, R., Kumar, K. R., Ma, J., Zhang, Q., Jiang, Y., et al., (2016). Dust aerosol properties and radiative forcing observed in spring during 2001-2014 over urban Beijing, China. Environmental Science and Pollution Research,23, 15,432-15,442. https://doi.org/10.1007/s11356-016-6727-910.1029/2018JD029461.

Yue, X. G., & Liao, S. Y., (2012). A comparison of principal component analysis and principal factor analysis in estimating the intelligence structure. Social Behavior and Personality: an international journal, 40(9), 1477-1484.

Zakey, A. S., Solmon, F., and Giorgi, F., (2006a) Implementation and testing of a desert dust module in a regional climate model. Atmos Chem Phys 6:4687–4704.

Zakey, A. S., Solmon, F., and Giorgi, F., (2006b). Implementation and testing of a desert dust module in a regional climate model. Atmos Chem Phys 6:4687–4704.

Zhang X, Wang D, Hao H, Zhang F, Hu Y. Effects of Land Use/Cover Changes and Urban Forest Configuration on Urban Heat Islands in a Loess Hilly Region: Case Study Based on Yan'an City, China. Int J Environ Res Public Health. 2017 Jul 26; 14(8):840. doi: 10.3390/ijerph14080840. PMID: 28933770; PMCID: PMC5580544.

Zhang, H., and Henderson-Sellers, A., (1996). Impacts of tropical deforestation. Part I: process analysis of local climatic change. J. Clim. 9 (7), 1497-1517. https://doi.org/10.1175/1520-0442.

Zhang, J., and Reid, J. S., (2010). A decadal regional and global trend analysis of the aerosol optical depth using a data-assimilation grade over-water MODIS and Level 2 MISR aerosol products. Atmospheric Chemistry and Physics, 10(22), 10949-10963.

Zhao, C., Hu, Z., Qian, Y., Ruby Leung, L., Huang, J., Huang, M., and Streets, D. G., (2014). Simulating black carbon and dust and their radiative forcing in seasonal snow: a case study over North China with field campaign measurements. Atmospheric Chemistry and Physics, 14(20), 11475-11491.

Zhou, L., Dickinson, R. E., Tian, Y., Fang, J., Li, Q., Kaufmann, R. K., Tucker, C. J., and Myneni, R. B., (2004). Evidence for a significant urbanization effect on climate in China. Proc Natl Acad Sci U S A 101(26):9540–9544. doi:10.1073/pnas.0400357101.

Zhu, C., Levy, R. C., Ichoku, C., and Mattoo, S., (2007). MODIS observation of aerosols and estimation of aerosol radiative forcing over southern Africa during SAFARI 2000. Journal of Geophysical Research: Atmospheres, 112(D12).

APPENDIX

Aerosol Optical Depth (AOD)

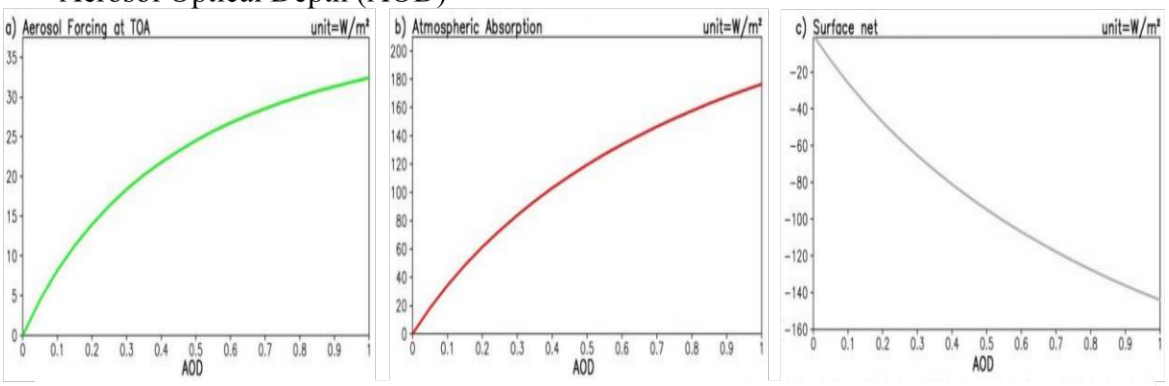

Appendix 1.1: Annual-mean clear-sky aerosol forcing as a function of AOD at 550nm which only considered solar radiation

Single Scattering Albedo (SSA)

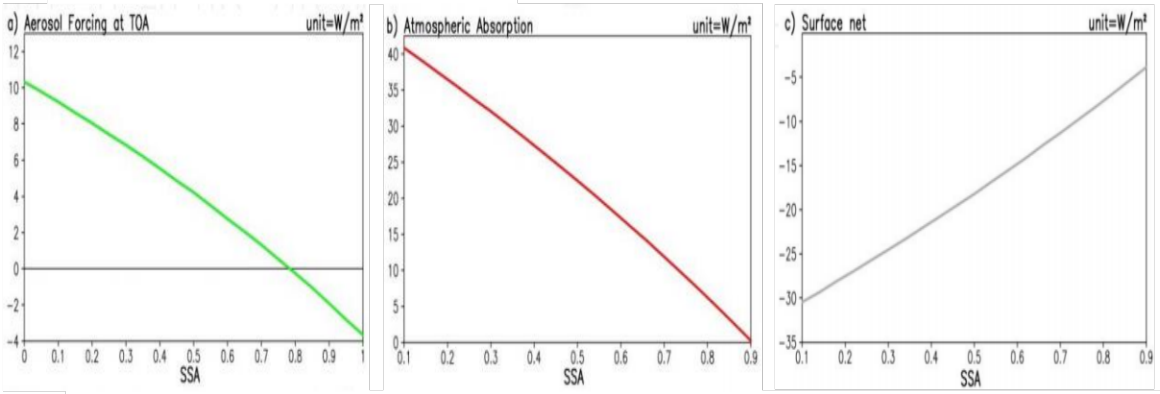

Appendix 1.2: Annual-mean clear-sky aerosol forcing as a function of SSA

Asymmetry Parameter

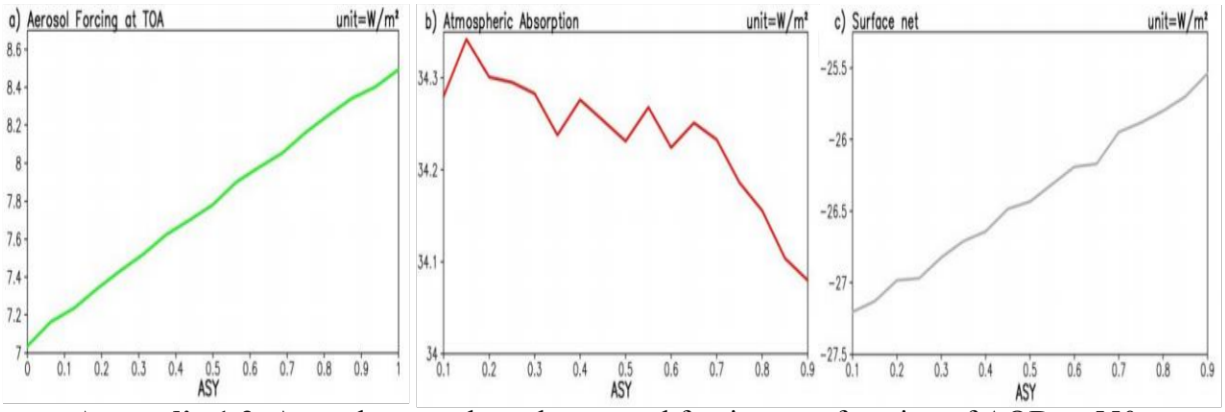

Appendix 1.3: Annual-mean clear-sky aerosol forcing as a function of AOD at 550nm which only considered solar radiation

AngstromExponent

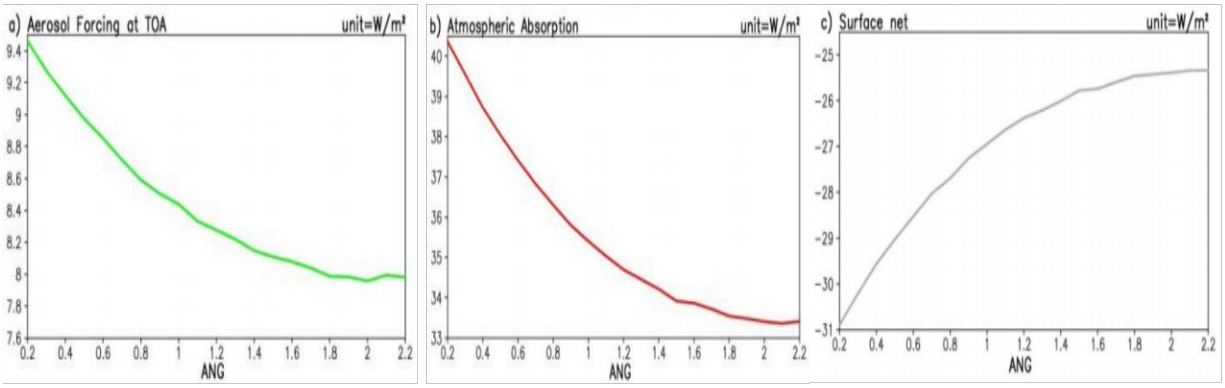

Appendix 1.4: Annual-mean clear-sky aerosol forcing as a function of α. AOD at 550nm

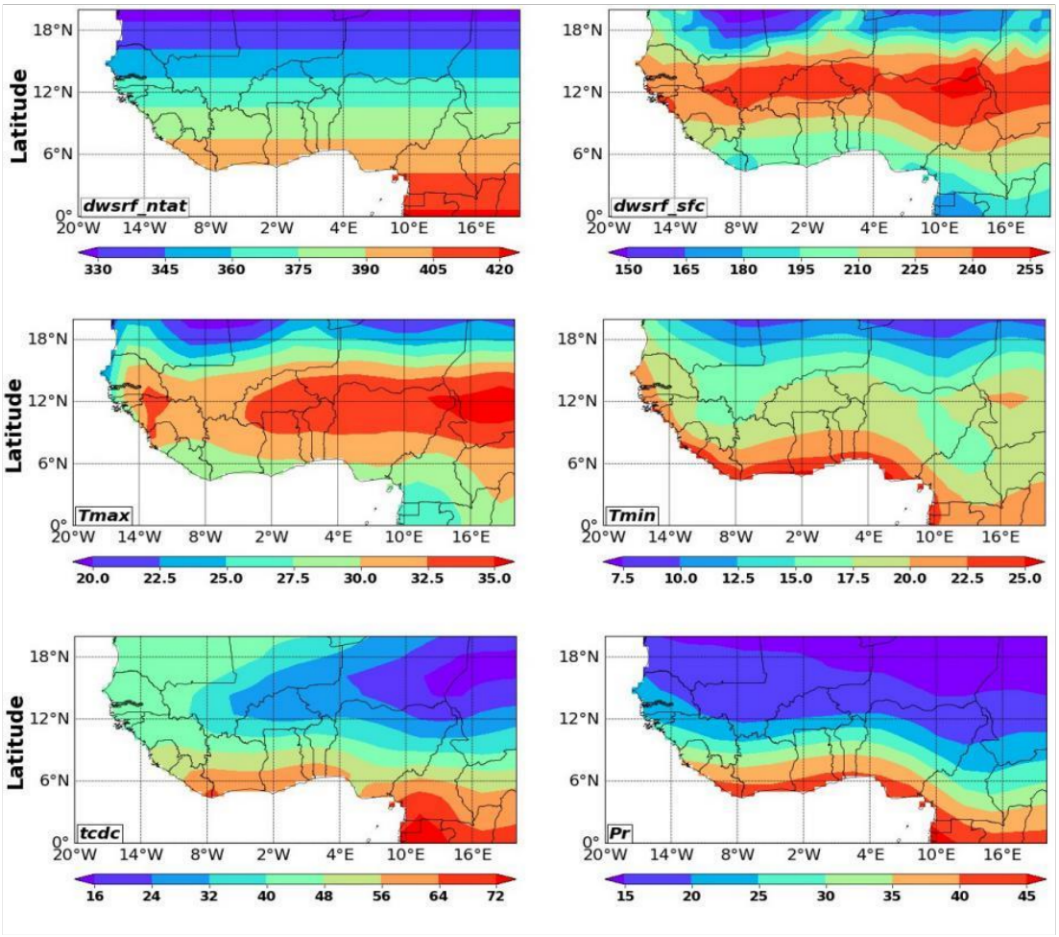

Appendix 1.5: Monthly variation of downward solar radiation flux at the top of the atmosphere (dwsrf_ntat) and at the surface (dwsrf_sfc, maximum temperature (Tmax), minimum temperature (Tmin), total cloud cover (tcdc) and precipitation (Pr)

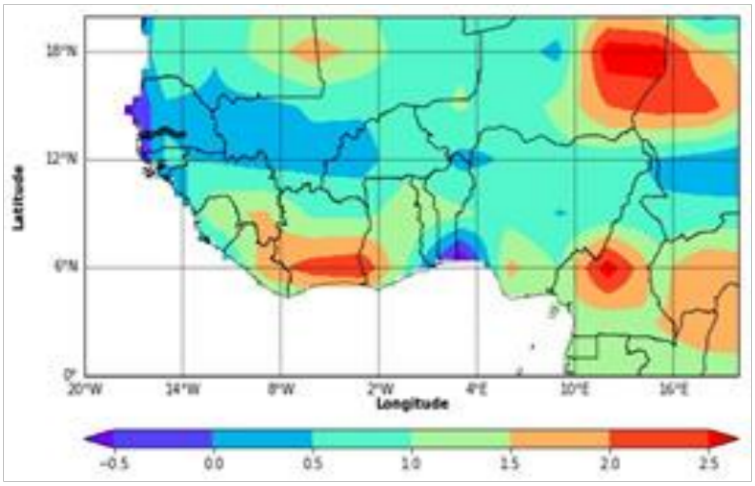

Appendix 1.6: Mean effective radiation flux at the TOA in DJF

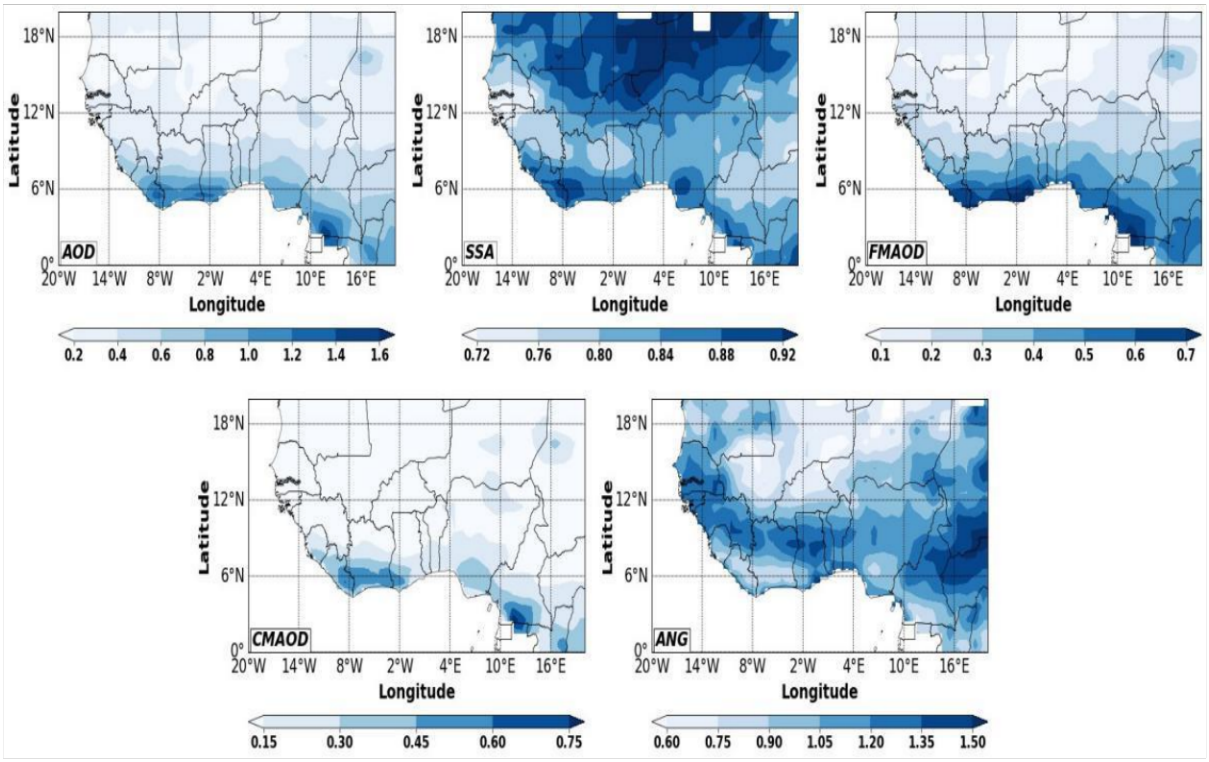

Appendix 1.7: Monthly fractional contributions of aerosol optical depth (AOD), single scattering albedo (SSA), fine-mode AOD (FMAOD), coarse mode AOD (CMAOD), and angstrom exponent (ANG) aerosol properties at 550nm.

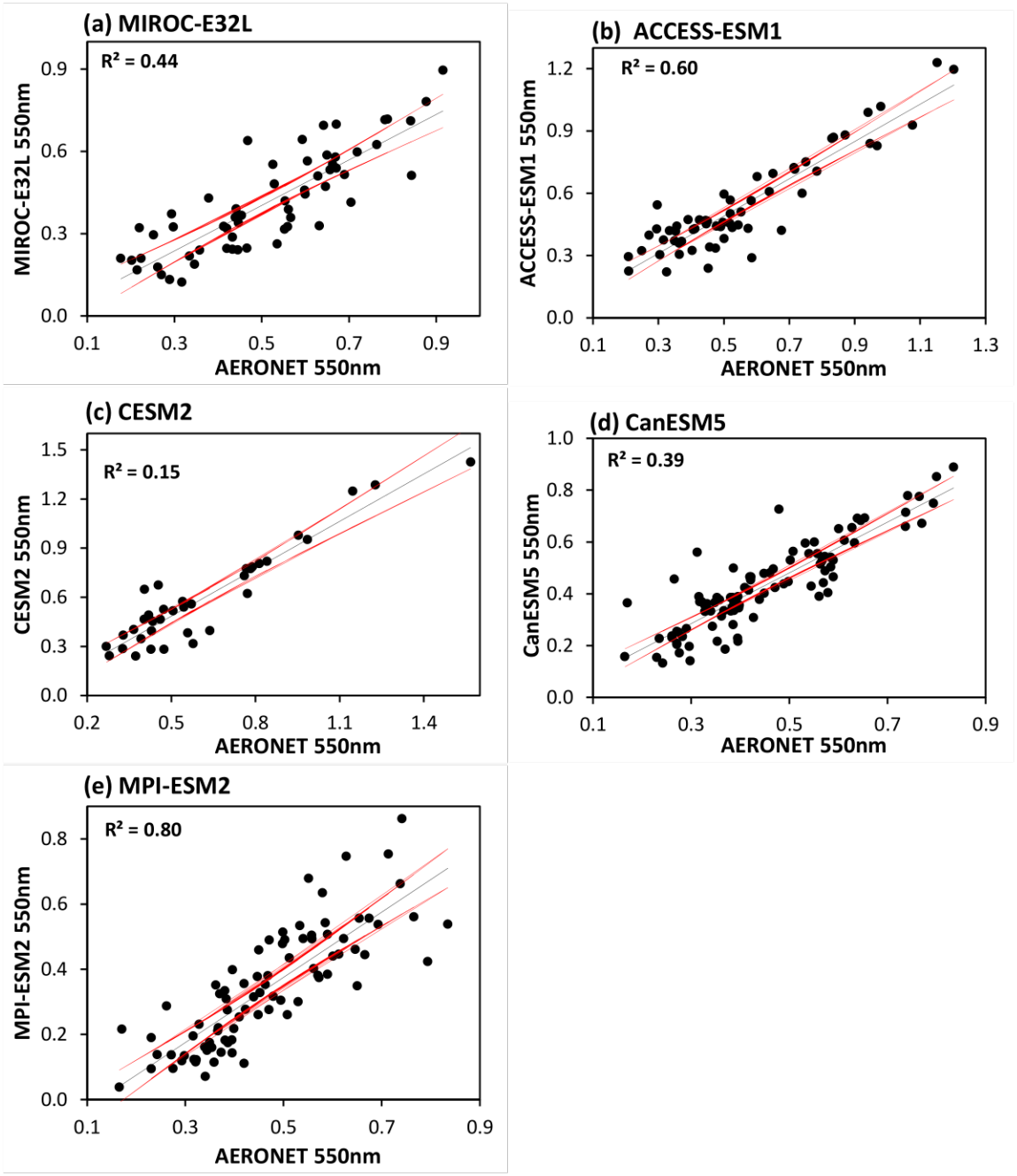

Appendix 1.8: Regression plots of aerosol optical depth values retrieved from AERONET at 550nm against different model data over West Africa with the true line of best-fit lying within the 95% confidence interval (red line)

Appendix 1.9: Prediction of aerosol optical properties by an ordinary least squares regression method: regressor coefficients (a), y intercept (a_0), squared correlations (R^2), and root mean square error (RMSE).

$y=a_0+a_1 \cdot x_1+\ldots+a_n \cdot x_n$

y	a_0	$a_1 \cdot$ln (QL)	$a_2 \cdot$ln (fad)	$a_3 \cdot$ln (Nint)	R^2	RMSE
MIROC	-0.557±0.0020	0.849±0.0004	-0.389±0.0006	–	0.59	-0.255
ACCESS-ESM1	-2.037±0.0019	0.808±0.0002	-0.043±0.0005	0.274±0.0003	0.60	-0.179
CESM2	-0.665±0.0024	0.860±0.0005	-0.065±0.0009	–	0.15	-0.172
MPI-ESM2	-2.437±0.0008	0.830±0.0001	-0.147±0.0001	0.303±0.0001	0.80	-0.019
CanESM5	-1.453±0.0056	0.843±0.0003	-0.132±0.0002	–	0.39	-0.265

Appendix 1.10: Pearson correlations between the logarithm of the radiative properties and the RCs. Degree of correlation (absolute values): (a) very weak: below 0.2, (b) weak: [0.2, 0.4), (c) moderate: [0.4, 0.6), (d) strong: [0.6, 0.8), and (e) very strong [0.8, 1.0]. Explained variance and cumulative explained variance by different components obtained from the PC analysis.

Models	**PC-1**	**PC-2**	**PC-3**	**PC-4**
MIROC	0.969	0.025	−0.001	0.201
ACCESS-ESM1	0.919	−0.282	0.076	0.237
CESM2	−0.896	−0.014	0.073	−0.183
MPI-ESM2	−0.062	−0.971	−0.192	−0.125
CanESM5	0.177	−0.937	0.285	0.094
EV (%)	**33.8**	**35.5**	**14.8**	**13.6**
CP (%)	**33.8**	**69.3**	**84.1**	**97.7**

Appendix 1.11: Mean and standard deviation of modelled AREs (W m−2) for the SW, LW, and NET (SW plus LW) radiation for the reference simulation over all the study days. ARE (Aerosol Radiative Effect) stands for the aerosol-radiation interaction effect, defined as the difference between the AREs at the top of the atmosphere (TOA) and the bottom of the atmosphere (BOA).

Ref.	ARE SW	ARE LW	ARE NET
TOA	-348.7±78.39	17.51±10.04	-331.2±77.27
ATM	32.94±12.11	-39.16±13.14	-6.225±12.98
BOA	-381.6±86.95	56.66±9.746	-324.9±86.51

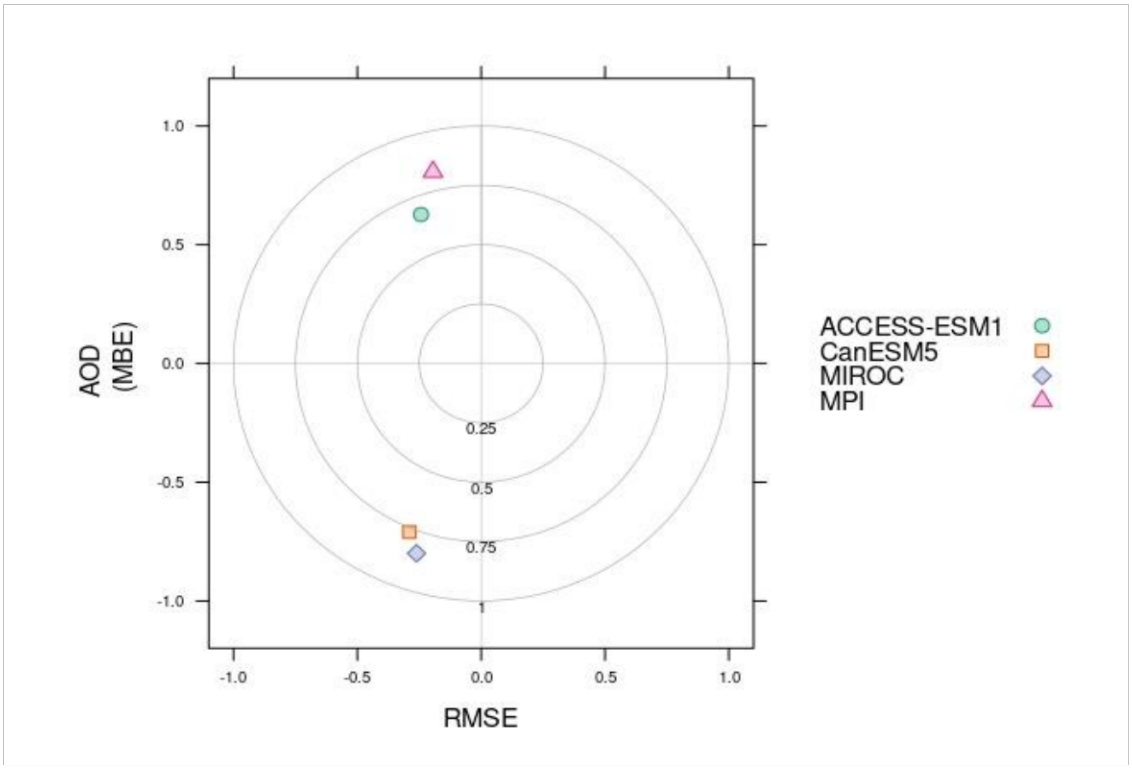

Appendix 1.12: Box plot showing the root mean square error (RMSE) and the mean bias error (MBE) of the models

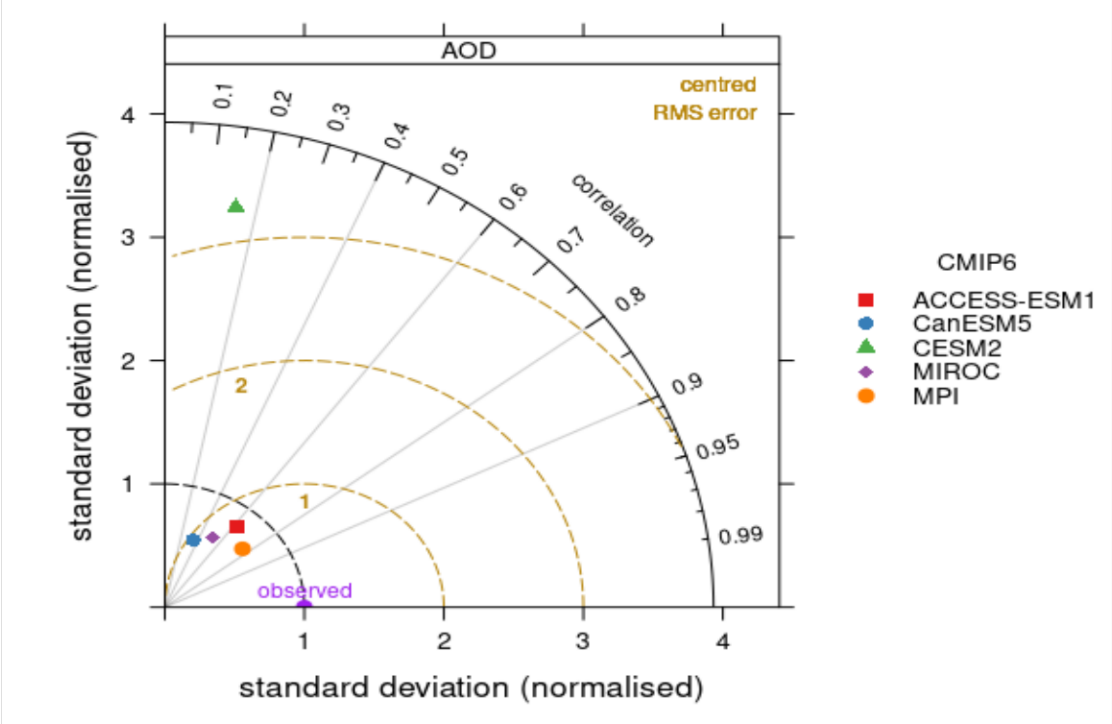

Appendix 1.13: Normalized Taylor's Plot

Appendix 1.14: Statistics of radiative properties of low-level clouds for all the case days individually and on average as simulated by cloud radiative kernels, n stands for the sample size. For the fraction of clouds, two values are presented: values in brackets denote the fraction of selected clouds (FC) according to the column selection, while values outside brackets stand for the actual cloud fraction (CF) in terms of the following threshold for the liquid water path, QL>1 g m−2.

Days	n (–)	QL (g m−2)	τ (–)	CBH (m)	CTH (m)	H (m)	fad (–)	CF (FC) (%)
24 December 2005	4822	31.9±21.7	14.0±1.38	541±160	507±146	253±52.2	0.11±0.20	2.25 (0.46)
25 December 2005	19542	119.1±15.5	17.4±33.8	2721±185	2132±627	124±173	0.45±0.24	4.38 (2.03)
5 January 2006	6465	56.2±28.8	22.0±10.7	1345±170	1900±324	208±128	0.24±0.12	3.11 (1.09)
29 January 2006	21661	15.3±26.3	19.3±38.8	1053±701	1279±567	234±202	0.40±0.30	6.99 (2.99)
14 February 2006	15105	124.3±92.7	36.1±40.3	679±523	1387±442	476±234	0.46±0.30	4.97 (3.08)
23 February 2006	34768	146.0±12.0	26.6±13.0	1681±674	351±376	423±230	0.13±0.51	37.4 (2.34)

Appendix 1.15: Monthly averages of radiative properties for CAMS-RA aerosol.

	AOD				SSA			ASY		
λ (μm)	Total	Coarse	Fine	Anthropogenic	Total	Coarse	Fine	Total	Coarse	Fine
0.45	0.144	0.058	0.087	0.043	0.902	0 .905	0.9	0.718	0.789	0.67
0.55	0.122	0.058	0.063	0.032	0.941	0.964	0.919	0.702	0.767	0.639
1	0.081	0.062	0.019	0.009	0.956	0.982	0.87	0.693	0.736	0.533

Appendix 1.16: Annual average climatology associated aerosol radiative effects at the top of the atmosphere (TOA), at the surface and for the atmosphere. Aside from total aerosol, effects of components and their anthropogenic contributions are also indicated. Considered fine-mode components are sulfate, organic matter, carbon component and the black carbon. Considered coarse-mode components are sea salts and dust.

Direct effect (W m−2)	TOA				Atmosphere				Surface			
	Total		Anthropogenic		Total		Anthropogenic		Total		Anthropogenic	
	All	Clear	All	Clear	All	Clear	All	Clear	All	Clear	All	Clear
Total	−1.1	−2.3	−0.35	−0.69	2.9	2.3	1.2	1.2	−4.0	−4.6	−1.6	−1.9
Fine	−0.80	−1.5	−0.36	−0.70	2.3	2.4	1.1	1.2	−3.1	−3.9	−1.5	−1.9
Sulphate	−0.83	−1.2	−0.41	−0.58	0.01	0.02	0	0.01	−0.84	−1.2	−0.41	−0.59
Carbon Component	0.08	−0.23	0.05	−0.10	2	2.2	1	1.2	−2.1	−2.5	−1.0	−1.3
Organic Matter	−0.45	−0.68	−0.22	−0.34	0.49	0.52	0.23	0.24	−0.94	−1.2	−0.45	−0.58
Black Carbon	0.55	0.46	0.28	0.24	1.7	1.8	0.89	0.94	−1.2	−1.4	−0.61	−0.70
Coarse	−0.34	−0.77	0.02	0.02	0.66	0.14	0.13	0.04	−1.00	−0.91	−0.11	−0.03
Sea Salt	−0.57	−1.00			0.01	−0.10			−0.58	−0.90		
Dust	0.23	0.24	0.015	0.01	0.68	0.25	0.12	0.13	−0.45	−0.01	−0.11	−0.033

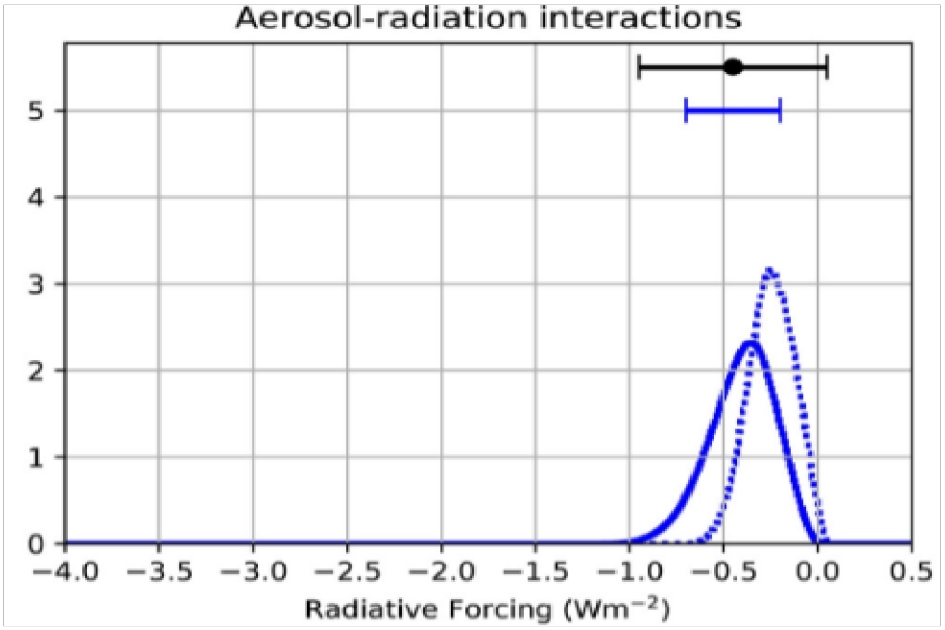

Appendix 1.17: Probability distribution functions of aerosol radiative forcing (dashed lines) and effective radiative forcing (solid lines), in W/m^2

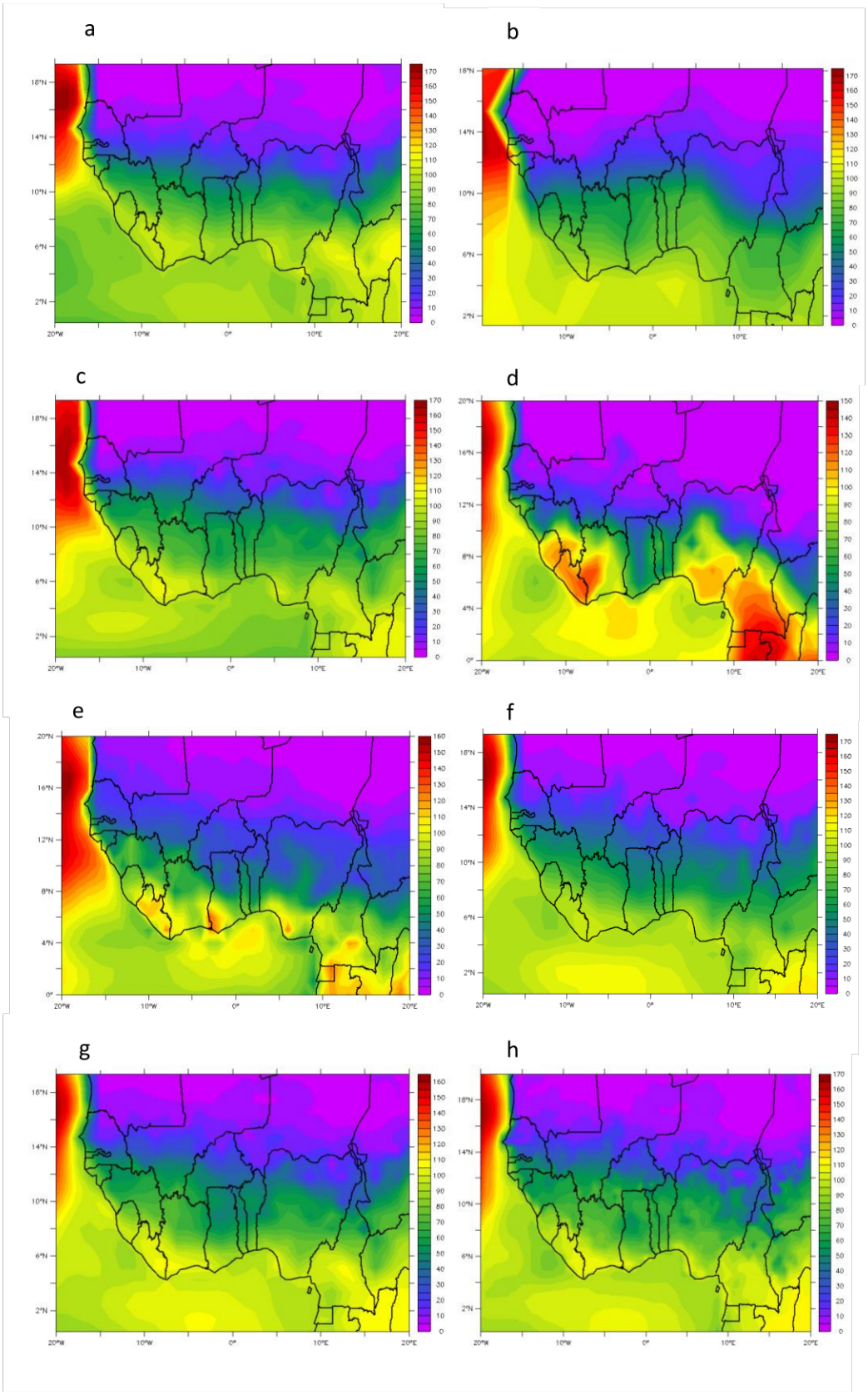

Appendix 1.18: Surface Latent Heat Radiation flux (normalised radiative forcing); (a) CAM4 (b) CanESM2 (c) CESM1 (d) ESRL GFS (e) GEOS-5 (f) LBNL-CAM5 (g) PSL-1deg (h) PSL-0.5deg

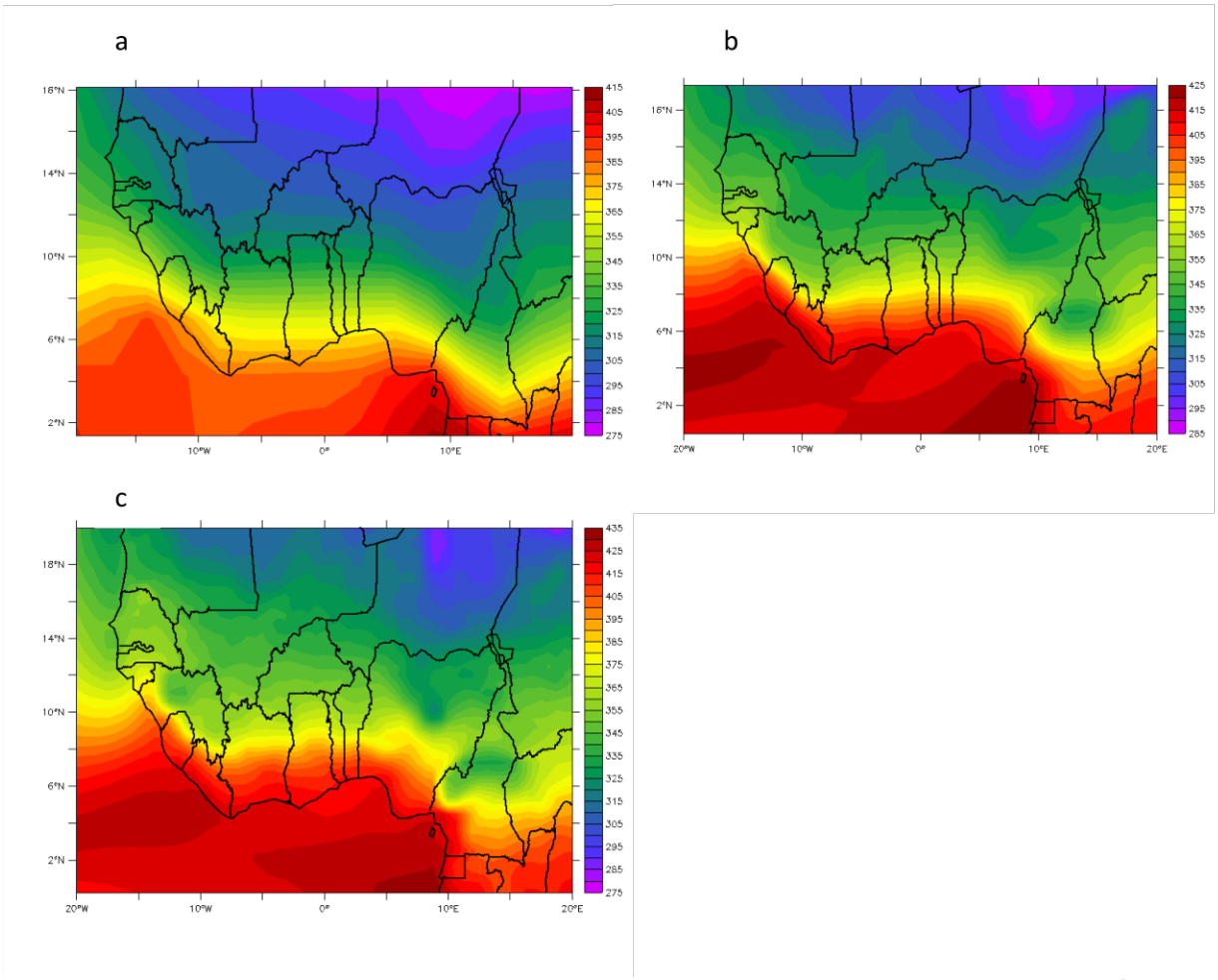

Appendix 1.19: Downward Longwave Radiation due to Aerosol Forcing (W/m^2): (a) CanESM2 (b) CESM1 (c) PSL